1-1-1974

Evaporation, Infiltration, And Rainfall-Runoff Processes In Urban Watersheds

A. Hossain

J. W. Delleur
delleur@purdue.edu

A. R. Rao

TECHNICAL REPORT NO. 41

EVAPORATION, INFILTRATION AND RAINFALL-RUNOFF PROCESSES IN URBAN WATERSHEDS

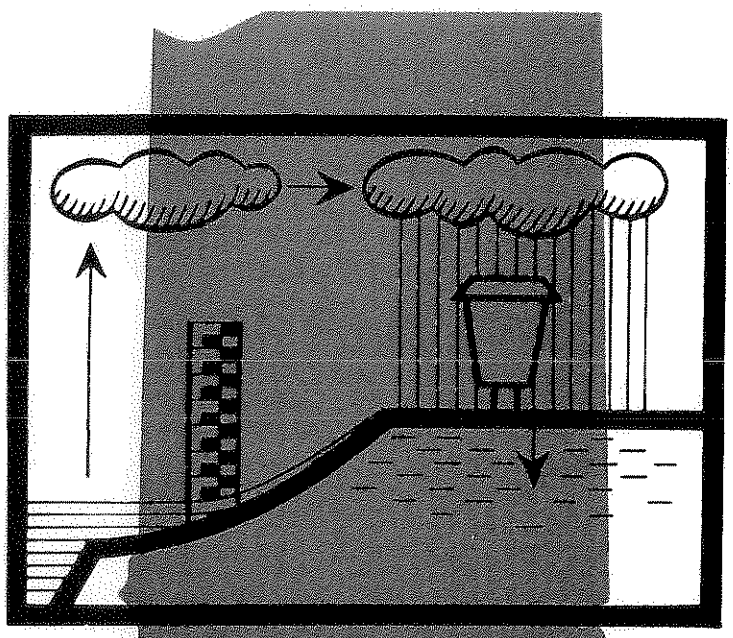

by

Aolad Hossain

Jacques W. Delleur

Ramachandra A. Rao

JANUARY 1974

PURDUE UNIVERSITY
WATER RESOURCES RESEARCH CENTER
WEST LAFAYETTE, INDIANA

Water Resources Research Center
Purdue University
West Lafayette, Indiana

EVAPORATION, INFILTRATION AND RAINFALL-RUNOFF PROCESSES IN URBAN WATERSHEDS

by

Aolad Hossain
Jacques W. Delleur
Ramachandra A. Rao

The work upon which this report is based was supported in part by funds provided by the United States Department of the Interior, Office of Water Resources Research, as authorized by the Water Resources Research Act of 1964 (PL 88-379 as amended).

Period of Investigation: September, 1970 - December, 1973
Final Report for OWRR-B-022-IND
Matching Fund Agreement No. 14-31-0001-3801

Purdue University Water Resources Research Center
Technical Report No. 41
January 1974

ABSTRACT

The rainfall-runoff transfer has been simulated by linear, nonlinear, time invariant and time variant deterministic models. Most of these models, particularly those based on the linear analysis concept, use the rainfall excess as the input. The weakest link in the rainfall-runoff transfer models is the proper estimation of the input, the effective rainfall. The principal objective of this study was the development and testing of methods of estimation of the rainfall excess. The other objectives of the study were the testing of linear and nonlinear systems models in the determination of the response of watersheds at different stages of urbanization and the development of a model of the rainfall excess-direct runoff transfer.

The data for the study were obtained from eleven watersheds in Indiana, Texas and Illinois.

Several evaporation models were tested and evaluated to determine their suitability for the estimation of the evaporation losses from urban watersheds. The van Bavel and the Kohler models, both based on a combination of the diffusion and the energy balance approaches, were compared. The importance of the relative humidity in the evapotranspiration empirical estimators was analyzed by comparing the Blaney-Criddle and the Blaney-Morin estimators, although these formulas were not originally developed for the estimation of short term evapotranspiration. The van Bavel formula was found to be the best model, and the Blaney-Morin model, which incorporates the effect of relative humidity was found to give good results when the radiation and other meteorological data required by the van Bavel formula are unavailable.

The constant diffusivity form of the unsteady flow equation for the flow in porous media was solved making use of the linear systems approach, and an impulse response function was obtained for the relative soil moisture change. This unsteady flow equation is also the theoretical basis for the first two of the five models which were tested to estimate the rainfall excess in urban watersheds. These are the MIT model, the Minnesota model, the Holtan model, the Multicapacity Basin Accounting model and the Antecedent Retention Index model. All the models were modified in view of their application to urban watersheds. Some of the parameters of these models were optimized. The performances of these models were evaluated and the sensitivities of their parameters were analyzed. The Antecedent Retention Index model gave the best estimate of the total rainfall excess and the MIT model gave the best prediction of the time distribution of the rainfall excess.

A quasi-linear model of the rainfall-runoff transfer was developed. A dimensionless linear kernel was obtained. The instantaneous unit hydrograph (IUH) for a specific storm on a specific watershed may be obtained by rescaling the dimensionless kernel by using the peak discharge of the IUH, the time lag of the watershed and storm characteristics. The peak discharge of the IUH and the time lag of the watershed are obtained by the given regression relationships. The model was tested by predicting the direct runoff of an urban watershed the data from which were not used for the calibration of the model and the performance was found to be very satisfactory.

A nonlinear deterministic model involving two kernel functions was used to compute the direct runoff from the rainfall excess. The model performance was tested by predicting the direct runoff of an urban watershed for storms not used in the identification of the kernels.

PREFACE AND ACKNOWLEDGMENTS

This report covers the work performed between September 1970 and December 1973 under a project entitled "Effects of Urbanization on Hydrology of Watersheds". The research was supported as a matching fund project by the Office of Water Resources Research under grant OWRR-B-022-IND and agreement 14-31-0001-3801, by Purdue Research Foundation under grant XR-5997, and by Purdue University. This research extends the work performed under project OWRR-B-002-IND entitled "The Effect of Urbanization in Small Watersheds" between July 1966 and June 1969 which was summarized in Purdue University Water Resources Research Center Technical Report No. 9. (A Program in Urban Hydrology, Part II. An Evaluation of Rainfall-Runoff Models for Small Urbanized Watersheds and the Effect of Urbanization on Runoff by P. B. S. Sarma, J. W. Delleur and A. R. Rao, October 1969. Copies are available from NTIS under call number PB 189043.)

The work reported herein is a summary of the doctoral thesis entitled "The Effects of Urbanization on Hydrology of Watersheds with Special Reference to Rainfall Excess", submitted by A. Hossain to the Graduate Faculty at Purdue University in December 1973. This work was performed under the supervision of Professors J. W. Delleur and R. A. Rao. For further details and for the complete listing of the computer programs, the reader is referred to the thesis (3.7) which may be obtained from University Microfilms, Ann Arbor, Michigan.

The authors wish to express their appreciation to Dr. Dan Wiersma, Director of the Water Resources Research Center at Purdue University for his help in the administration of the project and for the loam of a neutron meter for soil moisture measurements, and to Dr. J. F. McLaughlin, Head of the School of Civil Engineering at Purdue University, for his assistance in the administration of the project.

The authors wish to express their gratitude to their sponsors for their support without which this work could not have been undertaken.

TABLE OF CONTENTS

LIST OF TABLES

LIST OF FLOW CHARTS

1. OBJECTIVES OF THE STUDY

There is an abundance of models of the rainfall-runoff transfer which have been published in the literature. They can be deterministic or stochastic, distributed or lumped, linear or nonlinear, time variant or time invariant. This report is concerned with lumped time invariant deterministic models. Most of these models, particularly those based on the linear systems analysis concept, use the rainfall excess as the input. The methods of computation of the rainfall excess are arbitrary as well as those for the separation of the base-flow from the total hydrograph. It appears that the weakest link in the rainfall-runoff transfer model is the proper estimation of the input, which is the rainfall excess. Consequently the main objective of the study is the development and testing of methods of estimation of the rainfall excess from the total rainfall.

The majority of the existing rainfall-runoff models used in urban watersheds are linear and deterministic. The application of nonlinear systems analysis has been concentrated on rural basins. Therefore, it appears desirable to explore the possible improvements that may be obtained through the use of nonlinear system models of the rainfall-runoff process.

The specific objectives of the present study are thus as follows:

1. To study different evaporation models and to evaluate their performance so that they may be used to estimate the evapotranspiration losses from an urban watershed.
2. To study, develop and improve models to estimate the rainfall excess in urban watersheds. This includes the study of the sensitivity of the parameters and the evaluation of the performance of the models.
3. To use the linear system analysis method in the determination of the response of watersheds at different stages of urbanization due to a single storm event.
4. To develop a regional model for the rainfall excess-direct runoff transfer by relating the model parameters to storm and physiographic characteristics of urban watersheds.
5. To test the model by using data from watersheds other than those used for the calibration of the model.
6. To explore the application of nonlinear system models to the determination of the response of urban watersheds due to a short sequence of storm events.

2. DATA USED FOR ANALYSIS

2.1 Meteorological Data

The meteorological data used for the present study were measured at the Purdue Agronomy Farm located approximately six miles northwest of Lafayette, Indiana, and were obtained from the office of the state climatologist. The following data were used in the present study.

a. Maximum and minimum daily air temperature, °F
b. Maximum and minimum daily relative humidity, percent
c. Average daily wind velocity 20 feet above ground, mph
d. Daily evaporation from a class A pan, in.
e. Daily direct solar radiation, langley
f. Daily soil temperature at 4 inch depth under sod cover, °F.

The radiation and wind data were read from charts which run from midnight to midnight. All other data were recorded at 8:00 a.m. EST.

Some data of daily air temperature, relative humidity, wind velocity, class A pan evaporation and direct solar radiation were missing. Direct solar radiation data for as long as a month were at times found missing. The missing daily solar radiation data for one day were estimated from data for part of the day whenever such data were available. The solar radiation data which were found missing for one or two days were estimated by linear interpolation. Whenever the data were missing for more than a few days the solar radiation data from Indianapolis Airport were substituted. A similar procedure was adopted for the missing average wind velocity data.

2.2 Hydrological Data

The hydrologic data were acquired for eleven watersheds. Some of the characteristics of these watersheds are given in Table 2.1.

Table 2.1 List of Watersheds

Watershed	Area $mi.^2$	Stream length mi.	Stream slope ft/mi	% Area impervious	Avg. Lag hr.	Description in ref. No.
1. Ross Ade Upper, W. Lafayette, IN	0.0455	0.6613	112.000	38.0	0.210	2.1
2. Waller Creek at 38th St., Austin, TX	2.3100	4.3700	47.000	27.0	1.440	2.2
3. Waller Creek at 23rd St., Austin, TX	4.1300	5.2300	47.000	37.0	1.580	2.2
4. Wilburger Creek, near Austin, TX	4.6100	3.1670	45.940	0.0	2.890	2.2
5. Lawrence Creek at Ft. Benjamin Harrison, IN	2.8600	1.7050	32.210	0.0	2.050	2.1, 2.3
6. Bear Creek near Trevlac, IN	7.0000	3.8640	39.070	0.0	5.440	
7. Bean Blossom Creek near Bean Blossom, IN	14.6000	6.4400	32.740	0.0	6.560	2.1, 2.3
8. Little Eagle Creek at Speedway, IN	19.3100	11.1000	23.230	2.1	9.340	2.1
9. Pleasant Run at Arlington, Ave., Indianapolis, IN	7.5800	3.8220	12.670	10.5	3.570	2.1
10. Pleasant Run at Brookville Rd., Indianapolis, IN	10.1000	5.6440	14.260	15.5	3.720	2.1
11. Boneyard Creek, Urbana, IL	4.70	2.840	9.504	44.1	1.152	2.6

The hydrologic data of the Ross Ade upper watershed were used for studying the rainfall excess models. The rainfall and runoff data recorded continuously on a 20 inch chart were digitized at one-minute intervals. The rainfall and direct runoff values were then computed at 15 minute intervals for the period of April through December 1970 and 1971. The storm of April 18, 1970, for which the rainfall and runoff data were available at 15 minute intervals, was used for the parameter sensitivity analyses of the several models.

The method of estimating the direct runoff and the rainfall excess data used for the linear and nonlinear system analyses are given in Chapter III of the reference 2.1.

Table 2.2 Data Used for Ross Ade Upper Watershed

Rainfall and Runoff Characteristics

	1970	1971	4/18/73
No. of storms in sequence	66	63	1
Measured direct runoff, in.	4.3695	5.0749	1.164
Volume of rainfall, in.	29.90	27.16	4.617

Physiographic Characteristics

	Pervious	Impervious
Area, acres	18.170	10.990
Static storage, in.	0.25	0.0625
Initial depression storage (for sensitivity analysis), in.	0.25	
Impervious area draining directly to storm sewer, acres		4.180
Impervious area draining over pervious area, acres		6.810

2.3 Soil Data

The locations of the principal soils in the Ross Ade upper watershed are shown in Figure 2.1 which was taken from reference (2.4) and enlarged. The types of soils in the watershed are given in Table 2.3.

Table 2.3 Soils Types in Ross Ade Upper Watershed

Symbol	Soil Type	Depth of top layer, in. A	Area, % B	Effective Depth of storage, in. A x B
Ec	Eel silt loam 0-3% slope	6.0 to 8.0	16	1.12 in
Ms	Miami silt loam 3-8% slope	3.0 to 8.0	13	0.71
Mr	Miami silt loam 3-8% slope	7.0	12	0.84
Ch	Crosby silt loam 0-3% slope	7.0	5	0.35
Mw	Miami silt loam 12-25% slope	3.0 to 8.0	5	0.27
Mv	Miami silt loam 12-25% slope	8.0 to 12.0	49	4.90
		Avg. Depth		8.19 in

The soil moisture was measured once a week at Ross Ade upper watershed near the Hydrologic Station at 6, 12, 18, 24, 30 and 36 inch depths using soil moisture cells placed at these depths. The cells were manufactured by Soil Test, Inc. The soil moistures at the same depths were also measured by means of a Troxler Neutron Probe. Attempts were made to measure the hydraulic conductivity of soils from the Ross Ade upper watershed using an apparatus and a method very similar to those described by Klute (2.5). A suction of up to 27 inches of mercury was applied to the sample and the pressure on the water was about 5 inches of mercury, for about seven days. As there was no flow through the sample and as only the top layer of the sample was wet it was concluded that the hydraulic conductivity of the soil samples from this watershed could not be measured by this method. Consequently, three types of soils were selected, the characteristics of which were close to the average soil properties of the watershed: the Guelph loam, the Ida silt loam and the Yolo light clay. Figure 2.2 shows plots of the hydraulic conductivity vs. the soil moisture content by volume along with the slopes of the curves, ρ', for these soils. Other properties of the Guelph loam and Yolo light clay are listed in table 2.4.

Table 2.4 Soil Characteristics and Other Constants for Infiltration Models

Soil Characteristics	Guelph Loam	Yolo Light Clay
Porosity, vol. $vol.^{-1}$	0.523	0.499
Saturated hydraulic conductivity, in. $hr.^{-1}$	0.5202	0.01743
Moisture Diffusivity, $in^2\ hr^{-1}$	6.665	0.279
Effective soil storage, in.	3.50	
Area under $S\text{-}K_r$ curve, S_{av}, in.	12.55	8.80
Other Constants		
Basal area of plant stems, a, percent	0.90	
Constant rate of infiltration after prolonged wetting, f_c, in $hr.^{-1}$	0.15	
Exponent n' in Holtan's formula	1.40	
Free water, G, in.	S/2.74	
Available moisture capacity, AWC, in.	S-G	
Soil storage capacity, S, in.	3.5	
Ratio AWC/G	1.74	

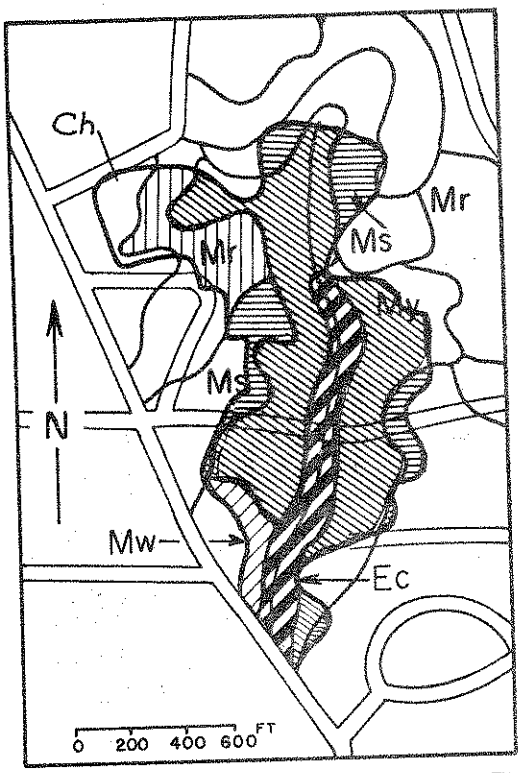

FIGURE 2.1 SOIL MAP OF ROSS ADE UPPER WATERSHED

DATA ARE TAKEN FROM REFERENCE NO 174

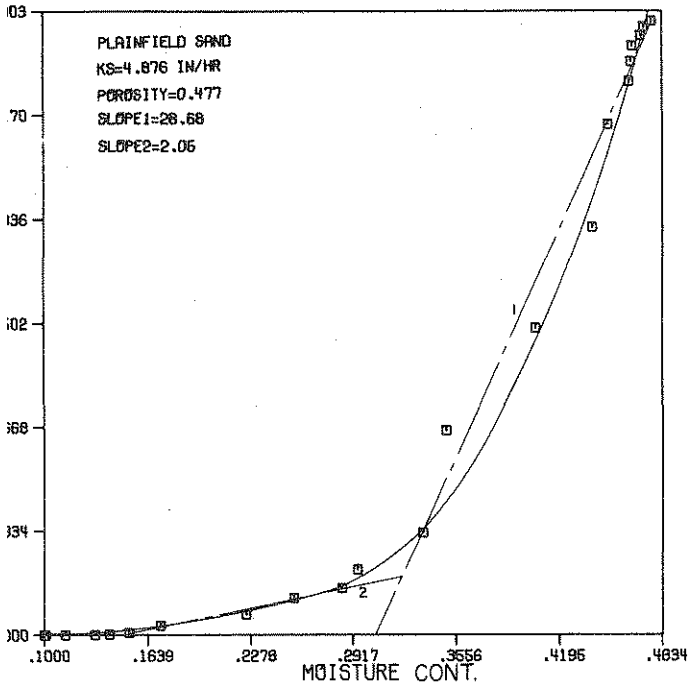

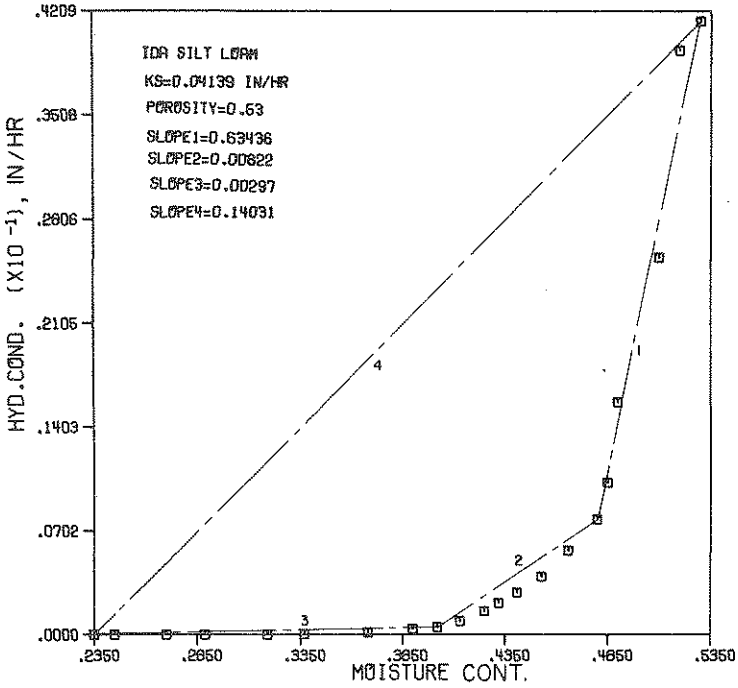

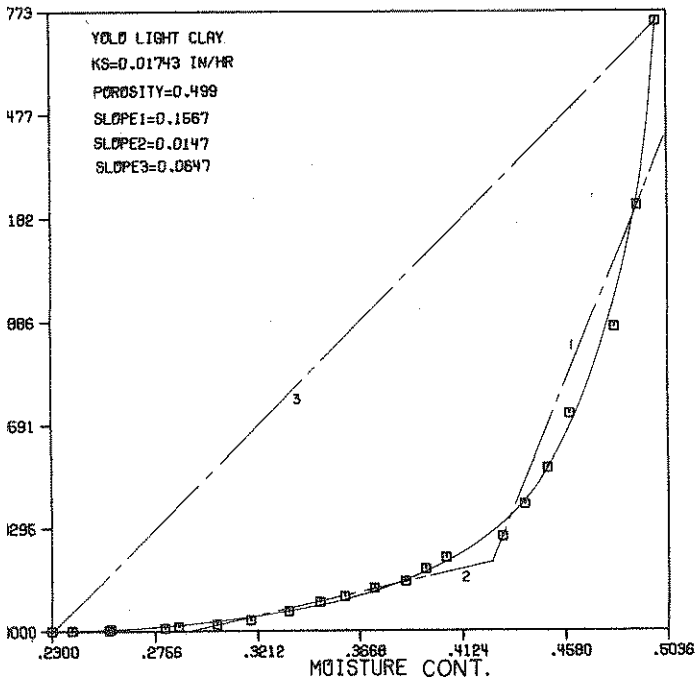

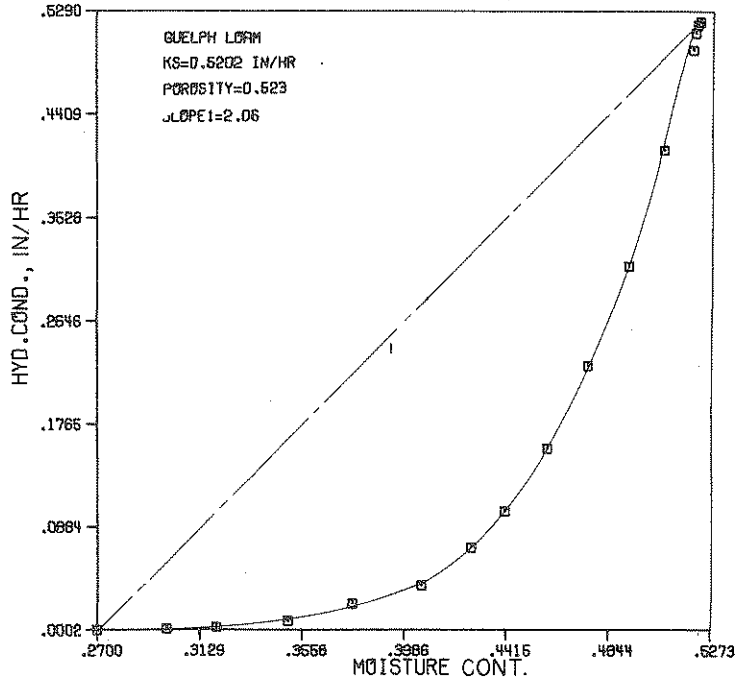

FIGURE 2.2 VARIATION OF HYDRAULIC CONDUCTIVITY WITH SOIL MOISTURE CONTENT

3. ESTIMATION OF EVAPORATION AND EVAPOTRANSPIRATION LOSSES

3.1 Introduction

The evaporation and evapotranspiration losses affect the runoff from a watershed by controlling the direct loss of water into the atmosphere and more importantly by affecting the infiltration process. Therefore, an estimate of evapotranspiration losses is important in estimating not only the evaporation but also the infiltration losses. Several models have been proposed to estimate the evapotranspiration rates from watersheds, although an analysis of their comparative performance is not available. In the present chapter, the prediction performance of the modified Penman equation (3.1) as developed by van Bavel (3.2, 3.3) and Kohler et al. (3.4) are compared with the objective of selecting the better of the two models. The importance of the role played by the relative humidity in the evapotranspiration estimation is analyzed by considering the Blaney-Criddle (3.5) and Blaney-Morin (3.6) evaporation estimators, although it is recognized that the Blaney-Criddle and Blaney-Morin estimators were not originally developed to estimate evapotranspiration losses on a daily basis.

3.2 Estimation of Evaporation by Using the Modified Penman Equation

3.2.1 van Bavel's Approach

The modified Penman's equation (3.1, 3.2) was used by van Bavel to estimate evaporation from different surfaces. The approach taken in the present study follows van Bavel's. The modified Penman equation is given in eq. 3.1.

$$E = \frac{1}{\rho_e L} \frac{(\Delta/\gamma)\ (\bar{Q}/A_s) + LB(e_{s2} - e_2)}{(\Delta/\gamma + 1)} \tag{3.1}$$

The following variables are used in eq. 3.1: E(cm./min.): evaporation. Δ/γ (Dimensionless): parameter dependent on the air temperature at height Z_2. $\bar{Q}$ (cal. min.$^{-1}$): sum of all energy inputs at the surface exclusive of the sensible heat and of the latent heat of vaporation. A_s (cm^2): water surface area. L (cal. gm.$^{-1}$): latent heat of vaporization. B (cm.$^{-1}$ min.): the turbulent transfer coefficient and is given by eq. 3.2. e_{s_2}(mb): saturation vapor pressure at temperature T_2(°C) at elevation Z_2(cm). e_2(mb): vapor pressure at temperature T_2 and elevation Z_2. ρ_e (gm. cm.$^{-3}$): density of evaporated water. Δ(mb. °C^{-1}) = $(e_s - e_{s_2})/(T_s - T_2)$ where e_s(mb) is the saturation vapor pressure at the surface temperature T_s(°C) and e_{s_2}(mb) is the saturation vapor pressure at elevation 2, a short distance above the surface where the temperature is T_2(°C). $\gamma = C_B p$ (mb °C^{-1}) where p (mb) is the surface atmospheric pressure intensity and C_B (°C^{-1}) is the Bowen Constant. $C_B = (C_p K_h)/(0.622\ L\ K_w)$ where C_p (cal gm^{-1} °C^{-1}) is the specific heat of the water vapor, K_h (cm^2 min^{-1}) is the thermal diffusivity, and K_w (m^2 min.$^{-1}$) is the vapor diffusivity.

The parameter B in eq. 3.1 is a turbulent transfer coefficient (cm^{-1} min) and is given by eq. 3.2

$$B = K \frac{\bar{U}_2}{\ln^2(Z_2/Z_1)} \tag{3.2}$$

In eq. 3.2, $K = 0.622\ K_w \rho/(K_m p\ C_1^2)$, where K_m (cm^2 sec^{-1}) is the kinematic eddy viscosity, $\bar{U}_2$ (cm min.$^{-1}$) is the wind speed at height Z_2, and Z_1 (cm) is the surface roughness parameter.

The data required for computation are summarized in table 3.1 along with the values of the physical constants used in the present study. Computational details involved in using van Bavel's approach may be found in ref. 3.7, and a discussion of the method is found in ref. 3.2.

Plots of the daily Class A pan evaporation measured at the Purdue Agronomy farm and the evaporation estimated by using eqs. 3.1 and 3.2 are shown in fig. 3.1. Most of the estimates are close to the measured values except for very few days when they are substantially different. These discrepencies are caused by (a) substitution of solar radiation values observed at the Weather Bureau station in Indianapolis for the Agronomy farm data to make up the missing data at the Agronomy farm, (b) interpolating the observed values to estimate missing data, and (c) possible errors in the measurement of evaporation.

Some of the statistics of the measured and estimated daily evaporation values are given in table 3.2. The variance of the estimated evaporation is larger than that of the measured evaporation and, in general,

the statistical parameters indicate that the estimated values are very close to the measured ones.

One of the parameters which must be empirically estimated in eq. 3.2 and hence in eq. 3.1, is the roughness parameter Z_1. The sensitivity of the potential evapotranspiration estimation to the changes in Z_1 was analyzed by varying the Z_1 values for the data of the years 1967-71. The different Z_1 values used were taken from ref. 3.2. The results of the analysis are shown in fig. 3.2, in which the ratio of the potential evapotranspiration (PET) to the measured (class A pan) evaporation is plotted against the natural logarithms of Z_1 where Z_1 is in cm. The ratio of PET to the measured evaporation is not sensitive to variations in Z_1 if the Z_1 values are small. When Z_1 is larger than about 15 cm, which corresponds to small bushes (1.3m = 4.3 ft. tall), the estimated PET will be much larger than the measured values. Thus for water surfaces, grass, most crops and bushes, the calculated evapotranspiration is insensitive to the choice of Z_1. However, the calculated evapotranspiration will be very sensitive to Z_1 for the values attributed to trees and forests (50 cm < Z_1 < 300 cm). Some of these results are summarized below.

Table 3.4 Percentage Error in Average PET with Change in Z_1 Values and Ratio of Average of Calculated PET to Average Pan Evaporation at the Agronomy Farm (West Lafayette, Indiana) for the Years Indicated.

Z_i cm	Z_j cm	% error = $\frac{\overline{PET\ Z_i} - \overline{PET\ Z_j}}{\overline{PET\ Z_i}} \times 100$			
		1967	1968	1969	1970
0.001	0.005	0.66	0.82	0.66	0.71
0.001	0.02	1.51	1.74	1.52	1.73
Z_1 (cm)		$\overline{PET\ Z_1}/\overline{MET}$			
0.001		1.060	0.977	1.056	0.985
300		9.591	10.173	9.809	9.847

$\overline{PET\ Z_i}$ = mean of computed daily potential evapotranspirations with Z_1 in eq. 3.2 equal to Z_i for the year shown (number of days of observation listed in Table 3.2)

$\overline{MET}$ = mean of measured class A pan evaporations for year shown.

3.2.2 Kohler's Approach

A graphical correlation between the meteorological variables and the daily water surface evaporation was obtained by Kohler (3.4). This graphical correlation is based on the functional form of Penman's equation (3.1). An analytical form of this correlation is given by Lamoreux (3.8) as eq. 3.3.

$$E = \frac{\mathrm{Exp}[(T_a - 212.0)\ (0.1024 - 0.010661\ \ln R)] - 0.0001 + 0.0105\ \Delta p^{0.88}(0.37 + 0.0041\ \bar{U})]}{0.015 + (T_a + 398.36)^{-2}\ (6.8554)\ 10^{10}\ \mathrm{Exp}[-7482.6/(T_a + 398.36)]} \qquad (3.3)$$

$$\Delta p = 6.41326 \times 10^6 \left[\mathrm{Exp}\left(\frac{-7482.6}{T_a + 398.36}\right) - \mathrm{Exp}\left(\frac{-7482.6}{T_d + 398.36}\right)\right] \qquad (3.4)$$

In eqs. 3.3 and 3.4, R (langley) is the net solar radiation, T_a (°F) is the mean daily air temperature, T_d (°F) is the mean daily dew-point temperature, $\bar{U}$ (miles day^{-1}) is the wind velocity at 2 ft. above the surface and E (inch day^{-1}) is the evaporation from free water surface.

Equations 3.3 and 3.4 give estimates of the evaporation from a free water surface of extended proportions, without advected heat transfer and assuming no change in the heat storage in the underlying water body. The data required for computing the evaporation from eq. 3.3, which are summarized in table 3.1, are much less than the data required to use the van Bavel's method.

The measured daily class A pan evaporation and the values computed by using eq. 3.3 are shown in fig.

3.3. Some of the statistics pertaining to the measured and the computed evaporation values are given in table 3.2. Kohler's method, which is a functional form of Penman's equation, also gives good evaporation predictions, as seen by the results given in table 3.2. The reasons for some of the large discrepancies between the computed and the measured values in Kohler's approach were the same which gave large discrepancies in van Bavel's method. These have been discussed in the previous section.

3.3 The Significance of Relative Humidity in Evapotranspiration Estimation

A numerical experiment was conducted to determine the significance of the relative humidity in the evapotranspiration computations. The Blaney-Criddle (3.5) and the Blaney-Morin (3.6) evapotranspiration models were used for this purpose. The original objective in the development of these formulas, however, did not include the estimation of evapotranspiration on a daily basis. However, they were investigated in the present study to test the effect of relative humidity and to determine their capabilities to estimate the daily evapotranspiration.

3.3.1 Blaney-Criddle Model

The original Blaney-Criddle evapotranspiration model is given in eq. 3.5.

$$U = KF = \Sigma K_i F_i = \Sigma(K_i t_i p_i/100) \tag{3.5}$$

In eq. 3.5, U (in) is the estimated evapotranspiration for the season, K is an empirical seasonal coefficient, F is the sum of the monthly evapotranspiration factors defined in terms of F_i, $F_i = t_i p_i/100$, where t_i (°C) is the mean monthly temperature, p_i is the mean monthly percent of annual daytime hours, and K_i is an empirical monthly coefficient.

In the present study, eq. 3.5 has been put in the form of eq. 3.6 to compute the daily evaporation from a water surface:

$$E = K_b' \cdot A \cdot T \tag{3.6}$$

In eq. 3.6, E (in.) is the estimated daily evaporation, K_b' is an empirical constant, T (°F) is the mean daily temperature, A is the monthly percentage of daytime hours of the year for the latitude of the place divided by the number of days in the month. The empirical constant K_b' is assumed to be unity for open water surface.

The measured evaporation and the evaporation computed by eq. 3.6 are shown in fig. 3.4. Some of the statistics of the measured and the computed evaporation values are given in table 3.2. From the results presented in fig. 3.4 and table 3.2, it is clear that the Blaney-Criddle model can give evaporation estimates which can be taken only as average values and that the model is not sensitive to the day to day variations.

3.3.2 Blaney-Morin Model

The Blaney-Morin model, given in eq. 3.7, is different from eq. 3.6 only in the relative humidity term R'.

$$E = K_b\, AT(114 - R') \tag{3.7}$$

In eq. 3.7, E (in) is the estimated daily evaporation, K_b, is the empirical consumptive use coefficient, assumed to be 0.0164 (ref. 3.6), A is the monthly percentage of daytime hours of the year for the place divided by the number of days in the month, T (°F) is the daily mean temperature (°F), R' is the daily mean relative humidity (%). The data required to use the Blaney-Morin model is summarized in table 3.1.

The pan evaporation computed by using eq. 3.7 and the measured values are shown in fig. 3.1 and some statistics relevant to evaporation estimation are given in table 3.2. The outstanding feature, between the results obtained from using Blaney-Criddle (fig. 3.4) and Blaney-Morin (fig. 3.1) models is that the Blaney-Morin model predicts the daily evaporation much better than the Blaney-Criddle model. Consequently, it can be concluded that the relative humidity term is very significant in estimating the evaporation from humid areas. Furthermore, the differences between the measured and computed evaporation values (table 3.2) for the Blaney-Morin model are of the same order, or are less than the values obtained by Kohler's model. In fact,

the performance of the Blaney-Morin model is comparable to that of Kohler's model.

The coefficients K_b' and K_b in eq. 3.6 and 3.7 must be estimated empirically. Blaney and Morin have suggested a few values for K_b. If the Blaney-Morin model is to be used at locations where the K_b values are unknown, they may be estimated by using eq. 3.7. The value of K_b assumed in the present study is very approximate and it appears that the predictions can be improved by using better estimates of K_b values. An investigation of the variation of the mean error in evaporation prediction with a variation in K_b indicated that the mean error reached minimum for a value of K_b equal to 0.015 (3.7).

3.4 Evaluation of Evaporation Models and Discussion

The following statistical measures, which are also shown in table 3.3, were used to evaluate the relative performances of the various evaporation models: (a) The correlation coefficient of the measured and computed evaporation, (b) the special correlation coefficient, (c) sum of the squares of errors, (d) the sum of errors and (e) the variance of the computed and measured evaporation. The model which gives the most favorable values of the statistics cannot necessarily be selected as the best model because some of the parameters (such as K_b in the Blaney-Morin model) are selected by trial and error. In spite of these subjective considerations, the statistics such as those indicated in table 3.3 give a measure of the performances of the different models.

The overall correlation coefficients between the measured and the computed evaporation values are higher for the van Bavel and the Kohler methods than for the Blaney-Criddle and the Blaney-Morin models. According to the results in tables 3.2 and 3.3, the evaporation estimates obtained by Kohler's method are sometimes better than those obtained by van Bavel's method. However, Kohler's method can be used only to estimate evaporation from open water surfaces. van Bavel's method gives better evaporation estimates than all the other models, in general, and it has the advantage that it can be used to compute the potential evaporation from any type of surface. As one of the objectives of the present study is to arrive at better methods of the computation of losses from urban areas, the van Bavel model is selected as the best model.

However, a considerable amount of data is required to use the van Bavel model. Where such data are not available, especially where the climate is humid, either Kohler's model or the Blaney-Morin model may be used. The Blaney-Morin model has the advantage that it is one of the simplest models and, therefore, it can be used where net solar radiation data are not available. It must be noted, however, that the parameter K_b in the Blaney-Morin model must be carefully selected.

van Bavel's Model

a. The mean air temperature, T_2, °C
b. The relative humidity at air temperature T_2
c. The surface atmospheric pressure intensity, mb
d. The net radiant energy, ly/min
e. The data measurement height, Z_2, cm
f. The temporal mean wind velocity at Z_2, cm min^{-1}
g. Values of temperature and corresponding values of Δ/γ

$$\rho_l = 1.0 \times .0^{-3} \text{ gm cm}^{-3}$$
$$K_w/K_m = 0.98$$
$$L = 583 \text{ cal gm}^{-1}$$
$$A_s = 1.0$$

h. Roughness parameter Z_1, cm.

Kohler's Model

a. The net solar radiation, ly
b. The mean daily air temperature, °F
c. The mean daily dew-point temperature, °F
d. The wind movement at 2 ft., miles day^{-1}.

Blaney-Criddle Model

a. Empirical consumptive use coefficient
b. The mean daily temperature, °F
c. Monthly percentage of daytime hours of the year for the place/number of days in the month.

Blaney-Morin Model

a. The mean daily temperature, °F
b. The mean daily relative humidity, percent
c. Empirical consumptive use coefficient
d. Monthly percentage of daytime hours of the year for the place/number of days in the month.

Table 3.1 Data Requirements for Evaporation Models

Table 3.2 Statistics of the Measured and Calculated Daily Evaporations

	van Bavel Method				Kohler Method				Blaney-Criddle Model				Blaney-Morin (K_b=0.0164)			
Year	1967	1968	1969	1970	1967	1968	1969	1970	1967	1968	1969	1970	1967	1968	1969	1970
No. of days (N)	214	214	213	184	214	214	213	184	214	214	213	184	214	214	213	184
$\Sigma E_c(i)$ (in)	43.153	36.179	37.461	34.657	39.224	31.060	28.260	30.934	40.153	41.312	41.130	37.461	45.376	39.225	39.339	37.168
$\Sigma E_M(i)$ (in)	40.300	36.580	35.350	34.770	40.300	36.580	35.350	34.770	40.300	36.580	35.350	34.770	40.300	36.580	35.350	34.770
$\Sigma e(i)$	-2.853	0.401	-2.111	0.113	1.076	5.520	7.090	3.836	0.147	- 4.732	- 5.780	- 2.690	- 5.076	- 2.645	- 3.989	- 2.398
$\hat{E}[E_c(i)]$	0.202	0.169	0.176	0.188	0.183	0.145	0.133	0.168	0.188	0.193	0.193	0.204	0.212	0.183	0.185	0.202
$\hat{E}[E_M(i)]$	0.188	0.171	0.166	0.189	0.188	0.171	0.166	0.189	0.188	0.171	0.166	0.189	0.188	0.171	0.166	0.189
$\hat{E}[e(i)]$	-0.013	0.002	-0.010	0.001	0.005	0.026	0.033	0.021	0.001	- 0.022	- 0.027	- 0.015	- 0.024	- 0.012	- 0.019	- 0.013
$\hat{E}[\lvert e(i)\rvert]$	0.048	0.048	0.050	0.046	0.045	0.048	0.047	0.042	0.051	0.057	0.051	0.056	0.047	0.051	0.046	0.046
$\Sigma e^2(i)$	0.860	0.809	0.882	0.665	0.750	0.848	0.860	0.581	0.970	1.122	0.914	0.956	0.791	0.841	0.783	0.674
$\hat{E}[e^2(i)]$ x 10	0.040	0.038	0.041	0.036	0.035	0.040	0.040	0.032	0.045	0.052	0.043	0.052	0.037	0.039	0.037	0.037
$\sqrt{\hat{E}[e^2(i)]}$ x 10	0.043	0.042	0.044	0.044	0.040	0.043	0.044	0.041	0.046	0.050	0.045	0.053	0.042	0.043	0.042	0.045
$Var[E_c(i)]$ x 10	0.080	0.071	0.082	0.087	0.059	0.055	0.044	0.072	0.020	0.021	0.020	0.018	0.050	0.044	0.045	0.055
$Var[E_M(i)]$ x 10	0.074	0.064	0.063	0.077	0.074	0.064	0.063	0.077	0.074	0.064	0.063	0.077	0.074	0.064	0.063	0.077
Var[e(i)] x 10	0.039	0.038	0.041	0.036	0.035	0.033	0.029	0.028	0.046	0.048	0.036	0.050	0.031	0.038	0.033	0.035
Corr. Coeff.	0.750	0.720	0.727	0.781	0.741	0.723	0.737	0.816	0.628	0.505	0.665	0.608	0.760	0.658	0.700	0.745
Sp. Corr. Coeff.	0.952	0.946	0.937	0.957	0.958	0.943	0.938	0.963	0.946	0.923	0.934	0.938	0.956	0.943	0.944	0.957
Integral Square Error	2.301	2.459	2.658	2.363	2.149	2.518	2.623	2.208	2.444	2.507	2.705	2.812	2.207	2.507	2.504	2.362
$\frac{\Sigma E_c(i) - \Sigma E_M(i)}{\Sigma E_M(i)}$ x 100	7.07	-1.10	5.97	-0.32	- 2.67	-15.09	-20.06	-11.03	- 0.36	12.94	16.35	7.74	12.60	7.23	11.28	6.90
$\frac{\Sigma E_c(i)}{\Sigma E_M(i)}$	1.070	0.989	1.060	0.997	0.973	0.849	0.799	0.890	0.996	1.129	1.164	1.077	1.126	1.072	1.113	1.069
$\left\{\frac{Var[E_c(i)]-Var[E_M(i)]}{Var[E_M(i)]}\right\}$ x 100	8.11	10.94	30.16	12.99	-20.27	-14.06	-30.16	- 6.49	-72.97	-67.19	-68.25	-75.62	-32.43	-31.25	-28.57	-28.57

$E_c(i)$ = Computed evaporation (i = 1, ..., N); $E_M(i)$ = Measured evaporation (i = 1, ..., N); $\hat{E}[\cdot]$ = Mean; Var $[\cdot]$ = Variance; e(i) = error = $E_M(i) - E_c(i)$

$$\text{Integral Square Error} = \frac{\left[\sum_{i=1}^{N} (E_M(i) - E_c(i))^2\right]^{1/2}}{\sum_{i=1}^{N} E_M(i)} \times 100 \; ; \; \text{Special Correlation Coefficient} = \left[\frac{\left[2 \sum_{i=1}^{N} E_M(i)\, E_c(i) - \sum_{i=1}^{N} (E_c(i))^2\right]}{\sum_{i=1}^{N} (E_M(i))^2}\right]^{1/2}$$

Table 3.3 Statistics for the Evaluation of Evaporation Models

Model	Correl. Coeff.	Sp. Correl. Coeff.	Sum of Sq. of Error	Sum of Error	Per. of Error	Mean of Abs. Error	Var. of Mes. Ev.	Var. of Comp. Ev.
$E_{van\ Bavel}$								
1967	.7495	.9519	.8599	-2.853	- 7.07	.0484	.0074	.0080
1968	.7196	.9454	.8088	.401	1.09	.0480	.0064	.0071
1969	.7268	.9367	.8824	-2.111	- 5.97	.0497	.0063	.0082
1970	.7814	.9571	.6647	.113	0.32	.0456	.0077	.0087
E_{Kohler}								
1967	.7413	.9582	.7501	1.076	2.66	0.449	.0074	.0059
1968	.7233	.9426	.8484	5.520	15.09	.0480	.0064	.0055
1969	.7370	.9384	.8598	7.090	20.05	.0474	.0063	.0044
1970	.8156	.9626	.5808	3.836	11.03	.0418	.0077	.0072
$E_{Blaney-Morin}$								
1967	.7601	.9559	.7909	-5.076	-21.59	.0473	.0074	.0050
1968	.6584	.9431	.8410	-2.645	- 7.23	.0508	.0064	.0044
1969	.6996	.9441	.7833	-3.989	-11.28	.0462	.0063	.0045
1970	.7448	.9568	.6744	-2.398	- 6.89	.0462	.0077	.0055
$E_{Blaney-Criddle}$								
1967	.6275	.9456	.9697	.147	0.36	.0507	.0074	.0020
1968	.5053	.9234	1.1222	-4.732	-12.93	.0566	.0064	.0021
1969	.6652	.9344	.9141	-5.780	-16.35	.0510	.0063	.0020
1970	.6075	.9382	.9558	-2.690	- 7.73	.0556	.0077	.0018

Note:

$E_{van\ Bavel}$ Daily evaporation computed by van Bavel method, inch.

E_{Kohler} Daily evaporation computed by Kohler method, inch.

$E_{Blaney-Morin}$ Daily evaporation computed by Blaney-Morin model, inch.

$E_{Blaney-Criddle}$ Daily evaporation computed by Blaney-Criddle model, inch.

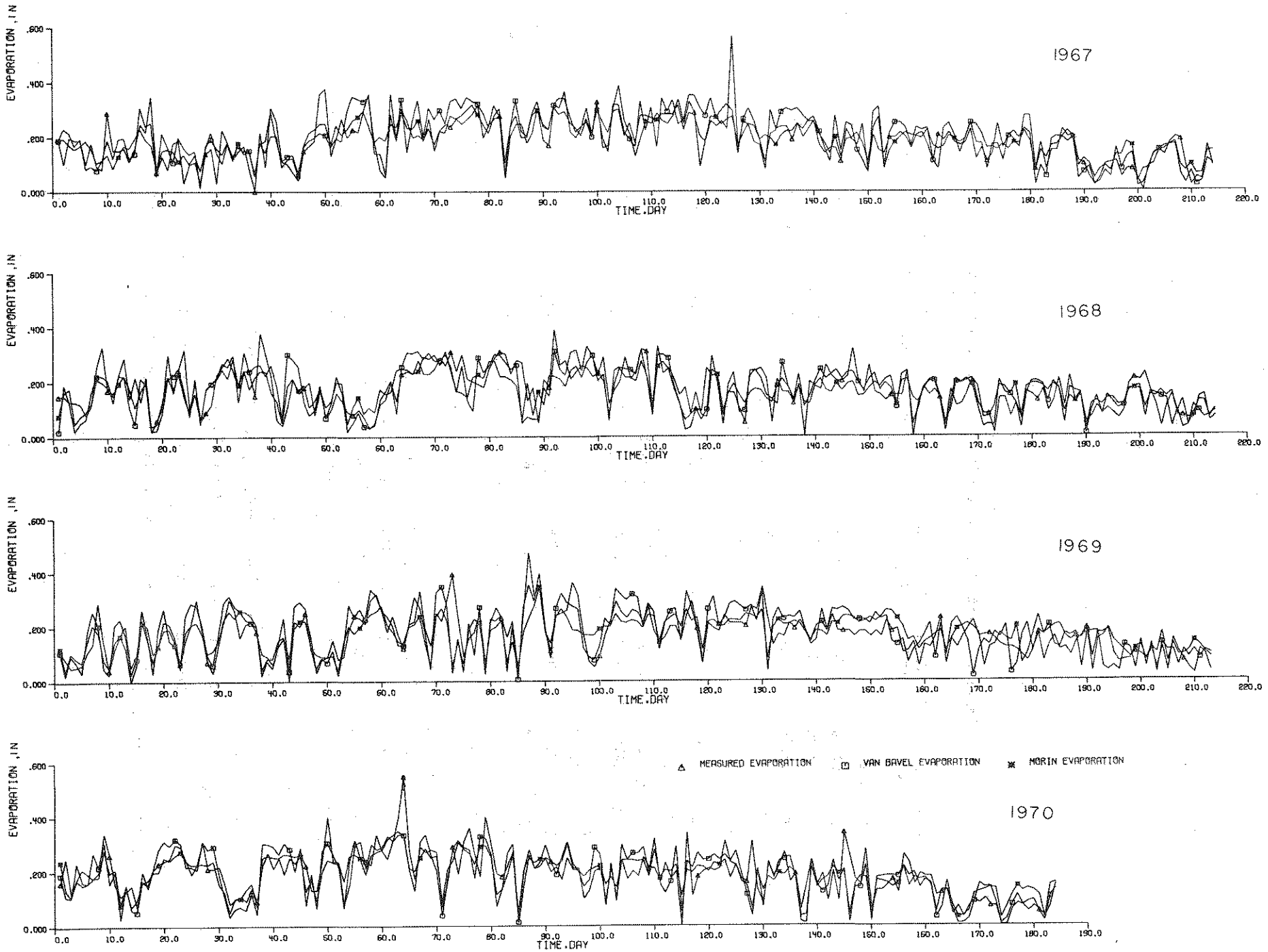
EVAPORATION ,IN
.600
.400
.200
0.000
0.0
10.0
20.0
30.0
40.0
50.0
60.0
70.0
80.0
90.0
100.0
110.0
120.0
130.0
140.0
150.0
160.0
170.0
180.0
190.0
200.0
210.0
220.0
TIME.DAY
1967
1968
1969
1970
MEASURED EVAPORATION
VAN BAVEL EVAPORATION
MORIN EVAPORATION

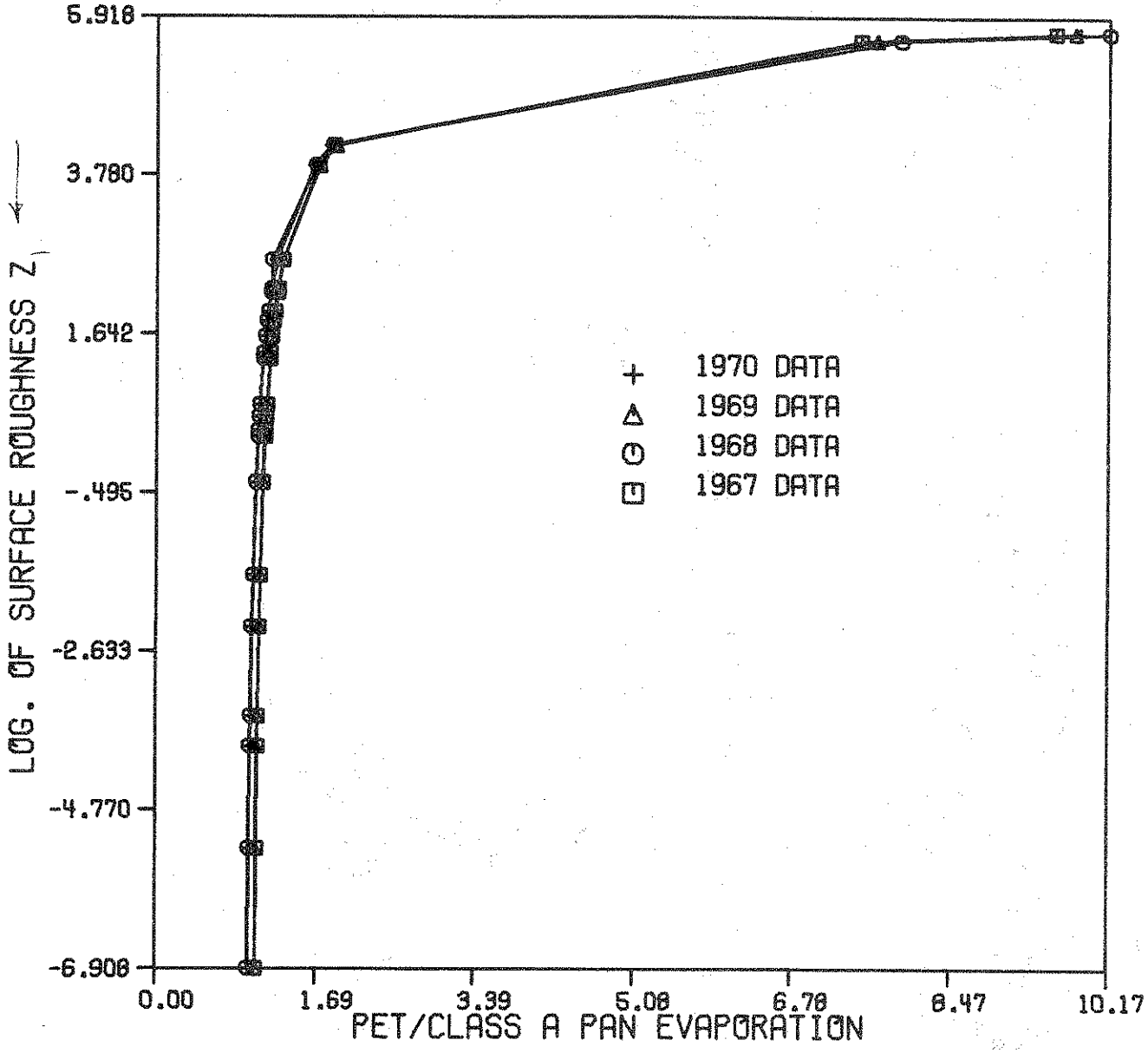

FIGURE 3.2 VARIATION OF THE RATIO OF CLASS A PAN EVAPORATION TO VAN BAVEL EVAPORATION WITH Z

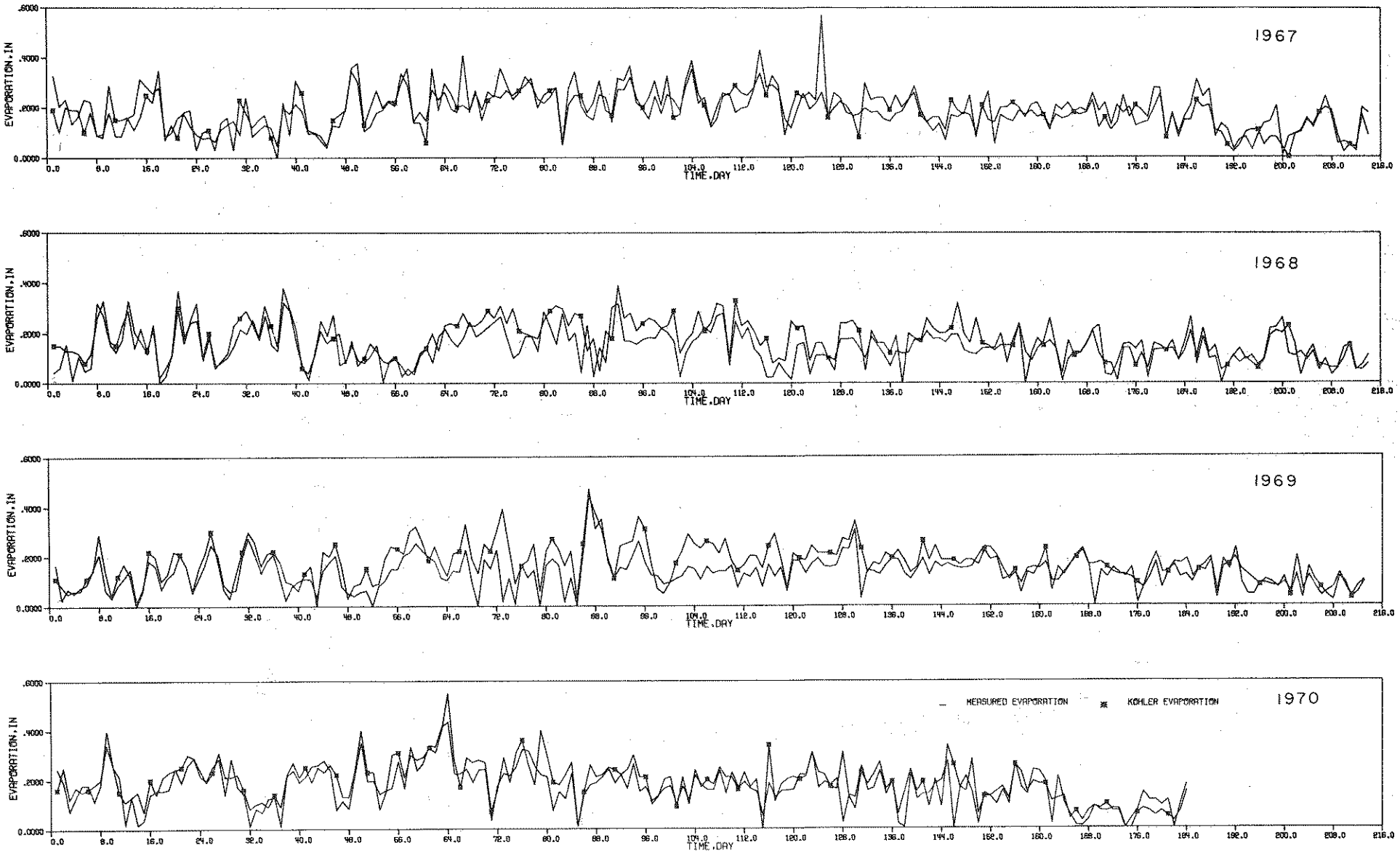

FIGURE 3.3 PLOT OF THE DAILY CLASS A PAN EVAPORATION AND OF THE DAILY KOHLER EVAPORATION.

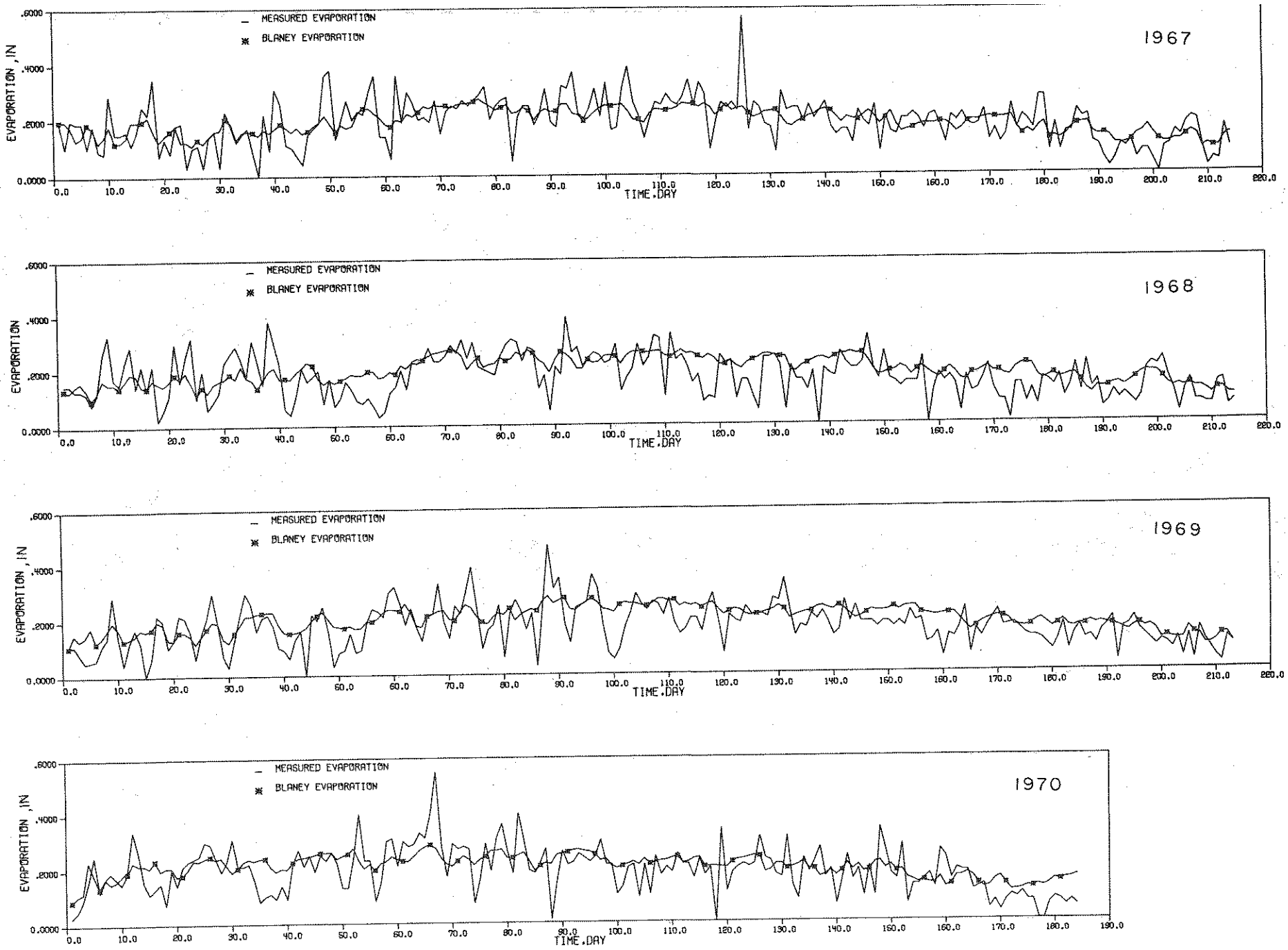

FIGURE 3.4 PLOT OF THE DAILY CLASS A PAN EVAPORATION AND OF THE DAILY BLANEY CRIDDLE EVAPORATION.

4. DETERMINATION OF THE RAINFALL EXCESS

The estimation of the rainfall excess depends on the determination of the interception loss, of the infiltration loss at the surface, of the loss in the static storage, of the evaporation and transpiration losses and of other losses from the watershed. In an urban watershed the interception loss may be very small compared to the other losses and thus it may be neglected. For estimating the infiltration loss, both the gain of soil moisture due to the rain and the losses of moisture from the soil must be taken into account. As the rate of rainfall exceeds the infiltration rate at the surface, the excess water begins to accumulate in the static surface storage. When the static storage capacity is exceeded the surface runoff begins. In a sewered area the water infiltrated through the soil surface cannot reappear as runoff. Consequently, the total direct runoff measured at a gaging station in the sewer may be taken to be equal to the total rainfall excess generated during the corresponding storm.

In this chapter the theoretical equations governing the infiltration phenomena are discussed first. The constant diffusivity form of the unsteady flow equation for the flow in porous media is solved by making use of the linear systems analysis approach. An impulsive response function is obtained for the soil moisture change. This is followed by the investigation of five models for estimating the rainfall excess. The first of these models is based on the theoretical infiltration equations discussed in the first section, the second is semi-empirical, the third is completely empirical and the last two are conceptual in nature. All the models were modified for their application to urban watersheds.

4.1 Theory

4.1.1 Governing Equations

The equation o continuity for the soilwater system can be expressed as

$$\frac{\partial(\rho q_x)}{\partial x} + \frac{\partial(\rho q_y)}{\partial y} + \frac{\partial(\rho q_z)}{\partial z} = - \frac{\partial(\rho\theta)}{\partial t} \tag{4.1}$$

where q_i = flux of water transmitted in the i direction, i = x, y or z, the z-coordinate being positive upward; ρ = density of water; θ = volumetric water content; t = time.

The movement of water in an unsaturated soil can be expressed by the Buckingham-Darcy equation:

$$q_x = -K_x(\theta) \frac{\partial h'}{\partial x}; \qquad q_y = -K_y(\theta) \frac{\partial h'}{\partial y}; \qquad q_z = -K_z(\theta) \frac{\partial h'}{\partial z} \tag{4.2}$$

where $K_i(\theta)$ = hydraulic conductivity in the i-direction expressed as a function of soil water content, i = x, y or z; $h' = z - h_s$ = hydraulic head; where z = elevation head and h_s = suction head.

Assuming that the medium is isotropic, then $K_x(\theta) = K_y(\theta) = K_z(\theta) = K(\theta)$. Expressing h' as a sum of the elevation head, z, and the suction head, h_s, and as $h_s = h_s(\theta)$, then $\theta = \theta(h_s)$, $K(\theta) = K[\theta(h_s)] = K(h_s)$. Assuming ρ = constant, equations 4.1 and 4.2 can be combined to form the h_s-based Richards' equation in the following form:

$$\frac{\partial}{\partial x}\left[K(h_s) \frac{\partial h_s}{\partial x}\right] + \frac{\partial}{\partial y}\left[K(h_s) \frac{\partial h_s}{\partial y}\right] + \frac{\partial}{\partial z}\left[K(h_s) \frac{\partial h_s}{\partial z}\right] - \frac{\partial K(h_s)}{\partial z} = - \frac{\partial\theta}{\partial t} \tag{4.3}$$

The above equation can also be written in terms of the water content, or θ-based equation as

$$\frac{\partial}{\partial x}\left[D(\theta) \frac{\partial\theta}{\partial x}\right] + \frac{\partial}{\partial y}\left[D(\theta) \frac{\partial\theta}{\partial y}\right] + \frac{\partial}{\partial z}\left[D(\theta) \frac{\partial\theta}{\partial z}\right] + \frac{\partial K}{\partial z} = \frac{\partial\theta}{\partial t} \tag{4.4}$$

where $D(\theta) = -K(\theta) \cdot \left(\frac{\partial h_s}{\partial x}\right)$ is the moisture diffusivity as a function of the water content.

Considering that the infiltration is the flow in the z-direction and using Z = -z, the one-dimensional Richards' equation can be written as

$$\frac{\partial}{\partial x}\left[D(\theta) \frac{\partial\theta}{\partial Z}\right] - \frac{\partial K}{\partial Z} = \frac{\partial\theta}{\partial t} \tag{4.5}$$

Detailed treatments of the development of Richards' equation have been given by Swartzendruber (4.1) and by Childs (4.2).

4.1.2 Solution of Richards' Equation

The following development differs somewhat from the classical presentation in that a linear system approach is used and an impulsive response function is obtained for the relative soil moisture change, c. (See eq. 4.7a for definition of c). The constant diffusivity form of the unsteady flow equation for the flow in porous media can be written as

$$\frac{\partial \theta}{\partial t} = \frac{\partial}{\partial Z}\left(D \frac{\partial \theta}{\partial Z}\right) - \frac{\partial K}{\partial Z} \tag{4.6}$$

where $\theta = nS$

n = Porosity

S = Degree of saturation

K = Hydraulic conductivity in the Z-direction

D = Constant moisture diffusivity

Z = Vertical coordinate (+ downward).

For semi-infinite depth of soil the following boundary conditions are considered:

$$\theta = \theta_n \; ; \; t = 0 \; ; \; z > 0 \text{ and } \theta = \theta_0 \; ; \; t \geq 0 \; ; \; z = 0 \tag{4.7}$$

The following transformations have been used as in references 4.2 and 4.3.

Let $$\frac{\partial K}{\partial \theta} = \rho' = \text{constant} \; ; \quad c = \frac{\theta - \theta_n}{\theta_0 - \theta_n} \; ; \quad T = \frac{\rho'^2 t}{D} \; ; \quad \xi = \frac{\rho' Z}{D} \tag{4.7a}$$

Taking the derivatives with respect to c, t and ξ, respectively, on both sides of eqs. 4.7a the following equations are obtained:

$$\frac{\partial c}{\partial \theta} = \frac{\theta_0 - \theta_n}{(\theta_0 - \theta_n)^2} \; ; \quad \frac{\partial T}{\partial t} = \frac{\rho'^2}{D} \; ; \quad \frac{\partial \xi}{\partial Z} = \frac{\rho'}{D} \tag{4.7b}$$

The derivatives appearing in Richards' equation are now evaluated as follows:

$$\frac{\partial K}{\partial Z} = \frac{\partial K}{\partial \theta} \cdot \frac{\partial \theta}{\partial Z} = \rho' \frac{\partial \theta}{\partial Z} \; ; \qquad \frac{\partial}{\partial Z} D \frac{\rho'}{D} (\theta_0 - \theta_n) \frac{\partial c}{\partial \xi}$$

$$\frac{\partial \theta}{\partial t} = \frac{\rho'^2}{D} (\theta_0 - \theta_n) \frac{\partial c}{\partial T} \; ; \qquad = \frac{\rho'}{D} \frac{\partial}{\partial \xi} \left[\rho (\theta_0 - \theta_n) \frac{\partial c}{\partial \xi}\right] \tag{4.7c}$$

$$\frac{\partial \theta}{\partial Z} = \frac{\rho'}{D} (\theta_0 - \theta_n) \frac{\partial c}{\partial \xi} \; ; \qquad = \frac{\rho'^2}{D} (\theta_0 - \theta_n) \frac{\partial^2 c}{\partial \xi^2}$$

Substituting eqs. 4.7a, 4.7b and 4.7c into eq. 4.6 it can be written as eq. 4.8.

$$\frac{\partial c}{\partial T} = \frac{\partial^2 c}{\partial \xi^2} - \frac{\partial c}{\partial \xi} \tag{4.8}$$

The boundary conditions given in eq. 4.7 may now be written as eq. 4.9.

$$c = 0 \; ; \; T = 0 \; ; \; \xi > 0 \text{ and } c = 1 \; ; \; T \geq 0 \; ; \; \xi = 0 \; . \tag{4.9}$$

By using the transformations given in eq. 4.9a,

$$u = ce^{-(\xi/2 - T/4)} \; ; \; c = ue^{(\xi/2 - T/4)} \tag{4.9a}$$

equation 4.8 can be written as eq. 4.10,

$$\frac{\partial u}{\partial T} = \frac{\partial^2 u}{\partial \xi^2} \tag{4.10}$$

and the boundary conditions 4.9 change to those given in eq. 4.11.

$$u = 0 \; ; \quad T = 0 \; ; \quad \xi > 0 \text{ and } u = e^{T/4} \; ; \quad T \geq 0 \; ; \quad \xi = 0 \tag{4.11}$$

By taking the Laplace transform of eq. 4.10 and using the initial condition, eq. 4.11 can be written as eq. 4.10a.

$$\frac{\partial^2 u}{\partial \xi^2} - p\bar{u} = 0 \tag{4.10a}$$

where $\bar{u}$ is the transform of u.

Substituting $q^2 = p$, eq. 4.10a can be written as eq. 4.12,

$$\frac{\partial^2 u}{\partial \xi^2} - q^2\bar{u} = 0 \tag{4.12}$$

with the boundary conditions given in eq. 4.13, which are derived from eq. 4.11.

$$\bar{u} = 0 \; ; \quad T = 0 \; ; \quad \xi > 0 \text{ and } \bar{u} = \frac{1}{p - 1/4} \; ; \quad T \geq 0 \; ; \quad \xi = 0 \tag{4.13}$$

The solution of eq. 4.12 subjected to the boundary conditions (eq. 4.13) is given by eq. 4.14,

$$\bar{u} = \frac{e^{-q\xi}}{p - 1/4} \tag{4.14}$$

and the transfer function in the frequency domain is given by eq. 4.15.

$$\bar{h} = e^{-q\xi} \tag{4.15}$$

Taking the inverse transform of eq. 4.15 the impulse response function, h, is obtained:

$$h = \frac{\xi}{2\sqrt{\pi}\, T^{3/2}} e^{-\xi^2/4T} \tag{4.15a}$$

The response u to an input θ is given by convolution integral

$$u = \int_0^\infty h(\xi,\tau)\; \theta(0,\, T-\tau)d\tau \tag{4.15b}$$

where τ is a dummy variable.

Substituting back the values of u and h, eq. 4.15b becomes, for an input $u = e^{T/4}$ at $\xi = 0$:

$$c = \int_0^T \frac{\xi}{2\sqrt{\pi}\, \tau^{3/2}} \cdot e^{-\xi^2/4\tau} \cdot e^{(T-\tau)/4} \cdot e^{(\xi/2 - T/4)}\, d\tau = \int_0^T \frac{\xi}{2\sqrt{\pi} \cdot \tau^{3/2}} \cdot e^{-(\tau-\xi)^2/4}\, d\tau \tag{4.16}$$

The impulse response function of c is thus given by I',

$$I' = \frac{\xi}{2\sqrt{\pi}\, T^{3/2}} \cdot \mathrm{Exp}\left[\frac{-(T-\xi)^2}{4T}\right] . \tag{4.17}$$

Substituting the values of ξ, T into eq. 4.17 the impulse response function of c, I' can be written as eq. 4.18.

$$I' = \frac{ZD^{1/2}}{2\sqrt{\pi}\rho'^2\, t^{3/2}} \cdot \mathrm{Exp}\left[\frac{-(\rho' t - Z)^2}{4Dt}\right] \tag{4.18}$$

For a constant input c = 1 at $\xi = 0$, i.e., Z = 0, the response of c is given by the convolution integral

$$c = \int_0^t \frac{ZD^{1/2}}{2\sqrt{\pi}\, \rho'^2\, \tau^{3/2}} \mathrm{Exp}\left[\frac{-(\rho'\tau - Z)^2}{4D\tau}\right] d\tau \tag{4.19}$$

where τ is a dummy variable which stands for t.

Substituting the value of c from eq.4.7a and solving for θ the following equation is obtained.

$$\theta = \theta_n + (\theta_0 - \theta_n) \int_0^t \frac{Z\, D^{1/2}}{2\sqrt{\pi}\, \rho'^2\, \tau^{3/2}} \cdot \mathrm{Exp}\left[\frac{-(\rho'\tau - Z)^2}{4D\tau}\right] d\tau \tag{4.20}$$

Equation 4.20 gives the water-content distribution within a semi-infinite region.

The flux of water through the surface (Z = 0) or the infiltration capacity can be written as

$$f = \left[-D \frac{\partial \theta}{\partial Z} - K_Z\right] | Z = 0 \qquad (4.21)$$

where K_Z is the hydraulic conductivity of the surface layer. Differentiating eq. 4.20 with respect to Z one obtains:

$$\frac{\partial \theta}{\partial Z} = (\theta_0 - \theta_n) \left[\int_0^t \frac{D^{1/2} Z}{2\sqrt{\pi}\, \rho'^2\, \tau^{3/2}} \cdot \mathrm{Exp}\left(\frac{-(\rho'\tau - Z)^2}{4D\tau}\right) \cdot \frac{2(\rho'\tau - Z)}{4D\tau}\, d\tau + \int_0^t \frac{D^{1/2}}{2\sqrt{\pi}\, \rho'^2\, \tau^{3/2}} \cdot \mathrm{Exp}\left(\frac{-(\rho'\tau - Z)}{4D\tau}\right) d\tau \right]$$

At the surface, i.e., Z = 0, the previous equation becomes eq. 4.22.

$$\frac{\partial \theta}{\partial Z} = \int_0^t \frac{D^{1/2}}{2\sqrt{\pi}\, \rho'^2\, \tau^{3/2}} \cdot \mathrm{Exp}\left(\frac{-\rho'^2 \tau^2}{4D\tau}\right) \cdot (\theta_0 - \theta_n) d\tau \qquad (4.22)$$

The flux of water through the surface is given by eq. 4.23 which is obtained by substituting eq. 4.22 into eq. 4.21:

$$f = \left[\int_0^t \frac{D^{3/2}}{2\sqrt{\pi}\, \rho'^2\, \tau^{3/2} \cdot \mathrm{Exp}\left(\frac{\rho'^2 \tau}{4D}\right)} \cdot (\theta_n - \theta_0) d\tau \right] - K_Z \qquad (4.23)$$

For solving equation (4.6) at Z = 0 subjected to the boundary conditions (eq. 4.7), the following assumptions were made:

a. The moisture diffusivity is constant.

b. The depth of the soil is semi-infinite.

c. The slope of the hydraulic conductivity vs. soil moisture curve is constant. (See Figure 2.2).

d. The water content at the surface is constant.

e. The soil mass is homogeneous.

f. The hydraulic conductivity has a constant value.

Figures 4.1 and 4.2 show the plots of the impulse response function, I' (eq. 4.18), and of the infiltration capacity, f (eq. 4.23), for different types of soil and initial moisture conditions respectively.

4.2 Rainfall Excess Models

Five models for estimating the rainfall excess in urban watersheds have been studied. The MIT model is based on the theory discussed in the preceding section. The Minnesota model is based on Darcy's law in conjunction with some empirical assumptions. The Holtan model is empirical. The multicapacity basin accounting model and the antecedent retention index model may be classified as conceptual models. These models were originally formulated for rural watersheds. They were modified in the present study for application to urban watersheds. The basic equations, the data requirements, and a sensitivity analysis of the parameters are given for each model along with the evaluation of their respective performances based on an application to the Ross Ade upper watershed. The models are then compared and evaluated for their application to urban catchments.

4.2.1 Modifications of the Models

The models discussed in the following sections have been modified in order to meet the following two objectives: (a) to estimate the rainfall excess from continuous records of rainfall events and from estimated infiltration and other losses and (b) to keep an accounting of the soil moisture exfiltrated by the evaporation processes. The five modifications of the models are as follows.

a. A loss of 1/16 inches was assumed for each storm to account for the water required to moisten the streets and sidewalks and also to fill the static storage in the small depressions of the paved areas. The deductions are made for streets, sidewalks and parking lots which drain directly into the storm sewer.

b. Some of the runoff from the impervious areas does not drain directly into the storm sewer but runs over lawns and other pervious areas. The impervious areas not connected to the storm sewer are expressed as a percentage as shown in Figures 4.3 and 4.4.

c. In the pervious areas, when the rate of rainfall exceeds the infiltration rate, the excess water begins to collect in the surface storage, which is assumed to be 0.25 inches for each storm. The local static

storage must be filled before any rainfall excess is generated. At the end of a storm, water in the static storage will infiltrate and the exfiltration phase will start only when static storage becomes empty.

d. To keep an accounting of the soil moisture carried over from one storm to another, an effective depth for the infiltrated soil moisture has been introduced. The total effective storage for the soil water is equal to the effective depth multiplied by the porosity of the soil. It is assumed that the moisture goes into storage by infiltration, and leaves the storage either by exfiltration or by percolation into the lower layer at a constant rate equal to the hydraulic conductivity of the lower soil layer. When the exfiltration starts, it is assumed that there is no loss from the effective storage layer into the lower layer due to percolation. Therefore, either after a storm, before a dry period or just before a storm the initial moisture content of the soil layer can be computed from the moisture content in the effective storage and the depth of the storage.

In the calculations of the infiltration and exfiltration rates (e.g. by eqs. 4.25 through 4.28) an equivalent rainfall intensity is used instead of the actual intensity. It is computed by adding the amount of rainfall during the time interval, Δt, to the amount of depression storage available at that time divided by the time interval, Δt.

4.2.2 Calibration and Verification of the Models

The models described in the following sections were tested by using the data of the Ross Ade upper watershed listed in Chapter 2. The models were calibrated and verified by using the rainfall and runoff records of 1970 and 1971, respectively. The storm of April 18, 1970, was used for the parameter sensitivity analyses of the models.

4.3 The MIT Model

The original model was suggested by Eagleson (3.2) and was incorporated in the MIT catchment model by Harley et al. (4.4). It is based on the constant diffusivity form of Richards' equation.

The infiltration rate and the volume of infiltration or exfiltration up to time t are given, respectively, by:

$$f = (\theta_i - \theta_0)\left(\frac{D}{\pi t}\right)^{1/2} - K_0 \quad ; \quad V = \frac{2(\theta_i - \theta_0)^2 D}{\pi f} \qquad (4.24a,b)$$

The infiltration rate is calculated by:

$$\text{a.} \quad f_{in} = (\theta_i - n)\left(\frac{D}{\pi t}\right)^{1/2} - K_0 \qquad i > f_{in} \qquad (4.25)$$

$$\text{b.} \quad f_{in} = i = (\theta_i - \theta_0)\left(\frac{D}{\pi t}\right)^{1/2} - K_0 \qquad \text{otherwise} \qquad (4.26)$$

and the exfiltration rate is calculated by

$$\text{a.} \quad f_{ex} = (\theta_i - 0)\left(\frac{D}{\pi t}\right)^{1/2} - K_0 \qquad PE > f_{ex} \qquad (4.27)$$

$$\text{b.} \quad f_{ex} = PE = (\theta_i - \theta_0)\left(\frac{D}{\pi t}\right)^{1/2} - K_0 \qquad \text{otherwise} \qquad (4.28)$$

where: θ_i = initial moisture content in soil profile, θ_0 = surface moisture content at $t > 0$, K_0 = hydraulic conductivity of the surface layer, f_{in} = infiltration rate, in hr^{-1}; f_{ex} = exfiltration rate, in hr^{-1}; i = rainfall intensity, in hr^{-1}; and PE = potential evapotranspiration rate, in hr^{-1}.

4.3.1 Computational Procedure

A Fortran IV program was written to compute the rainfall excess at 15 minute intervals making use of the modifications described in Section 4.2.1 The computational procedure is presented in Flow Chart 4.1 for the pervious area and in Flow Chart 4.2 for the impervious area in which the following notations are used:

θ_i, θ_0 — Initial moisture content in the soil profile, and on the surface respectively.

S_{at} — Degree of saturation.

n	Porosity.
DEP, MDEP	Depression storage on the pervious area, and the maximum value of DEP.
AKS	Saturated hydraulic conductivity of the soil.
t, Δt	Time count and the time step.
P	Rainfall intensity.
XKS	Volume of rainfall during Δt.
EDEP	Equivalent depth of rainfall.
f_{in}, f_{ex}	Rate of infiltration and of exfiltration, respectively.
V_{ft}, $V_{f_{t+\Delta t}}$	Volume of infiltration up to the end of the t^{th} or $t+\Delta t^{th}$ time step from the beginning of storm period, respectively.
ΔV_f, ΔV_e	Volume of infiltration and of exfiltration in time Δt, respectively.
S_t, $S_{t+\Delta t}$	Moisture storage value in the effective depth at the end of the t^{th} and $t+\Delta t^{th}$ time step, respectively.
PE	Potential evapotranspiration value during time step Δt.
V_{e_t}, $V_{e_{t+\Delta t}}$	Volume of exfiltration up to the end of t^{th} or $t+\Delta t^{th}$ time step from the beginning of the dry period, respectively.
RE	Rainfall excess volume in time step Δt from the pervious area, after satisfying the depression storage.
ER	Excess of rainfall volume over the infiltration volume in time step Δt from pervious area, before satisfying depression storage.
REV_t, $REV_{t+\Delta t}$	Rainfall excess volume at the end of t^{th} or $t+\Delta t^{th}$ time step from the pervious area, respectively.
EDPTH	Effective depth of storage.
MLOSS	Maximum value of the static storage on the impervious area.
$LOSS_t$, $LOSS_{t+\Delta t}$	Static storage available on the impervious area at the end of time step t or $t+\Delta t$, respectively.
$REXC_t$	Rainfall excess volume from the impervious area during time step t.
$RVOL_t$, $RVOL_{t+\Delta t}$	Total rainfall excess volume at the end of time step t or $t+\Delta t$, respectively.

The data required for implementing the MIT model are given in table 4.1.

4.3.2 Implementation of the Model and Sensitivity Analysis of the Parameters

The model was tested by using the Upper Ross Ade watershed data given in Chapter 2. In addition, the value of the moisture diffusivity, D, was optimized to give the best fit between the total measured direct runoff and the total computed rainfall excess for the 66 storms of 1970. The uniform volumetric moisture content, θ_i, at the beginning of the period of interest was taken equal to the porosity if the soil was completely saturated, equal to zero for a dry soil or estimated from the degree of saturation and the porosity. The effective soil storage value, S, was taken from Holtan's model where it had been optimized (see Section 4.5.3). The potential evapotranspiration input was computed by van Bavel's model (Section 3.2.1).

A sensitivity analysis of the parameters of the modified MIT model was made using the rainfall data of April 18, 1970, and the soil characteristics data of the Guelph loam and of the Yolo light clay. The values of the parameters that remained fixed were taken from Tables 2.2 and 2.4, those which varied took the ranges of values shown in Fig. 4.5. Figure 4.5 also shows the values in percent of the difference between the measured direct runoff and the computed rainfall excess. Isoerror lines, i.e., the contour of the same percent of error, at an interval of 100 percent are shown in figures.

a. Hydraulic conductivity. The values of the maximum and initial depression storage and of water diffusivities are given in tables 2.2 and 2.4. For $0.4 < \theta_i < 0.5$ for the Guelph loam and $\theta_i > 0.35$ for the Yolo light clay the zero isoerror line is nearly vertical showing that within this range the infiltration rate is very sensitive to the values of the initial moisture content and practically insensitive to the values of the hydraulic conductivity.

b. Diffusivity D. The values of the maximum and initial depression storages and of hydraulic conductivities are given in tables 2.2 and 2.4. For the Guelph loam the isoerror line remains horizontal for $0 < \theta_i < 0.2$ and $0.01 < D < 0.7$. The model is very sensitive to D in this range. For $0.2 < \theta_i < 0.4$ and $0.7 < D < 2.7$ the isoerror line is approximately a 45 degree line showing that in this range the model is

equally sensitive to both variables. For $\theta_i > 0.4$ and $D > 2.7$ the isoerror line becomes nearly vertical thus showing an insensitivity to the D values. For the Yolo light clay the zero isoerror line is approximately a 45 degree line for $0.10 < \theta_i < 0.35$ and for $0.025 < D < 0.2$. For $0.35 < \theta_i < 0.4$ the zero isoerror line becomes vertical showing that the model is insensitive to D within that range.

c. Maximum static storage, MDEP. The value of the initial depression storage, water diffusivities and hydraulic conductivities are given in tables 2.2 and 2.4. For the Guelph loam the zero isoerror line is nearly horizontal for $0.02 < MDEP < 0.045$ and $0 < \theta_i < 0.36$. For $0.37 < \theta_i < 0.42$ the zero isoerror line becomes nearly vertical. The model is very sensitive to MDEP values. The later statement is true for Yolo light clay for $\theta_i > 0.3$.

d. Static storage (before the storm), DEP. The values of the maximum depression storage, hydraulic conductivities, and water diffusivities are given in tables 2.2 and 2.4. For $0.42 < \theta_i < 0.47$ for Guelph loam the zero isoerror line becomes vertical. For Yolo light clay this is true for $0.35 < \theta_i < 0.4$. This means that the model is very sensitive to θ_i for $\theta_i > 0.42$ for Guelph loam and $\theta_i > 0.35$ for Yolo light clay and not at all sensitive to DEP within that range.

4.3.3 Evaluation of the Results

Out of the three types of soils tested, it was found that the Guelph loam gave the best fit between the measured direct runoff and the computed rainfall excess for the 66 storms in the year 1970. The minimum of the sum of squares of the errors was taken as the criterion for the selection. The model was then run with the rainfall data of 63 storms for the year 1971 to predict the rainfall excess at 15 minute intervals. The scatter diagrams of the computed rainfall excess plotted against the measured direct runoff of each storm for the years 1970 and 1971 are shown in Figure 4.6. Table 4.2 gives the statistics of the rainfall excess computed by the modified MIT model. Figure 4.7 gives the distribution of the differences between the measured direct runoff and the computed rainfall excess for each storm for the years 1970 and 1971.

The computed rainfall excess volume compares fairly well with the measured direct runoff for the year 1970. For the year 1970 more than 75 percent of the error is between -0.02 and 0.02 in. This percentage decreases to about 65 percent for 1971. The error in the computed rainfall excess volume for the whole year is 1.90 percent for the year 1970 but for the year 1971 it is 11.30 percent. The reason for this increase in error may be explained as follows:

The total amount of rainfall for the eleventh storm in the year 1971 was 3.59 inches whereas the direct runoff was 0.44 inches. The amount of direct runoff seems small compared to the direct runoff from similar amounts of rainfall under approximately similar watershed conditions. The computed rainfall excess for the storm was 1.12 in. which explains about 58 percent of the sum of squares of error for the year 1971. It should also be pointed out that inlets exist along the Ross Ade upper watershed boundary which are part of a combined sewer system which does not pass through the gage. During large storms these inlets may be overtopped, causing runoff to flow into the watershed (4.5). Consequently the area of the watershed contributing rainfall excess was variable for excessive storms.

4.4 The Minnesota Model

Russel G. Mein (4.6) at the University of Minnesota developed and tested the Minnesota infiltration model for computing the infiltration rate for a single rainfall event of uniform intensity. The model is based on Darcy's law and is philosophically identical to the Green-Ampt equation 4.7. The following assumptions are made:

a. The soil is homogeneous throughout the profile.
b. The initial moisture content of the soil profile is uniform.
c. The rainfall over the surface is uniform.
d. The initial moisture content before a rainfall event is small so that the relative hydraulic conductivity $[K_r = K(\theta)/K_s]$ is close to zero.
e. The rainfall intensity is greater than the hydraulic conductivity.
f. There is an abrupt wetting front with the soil beyond at the initial moisture content, the soil behind at saturation.
g. At the moment of surface saturation, the infiltration rate is equal to the rainfall rate.

There are three cases of infiltration under different rainfall conditions:

a. The rainfall intensity, I, is less than the saturated hydraulic conductivity, K_s.

b. The rainfall intensity, I, is greater than the saturated hydraulic conductivity, K_s, but less than the infiltration capacity, f_p, which can be defined as the maximum rate at which soil can absorb water through the soil surface.

c. The rainfall intensity, I, is greater than the infiltration capacity, f_p.

The original model was proposed for infiltration of constant intensity rainfall, $I > K_s$ into a soil of uniform moisture content, θ_i. The model deals with the cases b and c above. The hypothetical soil moisture profiles at the time of saturation and after the runoff has begun are shown in Figs. 4.8a and b, respectively.

4.4.1 Modifications of the Model

The Minnesota infiltration model was modified to allow for a non-uniform rainfall intensity, to estimate the time of surface saturation, to compute the infiltration losses for a series of the rainfall events interspaced by dry periods and to allow for combinations of pervious and impervious surfaces. As a result the model had to be modified to take care of both the infiltration and the exfiltration phases. The model was modified in the following way.

a. To allow for a non-uniform rainfall intensity and to estimate the time of surface saturation. The rainfall volumes that would infiltrate up to the surface saturation are Fs_1, Fs_2, Fs_3, Fs_4 corresponding to rainfall intensities of I_1, I_2, I_3, I_4 respectively (see Fig. 4.9). Up to the time of surface saturation the infiltration rate is equal to the rainfall intensity. The volume that would infiltrate up to surface saturation for a particular rainfall intensity may be calculated by using equation 4.30. Let I_1, I_2, I_3, I_4 be the sequence of rainfall intensities of duration x_1, x_2, x_3, x_4 and t_1, t_2, t_3, t_4 be the corresponding times to saturate the surface. For the duration $x_1 < t_1$ the amount of rainfall that would infiltrate is $Fx_1 < Fs_1$. The rate of infiltration during this duration is equal to the rainfall intensity. For the duration $x_2 < t_2$, the amount of rainfall that would infiltrate is Fx_2 where $Fx_1 + Fx_2 < Fs_2$. For the duration $x_3 < t_3$ the amount of rainfall that would infiltrate is Fx_3 where $Fx_1 + Fx_2 + Fx_3 \geq Fs_3$. If duration $x_1 = x_2 = x_3 = 1$ minute, then the surface would be saturated at the third minute. To find the time of surface saturation, subtract $Fx_1 + Fx_2$ from Fs_3. Let this be equal to Δs_3. Compute Δt_3, by dividing Δs_3 by I_3. The actual time of surface saturation is then equal to $x_1 + x_2 + \Delta t_3$ from the beginning of the rainfall event. Once the surface is saturated, the infiltration rate may be computed by using equation 4.31.

b. To allow for the exfiltration phase. It has been assumed that equation 4.31 is applicable to predict the exfiltration rate by changing F, the infiltration volume, to E, the exfiltration volume and replacing the moisture deficiency, XIMD, by the moisture content during the exfiltration phase XEMD ($= \theta_i - \theta_0$). The only constraint is that the value of f_p should not exceed the rate of evapotranspiration.

c. To allow for the pervious and impervious areas. The inclusion of static storages for pervious and impervious areas and the use of an equivalent rainfall intensity for handling the case of an impervious area draining on a pervious area are described in section 4.2.1.

d. Soil moisture accounting. An effective depth of storage has been introduced as described in section 4.2.1.

4.4.2 Basic Equations

The equations required to estimate the infiltration or the exfiltration are as follows:

During a storm period:

$$f_{in} = I \qquad \text{until } F = F_s \qquad (4.29)$$

$$F_s = \frac{S_{av} \cdot XIMD}{(I/K_s) - 1} \qquad I > K_s \qquad (4.30)$$

$$f_{in} = f_p = K_s\left(1 + \frac{S_{av}(XIMD)}{F}\right) \qquad F > F_s,\ I > f_p \qquad (4.31)$$

$$f_{in} = I \qquad \text{otherwise} \tag{4.32}$$

During a dry period:

$$f_{ex} = K\left(1 + \frac{S_{av}(XEMD)}{E_t}\right) \qquad PET > f_{ex} \tag{4.33}$$

$$f_{ex} = PET \qquad \text{otherwise}$$

where Fs (in.) = infiltration volume up to surface saturation, f_{in} (in. $hr.^{-1}$) = infiltration rate, f_p (in. $hr.^{-1}$) = infiltration capacity, f_{ex} (in. $hr.^{-1}$) = exfiltration rate, I (in. $hr.^{-1}$) = average intensity of the rainfall excess, S_{av} = area under the capillary suction vs. relative hydraulic conductivity curve: $S_{av} = \int_0^1 S.dK_r$; XEMD = THETAI - THETAO; XIMD = initial moisture deficit; THETAI (vol. $vol.^{-1}$) = initial moisture content of the soil; THETAO = moisture content at surface, assumed zero; K_s (in. $hr.^{-1}$) = saturated hydraulic conductivity.

4.4.3 Computational Procedure and Data Requirements

A Fortran IV program was developed to compute the rainfall excess at 15 minute intervals. The average daily evapotranspiration was supplied as an input. The computational procedure is presented in Flow Chart 4.3 in which the following notation is used.

THETAI, THETAS	Initial and saturated moisture content of the soil profile, respectively.
ERR	Equivalent rainfall intensity.
XIMD	Moisture deficiency.
ΔR	Depth of rainfall in time step Δt.
f_{in}, f_{ex}	Rate of infiltration, of exfiltration, respectively.
F, F_s	Volume of infiltration up to the current time step and up to surface saturation, respectively.
MDEP	Maximum depth of static storage.
S_t, $S_{t-\Delta t}$	Soil moisture storage value at the end of the t^{th} or $t-\Delta t^{th}$ time step, respectively.
AKS	Saturated hydraulic conductivity.
TA_t, $TA_{t-\Delta t}$	Volume of rainfall excess at the end of the t^{th} or $t-\Delta t^{th}$ time step, respectively.
$A_{\Delta t}$	Rainfall excess during the step Δt.
PET	Potential evapotranspiration rate.
E_t, $E_{t-\Delta t}$	Volume of exfiltration at the end of the t^{th} or $t-\Delta t^{th}$ time step, respectively.
$E_{\Delta t}$	Volume of exfiltration during time step Δt.
XEMD	Moisture content of the soil during the exfiltration phase.
n	Porosity of the soil.
DEPT	Effective depth of soil storage of the watershed.
DEP	Static storage during the current time step.
ER	Excess of rainfall volume over the infiltration volume in time step Δt from pervious area before satisfying depression storage.

The data required for the implementation of the modified Minnesota model are given in table 4.1.

4.4.4 Implementation of the Model and Sensitivity Analysis of the Parameters

The model was implemented for the Ross Ade upper watershed using the data given in tables 2.2 and 2.4. The effective soil storage value, S, was taken from Holtan's model as discussed in section 4.5.3. The soil properties for the Guelph loam gave the best result as was the case for the MIT model. The sum of squares of differences of measured direct runoff and computed rainfall excess for each storm was the criterion for the testing.

The model was run with different values of the saturated hydraulic conductivity to evaluate its effect on the sum of squares of errors between the measured direct runoff and the computed rainfall excess for the 1970 data. The sum of squares of errors was found to be minimum for a hydraulic conductivity of 0.13 for the Guelph loam.

Sensitivity analyses of the modified Minnesota model to changes in S_{av}, in the hydraulic conductivity, in the maximum depression storage and in the depression storage before the storm were made using the rainfall data of the storm of April 18, 1970. The results are shown on the Figs. 4.10 and 4.11. The values shown on

the figures are percentages of the difference between the measured direct runoff and the computed rainfall excess. Isoerror lines, at an interval of 100 percent are shown in the figures. In all cases the depression storage before the storm was 0.0 in.

a. Area under S-K_r curve, S_{av}. The values of the maximum depression storage and the hydraulic conductivities are given in tables 2.2 and 2.4. For the Guelph loam there is no zero isoerror line for the range of values used. For the Yolo light clay the zero isoerror line is a vertical line for 0.0 < XIMD < 0.05 inch and 0.8 < S_{av} < 8.8. The model is very sensitive to XIMD and insensitive to S_{av} within this range of values.

b. Hydraulic conductivity, K. The values of S_{av} and of the maximum depression storage are given in tables 2.2 and 2.4. For the Guelph loam the zero isoerror makes about ten degrees with the x-axis for 0.05 < XIMD < 0.4 and .047 < K < .14 whereas for the Yolo light clay the zero isoerror becomes a vertical line for 0 < XIMD < 0.05 and .0016 < K < .017 which shows that for the Yolo light clay the model is very sensitive to change in XIMD and insensitive to K values for the range of values used, whereas the opposite is true for the Guelph loam.

c. Maximum static storage, MDEP. The values of the hydraulic conductivities are given in table 2.4. There is no zero isoerror value for the sets of data used for Guelph loam. For the Yolo light clay the zero isoerror line is a vertical line for 0 < XIMD < 0.05 and 0.023 < MDEP < 0.25. The model is very sensitive to XIMD values but insensitive to MDEP values for this range of values.

d. Static storage, DEP, (before a storm). The value of the maximum depression storage and of the hydraulic conductivities are given in tables 2.2 and 2.4. There is no zero isoerror line for the Guelph loam for the range of the data used. For the Yolo light clay the zero isoerror line becomes vertical for 0 < XMID < 0.05 and 0.023 < DEP < 0.25. For these range of values the model is very sensitive to XIMD values and insensitive to DEP values.

4.4.5 Evaluation of the Results

Scatter diagrams of the computed rainfall excess plotted against the measured direct runoff of each storm for the years 1970 and 1971 are shown in Figure 4.6. The statistics of the computed rainfall excess calculated by the modified Minnesota model and the measured direct runoff for the year 1970 and 1971 are given in Table 4.2. The distributions of the differences between the measured direct runoff and the computed rainfall excess for each storm for the year 1970 and 1971 are given in Figure 4.7. In general, the computed rainfall excess volume compares fairly well with the measured direct runoff for the year 1970 (see Fig. 4.6 and Fig. 4.7). The percentage of error for the whole year and the sum of squares of the errors are somewhat larger for 1971 than for 1970. This increase is due in part to the error in the direct runoff of the eleventh storm of 1971 (already discussed in section 4.3.3) and in part to the approximate values of the porosity, the saturated hydraulic conductivity and S_{av} of Guelph loam used in the model. Nevertheless a little over 77 percent of the error is between -.02 to .02 inches for 1970 and this decreased to a little over 66 percent in 1971. The sensitivity analysis shows that soil characteristics significantly affect the performance of the model.

4.5 Holtan Model

H. N. Holtan (4.8, 4.9, 4.10) proposed the following empirical infiltration model: (see Fig. 4.12a)

$$f = a(S-F)^{n'} + f_c \tag{4.34}$$

where f = infiltration capacity, in $hr.^{-1}$.
a = percent basal area of plant stems.
S = soil storage capacity = G + AWC, in.
F = accumulated infiltration volume, in the overlying stratum, in.
n' = a constant for a given soil.
f_c = constant rate of infiltration after prolonged wetting, in $hr.^{-1}$.
G = free water, in.
AWC = available moisture capacity, in.

The following assumptions have been incorporated in eq. 4.34.

a. The volume of rainfall, P, at rates in excess of the infiltration capacity, f, must fill the surface depressions, V_d, before direct runoff can occur.

b. The greatest intake is in the vicinity of the plant stems. The percent basal area, a, of the plant stems is an index of the effective area of most rapid infiltration.

c. The final near-constant rate of infiltration, f_c, is associated with the impeding layer of soil.

d. The infiltration rate, f, approaches f_c when the storage, S, is exhausted by the accumulated infiltration, F, in the overlying soil strata.

e. When the rainfall ceases, the infiltration will continue to the extent of the depression storage.

f. When the rainfall ceases, the free water, G, will drain through the underlying strata at a constant rate, f_c. This provides an infiltration recovery.

g. During the periods of no rainfall the available storage, S_a, recovers through evapotranspiration to the extent of the available water capacity, AWC.

4.5.1 Modifications of the Model

In order to estimate the rainfall excess from an urban watershed the model has been modified as discussed in Section 4.2.2.

4.5.2 Computational Procedure

The final near-constant rate of infiltration, f_c, may be estimated from the hydrologic grouping of soils as the SCS Handbook (4.11) or from the Handbook of Applied Hydrology (4.12). The storage in the overlying horizon, S, may be computed as the total porosity in the A-horizon minus the moisture at a suction of fifteen bars. This may be found in USDAHL-70 model of Watershed Hydrology (4.13) and also in reference 4.12. The available soil moisture capacity, AWC may be estimated from the soil texture as in reference 4.10. The free or loosely held water, G, is estimated as the difference between S and AWC. The value of a is found to correlate with the density of vegetation and may be estimated by using Table 3 in reference 4.10

A Fortran IV program was written to compute the rainfall excess at 15 minute intervals using the procedure given in Flow Chart 4.4. The average daily evapotranspiration input was computed as indicated in section 3.2. The following notations are used in Flow Chart 4.4:

DELP	Volume of rainfall in the current time step, Δt.
DELF	Volume of infiltration in the current time step, Δt.
VD	Depression storage in the current time step, Δt.
DPE	Excess rainfall in the current time step, Δt.
S	Soil storage capacity.
F	Accumulated infiltration volume in the overlying strata up to the current time step.
f_c	Constant rate of infiltration after prolonged wetting.
G	Free water.
AWC	Available moisture capacity.
f_t, $f_{t-\Delta t}$	Infiltration capacity in the t^{th} and $t-\Delta t^{th}$ time step, respectively.
S_a	S-F
PE	Total excess rainfall for the storm.
RE	Rainfall excess in the current time step.
$\overline{DELF}$	Average volume of infiltration for two consecutive time steps.
ET	Evapotranspiration in the current time step.

For the impervious area the procedure is the same as in section 4.3.1 and Flow Chart 4.2.

The data required for the implementation of the modified Holtan model are given in table 4.1.

4.5.3 Implementation of the Model and Sensitivity Analysis

The data used for the implementation of the model are given in Tables 2.2 and 2.4. The values of MDEP, f_c, a, G, AWC were taken from references 4.9, 4.11, and 4.12, for the types of soils and vegetation in the Ross Ade upper watershed. An average weighted value for each of the above parameters was then estimated. The value of S was optimized to give the best fit between total measured direct runoff and total computed rainfall excess for the 66 storms in the year 1970. The value of S equal to 3.5 in. gave the best fit. The

minimum sum of squares of error was the criterion for the selection.

A sensitivity analysis of the parameters of the modified Holtan model was made using the rainfall data of the storm of April 18, 1970. The results of the sensitivity analysis are shown in Fig. 4.12b. The values shown on the figures are the percent of difference between the measured direct runoff and the computed rainfall excess. Isoerror lines at intervals of 100 percent are also shown on the figure.

a. Available storage, S_a = S-F. The values of n', V_d and AWC/G are given in table 2.4, and f_c = 0.25. For $1.0 < S_a < 2.0$ and $0.5 < S < 10$ the zero isoerror line is nearly horizontal. Thus the model is insensitive to S in this range. When $0 < S < 1.0$ and $1.5 < S_a < 10$ the zero isoerror line becomes vertical showing that the model is insensitive to S_a in this range but very sensitive to S.

b. The final near constant rate of infiltration, f_c. The values of n', V_d, AWC/G, and S are shown in Table 2.4. The zero isoerror line is a 45 degree line for $0.02 < f_c < 0.25$ and $1.3 < S_a < 3.5$. Thus the model is sensitive to both S and S_a values in this range.

c. Ratio of the available moisture capacity to free water capacity, AWC/G. The values of n', V_d, S, and f_c are shown in Table 2.4. The zero isoerror line is horizontal for $0.2 < AWC/G < 0.4$ and $0 < S_a < 3.5$, thus indicating that the model is insensitive to S_a in this range, but appears to be very sensitive to AWC/G.

d. Exponent, n'. The values of V_d, S, f_c, and AWC/G are shown in Table 2.4. For $1.0 < n' < 1.1$ and $0 < S_a < 3.5$ the zero isoerror line is nearly horizontal. Thus the model is very sensitive to n' and insensitive to S_a in this range.

e. Maximum depression storage, V_d. The values of S, f_c, AWC/G and n' are shown in Table 2.4. For values of $0.0 < V_d < 0.25$ and $0 < S_a < 1.3$ the isoerror line makes an angle of approximately 20 degrees, indicating that the model is more sensitive to V_d than to S_a within this range.

4.5.4 Evaluation of the Results

The scatter diagrams of the computed rainfall excess plotted against the measured direct runoff of each storm for the years 1970 and 1971 are given in Figure 4.6. The distribution of the differences between the measured direct runoff and computed rainfall excess for each storm for the year 1970 and 1971 are shown in Figure 4.7. The statistics of the rainfall excess computed by the modified Holtan model are given in Table 4.2. The computed rainfall excess volume compares well with the measured direct runoff for the year 1970. The percentage of error for the whole year is 0.46 percent in 1970 and for the year 1971 it becomes 1.98 percent. The reason for at least a part of this increase has been discussed in Section 4.3.3. It seems that although the total error for the prediction year 1971 is small yet the variation of computed rainfall excess from storm to storm is quite high as evident from the variance of the error and from the sum of the squares of the errors.

The model appears to be sensitive to n' and AWC/G and has a varying degree of sensitivity to S, f_c and S_a.

4.6 Multicapacity Basin Accounting Model

M. A. Kohler and M. M. Richards (4.14) developed a model for computing the runoff from rainfall events based on the concept that the usable moisture capacity varies from point to point over a watershed, and that the distribution of the moisture capacity may be simulated by several reservoirs with different storage capacities which correspond to different parts of the watershed (see Fig. 4.13). Accounting computations are carried independently for each of the several reservoirs. The loss, i.e. the rainfall minus the runoff, is equal to the rainfall at the beginning of the storm and it approaches the deficiency assymptotically as the rainfall continues. The relation may be expressed as

$$Q = (p^n + d^n)^{1/n} - d \qquad (4.35)$$

where Q = rainfall excess volume; d = integrated index of initial moisture deficiency in the reservoir; p = rainfall; n = c + K'd; c = constant; (see Fig. 4.13) and K' = constant. The deficiency in a reservoir at the end of a time interval may be computed from the continuity equation:

$$d_{t+\Delta t} = d_t - (P - Q) + E, \qquad 0 \leq d_{t+\Delta t} \leq S \qquad (4.36)$$

where d_t, $d_{t+\Delta t}$ = Moisture deficiency in the reservoir at the end of time periods t and $t+\Delta t$, respectively.

Q = Rainfall excess volume (equal to direct runoff volume for a particular storm).

E = Actual evapotranspiration losses during time period Δt.

S = Maximum storage capacity of the reservoir.

A linear regression equation can be developed using the measured direct runoff as the dependent variable and the computed direct runoff from the reservoirs as the independent variables:

$$Q_M = C + \sum_{i=1}^{i=m} C_i Q_i \qquad (4.37)$$

where C, C_i = constants; Q_i = computed direct runoff from the i^{th} reservoir; m = number of reservoirs; and Q_M = measured direct runoff.

4.6.1 Computational Procedure

A set of reservoirs of different capacities is selected and the initial deficiencies of the reservoirs are assumed.

The Flow Chart 4.5 illustrates the sequence of the calculations, in which the following notations are used:

S_i = maximum storage capacity of the i^{th} reservoir.

d_i = deficiency of the i^{th} reservoir.

Q_i = computed direct runoff from the i^{th} reservoir.

RE_i = rainfall excess from the i^{th} reservoir.

The only data required apart from the rainfall and the direct runoff are the evapotranspiration estimates at specified time intervals.

4.6.2 Implementation of the Model

The model was tested using the Upper Ross Ade watershed data given in Chapter 2. The daily evapotranspiration computed by van Bavel's method (Section 3.2.1) was used in the multicapacity basin accounting model. As the watershed is urbanized, it includes a range of perviousness which is simulated by reservoirs having a large range of storage capacities. A small storage capacity is used to represent the static storage in the impervious area and large values are used for the static and the soil moisture storages for the different types of soils in the pervious part of the watershed. Therefore, five sets of reservoirs each containing five reservoirs with the capacities shown in the lower part of Figure 4.14 were selected to compute the rainfall excesses. The initial deficiencies were also varied from zero to the maximum storage of the reservoirs in five equal steps. The reservoirs having capacities of 0.20, 0.40, 2.0, 4.0, 7.0 inches and initial deficiencies equal to 1/4 of the maximum storage capacities of each of the reservoirs gave the highest multiple correlation coefficient of 0.9923 and the following regression equation:

$$Q_i = 0.00496 - 0.11064 \cdot Q1_i + 0.38107 \cdot Q2_i - 0.39095 \cdot Q3_i + 1.47071 \cdot Q4_i - 1.30406 \cdot Q5_i \qquad (4.38)$$

where Q_i = total rainfall excess of the i^{th} storm. $Q1_i$, $Q2_i$, $Q3_i$, $Q4_i$, $Q5_i$ = rainfall excess values of the i^{th} storm computed from the reservoir with storage capacities of 0.2, 0.4, 2.0, 4.0 and 7.0 inches, respectively. The continuous record of April through December, 1970 was used for developing the above regression equation. During the month of April, 1970, the watershed was nearly saturated, so the regression equation was developed using initial deficiencies equal to 1/4th of the maximum storage capacity of each reservoir.

The model was run to compute rainfall excess in each reservoir for 63 storms and the intervening dry periods of 1971. The predicted rainfall excess for each storm was then computed by substituting the values of the rainfall excess calculated from each reservoir into the regression equation.

4.6.3 Evaluation of the Results

The statistics of the rainfall excess computed by the Multicapacity Basin Accounting model and the measured direct runoff for the calibration year of 1970 and for the prediction year of 1971 are given in Table 4.2. Scatter diagrams of the computed rainfall excess plotted against the measured direct runoff of each

storm for the years 1970 and 1971 are shown in Figure 4.6. The distribution of differences between the measured direct runoff and the computed rainfall excess for each storm for the years 1970 and 1971 are plotted in Figure 4.7. It is evident from Table 4.2 and Figures 4.6 and 4.7 that, in general, the computed rainfall excesses compared well with the measured direct runoffs both for 1970 and 1971. In 1970 nearly 70 percent of the errors are between -0.01 and 0.01 whereas in 1971 this decreased to about 50 percent. The ratio of computed rainfall excess to measured direct runoff is approximately one for 1970 and becomes 0.88 in 1971. The maximum error of 0.078 inch in a single storm in 1970 increased to 0.45 inch in 1971. The reason for this increase has already been discussed in Section 4.3.3.

4.7 Antecedent Retention Index Model

Keith E. Saxton and Arno T. Lenz (4.15) suggested a modified antecedent precipitation index model for soil moisture accounting which may be written as

$$ARI_i = (ARI_{i-1} + R_{i-1})K_1 \tag{4.39}$$

where ARI_i = antecedent retention index for the i^{th} day; R_i = retention = rainfall - runoff; t = time in days; K_1 = recession factor less than 1, assumed constant.

A linear regression equation can be developed correlating the rainfall excess volume of each storm, RE, as the dependent variable and the following independent variables: the antecedent retention index values before each storm, ARI, the daily soil temperatures before each storm, T, and the precipitation volume of each storm, P.

$$RE_i = C + a_1 P_i + a_2 ARI_i + a_3 T_i \tag{4.40}$$

where a_1, a_2, a_3 and c are constants and the subscript i refers to the i^{th} storm.

4.7.1 Computational Procedure

A Fortran IV computer program was written to compute the ARI values before each storm, and to develop a linear regression equation, to compute the multiple correlation coefficient and the standard error of estimate.

The initial value of ARI may be estimated from the measured value of the soil moisture at different levels of the soil profile at the beginning of the period of interest. If there is no measured soil moisture data, the computation may start from a day when the soil moisture is near the field capacity, that is, after a heavy rain or soon after a snowmelt. The computational procedure is summarized in Flow Chart 4.6. The data required for implementing the model are given in Table 4.1.

4.7.2 Implementation of the Model

The model was tested using the Upper Ross Ade watershed data given in Chapter 2. The soil moisture was measured by using a Neutron meter at 6, 12, 18, 24, 30 and 36 inches below the surface at the Ross Ade upper watershed near the gaging station for the year 1971. The average values of the soil moisture for the top 12 inches were computed. For the year 1970, the average daily soil temperature 4 inches from the surface under sod at the Agronomy farm near West Lafayette were used. The first average value of the soil moisture was taken as the initial ARI value both for years 1970 and 1971. The model was calibrated by using rainfall and direct runoff and soil temperature data for the year 1970. A recession factor of 0.992 gave ARI values before each storm with the maximum multiple correlation coefficient of 0.9637 and a standard error of estimate of 0.0441 in the linear regression equation for the rainfall excess volume of each storm:

$$RE = 0.01009 + 0.21778 \cdot P - 0.00845 \cdot ARI + 0.00054 \cdot T \tag{4.41}$$

4.7.3 Evaluation of the Results

The regression equation developed using the 1970 data was used to predict the rainfall excess of each storm of 1971. Figure 4.6 shows the scatter diagrams of the computed rainfall excess plotted against the measured direct runoff of each storm for the years 1970 and 1971. The statistics of the rainfall excess values computed by the model are given in Table 4.2. The distribution of the differences between the measured direct runoff and the computed rainfall excess for each storm for the years 1970 and 1971 is shown in

Figure 4.7. It is evident from the distribution of error and the scatter diagram, Fig. 4.7 and Fig. 4.6, respectively, that except for the eleventh storm of 1971, in general, the computed rainfall excess volume compares fairly well with the measured direct runoff for the years of 1970 and 1971.

For the data of 1970, about 65 percent of the error is between -.02 and .02 inches. For the data of 1971, this decreases to about 59 percent. The variations of the measured direct runoff and of the computed rainfall excess are in general very similar from storm to storm. This is also evident from the variance of error (see Table 4.2).

4.8 Evaluation of the Models

The comparison of the five rainfall excess predictors has been based on the following criteria:

a. The sum of the squares of the differences between the values of measured direct runoff and the computed rainfall excess.
b. The sum of the differences between the values of measured direct runoff and the computed rainfall excess.
c. The variance of the values of measured direct runoff and of the computed rainfall excess.

Out of the five rainfall excess predictors, the modified MIT model, the modified Minnesota model and the modified Holtan model compute the time distribution of rainfall excess during a storm whereas the Multicapacity Basin Accounting model and the modified Antecedent Retention Index Model compute the total volume of rainfall excess of each storm. The pertinent statistical properties of the measured direct runoff and the computed rainfall excess by the five models are shown in Table 4.2. The overall sum of the squares of the error for the Multicapacity Basin Accounting (MBA) Model and antecedent Retention Index (ARI) Model are lower than those of the modified MIT Model, Minnesota Model and the Holtan Model for the period of study. The sum of the squares of the errors for the ARI model during the calibration year of 1970 is 3 times that of the MBA Model, whereas for the prediction year of 1971 the sum of the squares of the errors for the ARI model is 0.33 percent less than that of the MBA model. The percentage of error in the MBA model increases from .03 percent in 1970 to 11.50 percent in 1971. In the case of the ARI model the percentage of error decreases from 11.27 in 1970 to 3.31 in 1971. The variance of the error for the prediction year is nearly the same for both the models. Although the sum of the squares of the error for the Holtan Model during the calibration year of 1970 is smaller than that for the ARI Model, for the prediction year of 1971 the modified Holtan Model has the highest sum of the squares of the errors among the five rainfall excess predictors considered.

Among the three rainfall excess predictors which are used to compute the time distribution of rainfall excess within a storm, the sum of the squares of errors of the modified Minnesota Model for the prediction year of 1971 is the least, followed by the modified MIT model. But the percentage of errors for the Minnesota model is quite high. It increases from 13.36 percent in 1970 to 22.51 percent in 1971, whereas for the modified MIT Model the percentage of error increases from 1.9 percent in 1970 to 11.30 percent in 1971. It may be noted that the overall percentage of error for the modified Holtan Model is the least among the five rainfall excess predictors considered in the present study.

4.9 Selection of Rainfall Excess Model and Discussion

Among the five total rainfall excess predictors, the MBA Model, which is a conceptual model and the ARI Model, which is based on a simple soil moisture accounting gave better results. These two models can be used to compute only the total volume of rainfall excess of the storm. Consequently, the use of these models is limited.

Out of the three rainfall excess models: the modified MIT model, the Minnesota model and the Holtan model, which may be used to compute the time distribution of the rainfall excess, the modified MIT model gave the best result if the sum of the squares of error and the percentage of error are used as criteria for evaluation. Although the sum of the squares of errors was the least for the modified Minnesota model the percentage of errors both for 1970 and 1971 was quite high. If only the sum of the squares of errors is considered, the performance of the modified Minnesota model was the best. Thus the modified Minnesota model, which is a simple algebraic equation based on Darcy's law, predicts fairly well the rainfall excess of storms

from urbanized watersheds.

The modified Minnesota model uses the same equation both for computing the infiltration after surface saturation and the exfiltration. The value of the hydraulic conductivity parameter of the model is assumed to be constant and equal to the value of saturated hydraulic conductivity both for infiltration and exfiltration phases. Moreover, unlike the modified MIT model or the modified Holtan model, none of the parameters in the Minnesota model was optimized. The model was run with parameter values of three types of soils. The soil type which gave the minimum sum of the squares of errors was accepted as the average soil type of the watershed. The sum of squares of errors could be decreased by using the measured average values of the parameters. This is also true for the modified MIT model.

The modified MIT model gave the best result as expected because it is based on the constant diffusivity form of the unsteady flow equation for flow in porous media. Actually, it was expected to give the least value of the sum of squares of errors. The reason for not obtaining the least value of the sum of squares of errors may be due to the type of soil data used for the model which may be considered as a gross approximation. The variance of the rainfall excess for the prediction year of 1971 was 63.8 percent more than the variance of the direct runoff for the modified MIT model, whereas for the modified Minnesota model this was 22.1 percent and for the modified Holtan model this was 182.8 percent. Although the sum of squares of errors of the modified Holtan model for the year 1970 was smaller than that obtained by using the modified MIT model or the ARI model, for the prediction year of 1971 the modified Holtan Model gave the highest sum of the squares of error. Consequently, it appears that for predicting the rainfall excess over an urbanized watershed, the modified Holtan model may not be a good choice. Out of the MBA and ARI models, the ARI model gave a slightly smaller sum of the squares of error, but the percentage of error for the MBA model was 248 percent more than that of ARI model for the prediction year of 1971. Considering both the percentage of errors and sum of squares of the errors, it seems that the ARI model is better than the MBA model for predicting rainfall excess values of storms over urbanized watersheds such as the Ross Ade upper watershed.

The selection of the rainfall excess model depends also on its ultimate use which in the present study is the identification of the linear and non-linear kernels of the watershed. If only the total volume of rainfall excess is required for the rainfall excess-direct runoff transfer model, the use of the ARI model is recommended, whereas if the time distribution of rainfall excess is required, the MIT model is suggested.

In an urban watershed the percentage of impervious area of the watershed which is directly connected to the storm sewer is an important parameter. The losses in the impervious areas are very small. Moreover, it was found from the results obtained by the rainfall excess predictors that the contribution of the pervious area to the total rainfall excess was small, except for large storms. In view of these factors, it appears that for an urban watershed with a high percentage of impervious area directly connected to the storm sewers, the precise measurement of this area may be as important or more important than the measurement of the soil parameters of the watershed. Table 4.3 gives, as an example, the ratio of the computed rainfall excess to the measured direct runoff in terms of hypothetical percentages of the impervious area directly connected to the storm sewer for the storm of April 18, 1970, on the Ross Ade upper watershed (see Table 2.2). The total impervious area is assumed to cover 50 percent of the watershed area and the initial moisture content is taken as 0.0. As can be seen from this hypothetical example, the ratio of the computed rainfall excess to the measured direct runoff is very sensitive to the percentage of area directly connected to the storm sewer.

Table 4.1

Data Requirements of the Rainfall Excess Models

Modified MIT Model

a. Percentage of impervious area in the watershed.
b. Percentage of impervious area draining directly to the storm sewer.
c. Static storage for the impervious area, in.
d. Static storage for the pervious area, in.
e. Porosity, n, of the soil.
f. The constant moisture diffusivity, D, $in.^2 hr.^{-1}$
g. The hydraulic conductivity, K, $in.hr^{-1}$.
h. The initial moisture content of the soil, vol. $vol.^{-1}$.
i. Rainfall data at specified time intervals, $in.hr^{-1}$.
j. Potential evapotranspiration data at specified time intervals, $in.hr^{-1}$.
k. Effective storage of the top soil layer of the watershed, S.

Modified Minnesota Model

a. Porosity, n.
b. Initial moisture content of the soil profile, THETAI = nD_{sat}, vol. vol^{-1}.
c. Area under the capillary suction vs. relative hydraulic conductivity curve between $K_r = 0.01$ and $K_r = 1$.
d. Saturated hydraulic conductivity of the soil, in hr^{-1}.
e. Maximum value of static storage both for impervious area and pervious area, in.
f. Percentage of pervious area of the watershed.
g. Percentage of impervious area to the total area directly connected with the storm sewer.
h. Percentage of impervious area to the pervious area not directly connected with storm sewer. Runoff from this area runs over the pervious area.
i. Effective storage of the top soil layer of the watershed, S, in.
j. Potential evapotranspiration rate at the specified time step, in hr^{-1}.
k. Rainfall data at specified time interval, in hr^{-1}.

Modified Holtan Model

a. Percent basal area of plant stems, a.
b. Soil storage capacity, S.
c. Free water, G.
d. Available moisture capacity, AWC.
e. Constant rate of infiltration after prolonged wetting, f_c.
f. Exponent n' assumed to be constant for a given soil.
g. Potential evapotranspiration data at the same time interval as rainfall, PE.
h. Maximum depression storage on the pervious area, MDEP.
i. Maximum depression storage on the impervious area, MLOSS.
j. Percentage of impervious area of the watershed which drains directly into the storm water.
k. Percentage of impervious area of the watershed which drains over the pervious area.
l. Rainfall data at specified time interval, Δt.

Multicapacity Basin Accounting Model

a. Evapotranspiration at specified time intervals.
b. Rainfall data at specified time intervals.
c. Runoff data at specified time intervals

Antecedent Retention Index Model

a. The initial value of the antecedent retention index.
b. The recession coefficient, K_1.
c. The rainfall and direct runoff data of a sequence of storms and time between storms.
d. The temperatures of the top layer of the soil profile before the storms.

Table 4.2 Statistics of the Rainfall Excess Models

	Modified MIT Model		Modified Minnesota Model		Modified Holtan Model		Multicapacity Basin Accounting Model		Modified ARI Model $K_1 = 0.992$	
	1970	1971	1970	1971	1970	1971	1970	1971	1970	1971
No. of storms	66	63	66	63	66	63	66	63	66	63
Sum of calculated rainfall excess, in	4.2861	4.5015	3.7855	3.9324	4.3898	4.9743	4.3708	4.4915	4.8618	4.9071
Sum of measured direct runoff, in	4.3695	5.0749	4.3695	5.0749	4.3695	5.0749	4.3695	5.0749	4.3695	5.0749
Rainfall excess/direct runoff	0.9809	0.8870	0.8663	0.7749	1.0046	0.9802	1.0003	0.8850	1.1127	0.9669
Sum of errors, (measured - calculated) in	0.0832	.5734	.5840	1.1425	-0.0203	.1006	- .0013	.5834	- 0.4923	0.1678
% of error	1.90	11.30	13.37	22.51	-0.46	1.98	-0.03	11.50	-11.27	3.31
Mean of rainfall excess	0.0649	.0715	.0574	.0624	0.0665	.0790	.0662	.0713	0.0737	0.0779
Mean of direct runoff	0.0662	.0806	.0662	.0806	0.0662	.0806	.0662	.0806	0.0662	0.0806
Mean of error	0.0013	.0091	.0088	.0181	-0.0003	.0016	- .0000	.0092	- 0.0075	0.0027
Mean of absolute error	0.0253	.0444	.0219	.0423	0.0144	.0569	.0112	.0332	0.0229	0.0377
Sum of sqs. of error	0.3615	.7864	.3240	.6590	0.0560	1.5666	.0260	.3295	0.1061	0.3284
Mean of sqs. of error	0.0055	.0125	.0049	.0105	0.0008	.0249	.0004	.0052	0.0016	0.0052
Variance of rainfall excess	0.0135	.0267	.0102	.0199	0.0250	.0461	.0257	.0260	0.0230	0.0170
Variance of direct runoff	0.0261	.0163	.0261	.0163	0.0261	.0163	.0261	.0163	0.0261	0.0163
$\frac{\text{Var CRE - Var ODR*}}{\text{Var ODR}} \times 100$	-48.28	63.80	-60.92	22.09	-4.21	182.82	-1.53	59.51	-11.88	4.29
Variance of error	0.0056	.0126	.0049	.0103	0.0009	.0253	.0004	.0052	0.0016	0.0053

*CRE = calculated rainfall excess, ODR = observed direct runoff.

Table 4.3 Variation in Rainfall Excess Volume with Percentage of Impervious Area Directly Connected with Storm Sewer Using MIT Model.

Storm of April 18, 1970, on Ross Ade Upper Watershed

Area Connected Directly with Storm Sewer, Percent	Computed Rainfall Excess ÷ Measured Direct Runoff
10.0	0.3912
20.0	0.7825
30.0	1.1737
49.0	1.5650

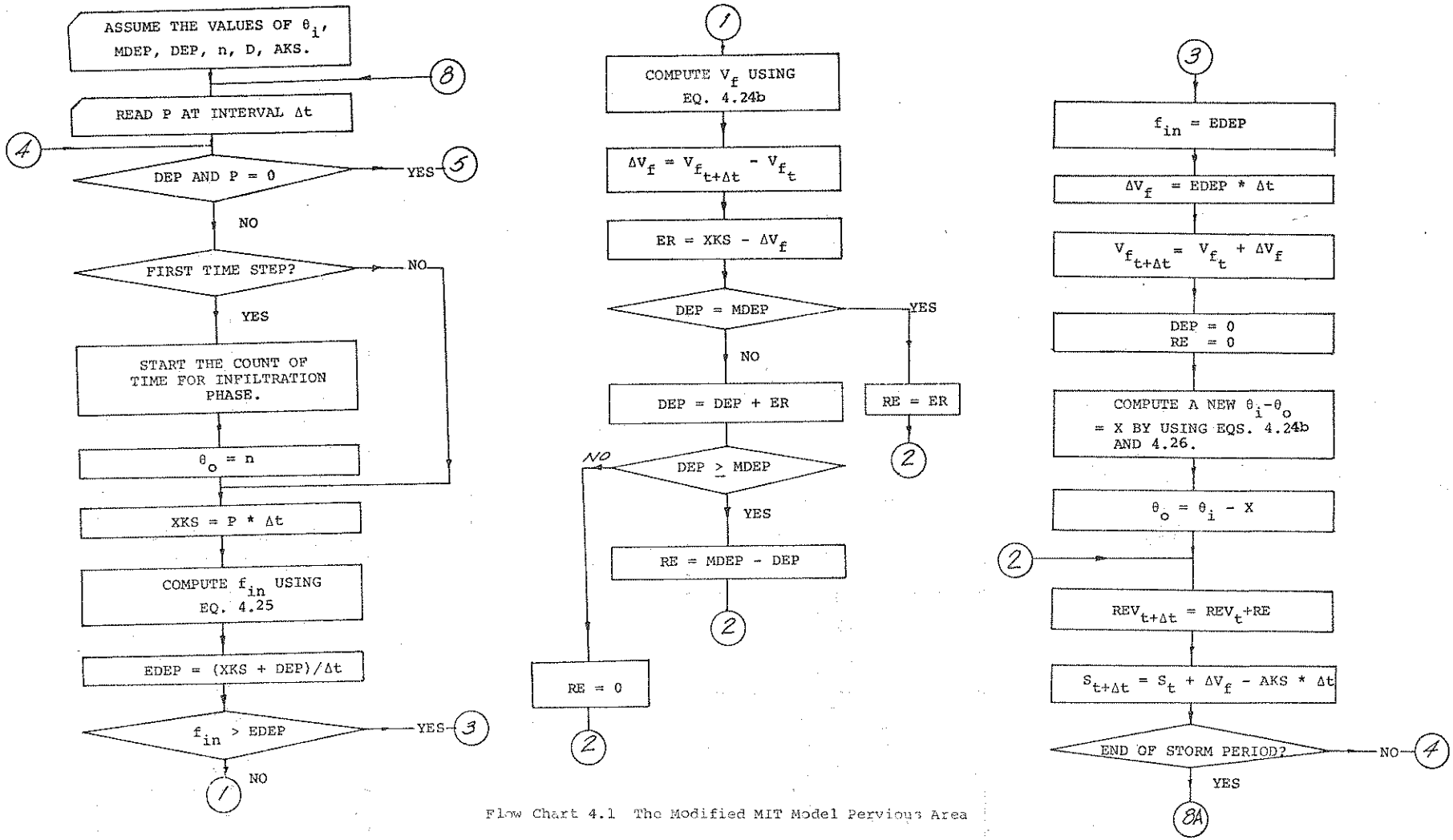

Flow Chart 4.1 The Modified MIT Model Pervious Area

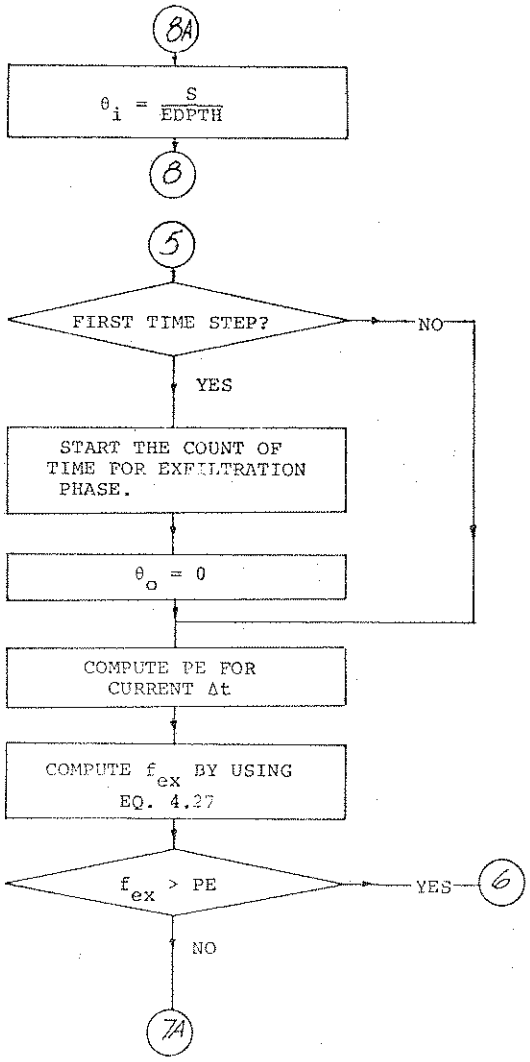
8A
$\theta_i = \frac{S}{EDPTH}$
8
5
FIRST TIME STEP?
NO
YES
START THE COUNT OF TIME FOR EXFILTRATION PHASE.
$\theta_o = 0$
COMPUTE PE FOR CURRENT Δt
COMPUTE f_{ex} BY USING EQ. 4.27
$f_{ex} > PE$
YES
6
NO
7A

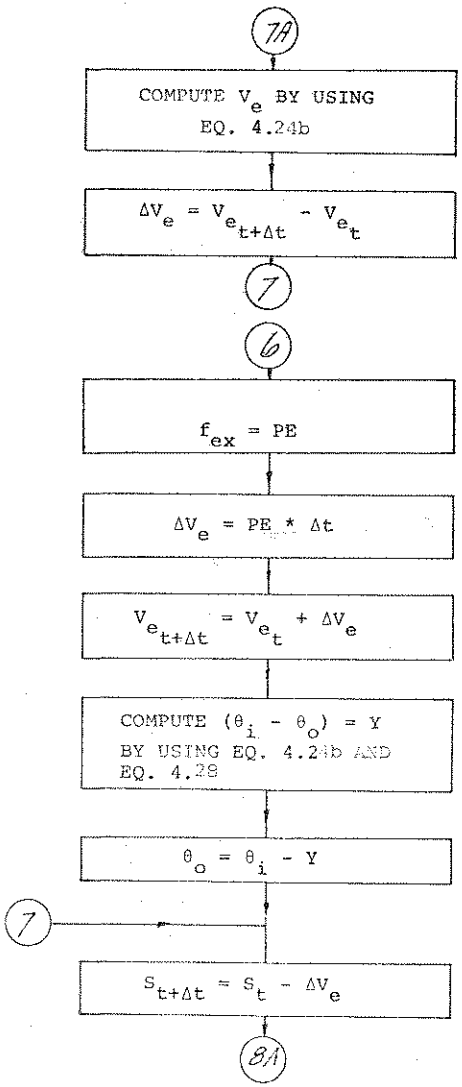
7A
COMPUTE V_e BY USING EQ. 4.24b
$\Delta V_e = V_{e_{t+\Delta t}} - V_{e_t}$
7
6
$f_{ex} = PE$
$\Delta V_e = PE * \Delta t$
$V_{e_{t+\Delta t}} = V_{e_t} + \Delta V_e$
COMPUTE $(\theta_i - \theta_o) = Y$ BY USING EQ. 4.24b AND EQ. 4.28
$\theta_o = \theta_i - Y$
7
$S_{t+\Delta t} = S_t - \Delta V_e$
8A

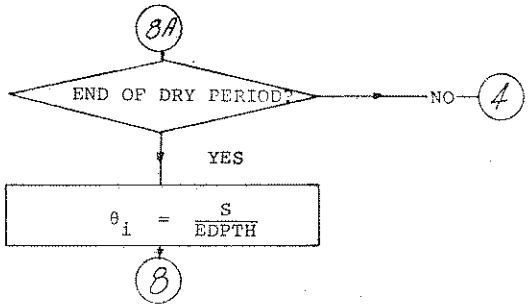
8A
END OF DRY PERIOD?
NO
4
YES
$\theta_i = \frac{S}{EDPTH}$
8

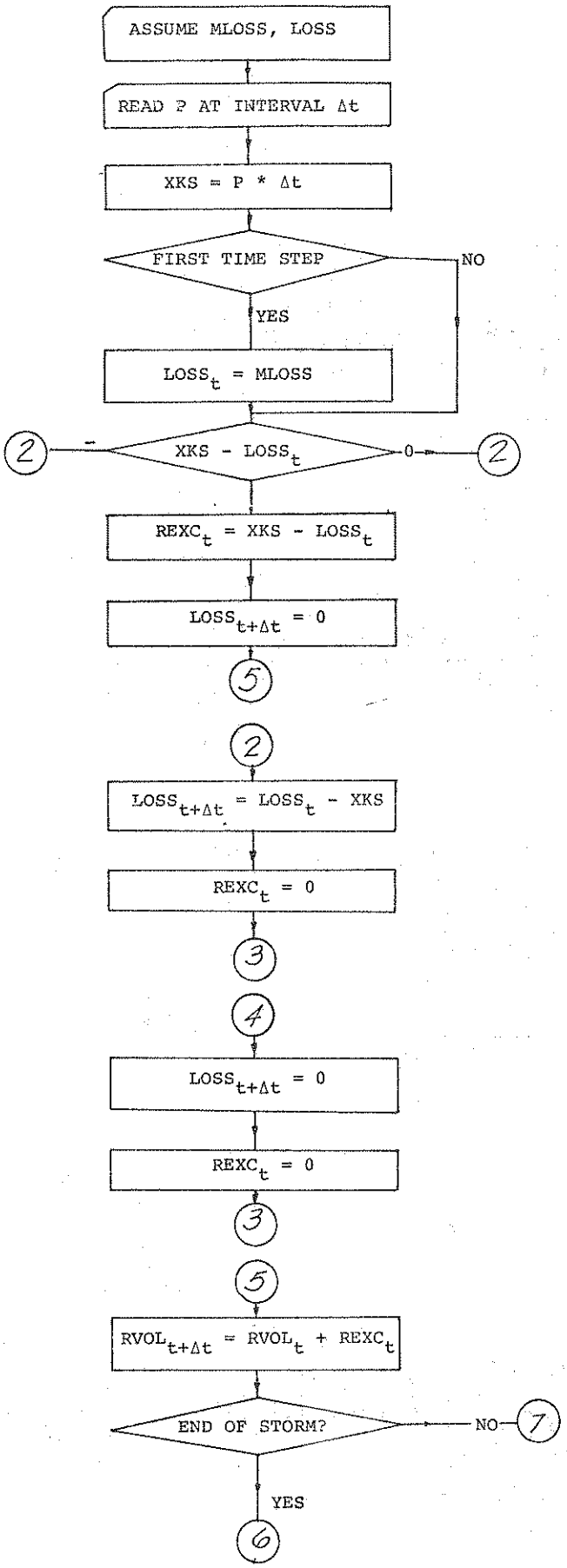

Flow Chart 4.2 The Modified MIT Model - Impervious Area

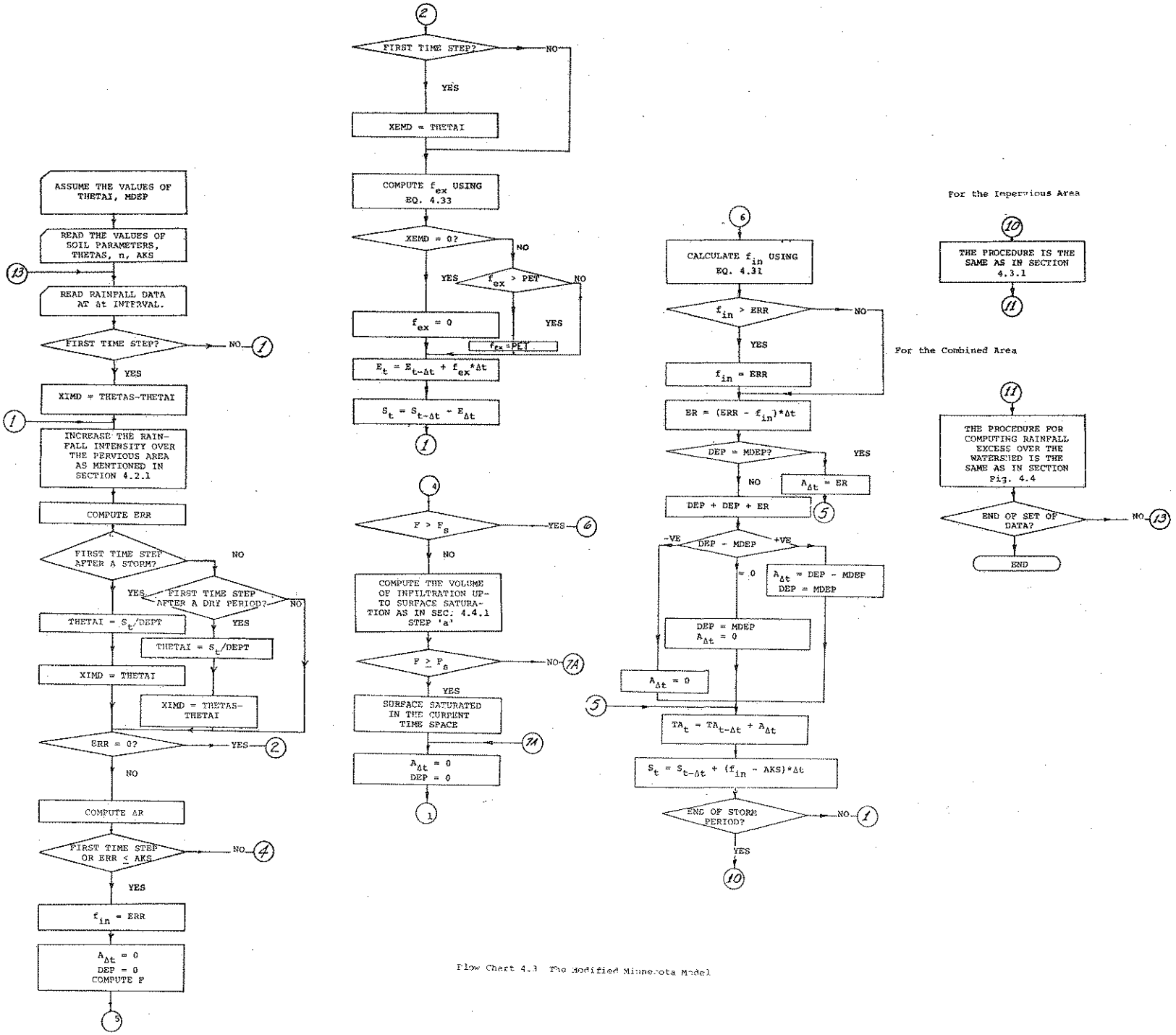

Flow Chart 4.3 The Modified Minnesota Model

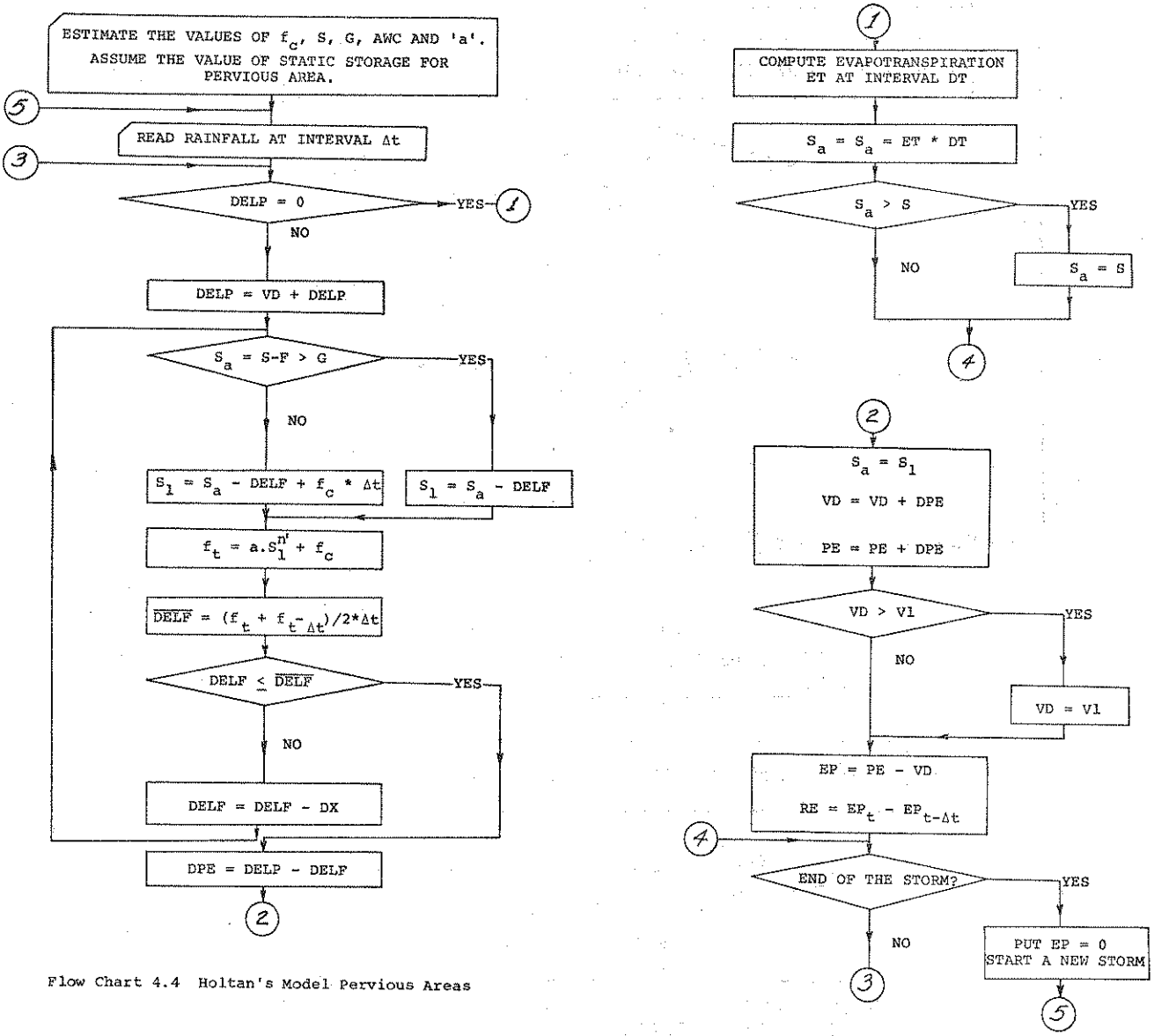

Flow Chart 4.4 Holtan's Model Pervious Areas

The flow chart for the impervious area is the same as Flow Chart 4.2.

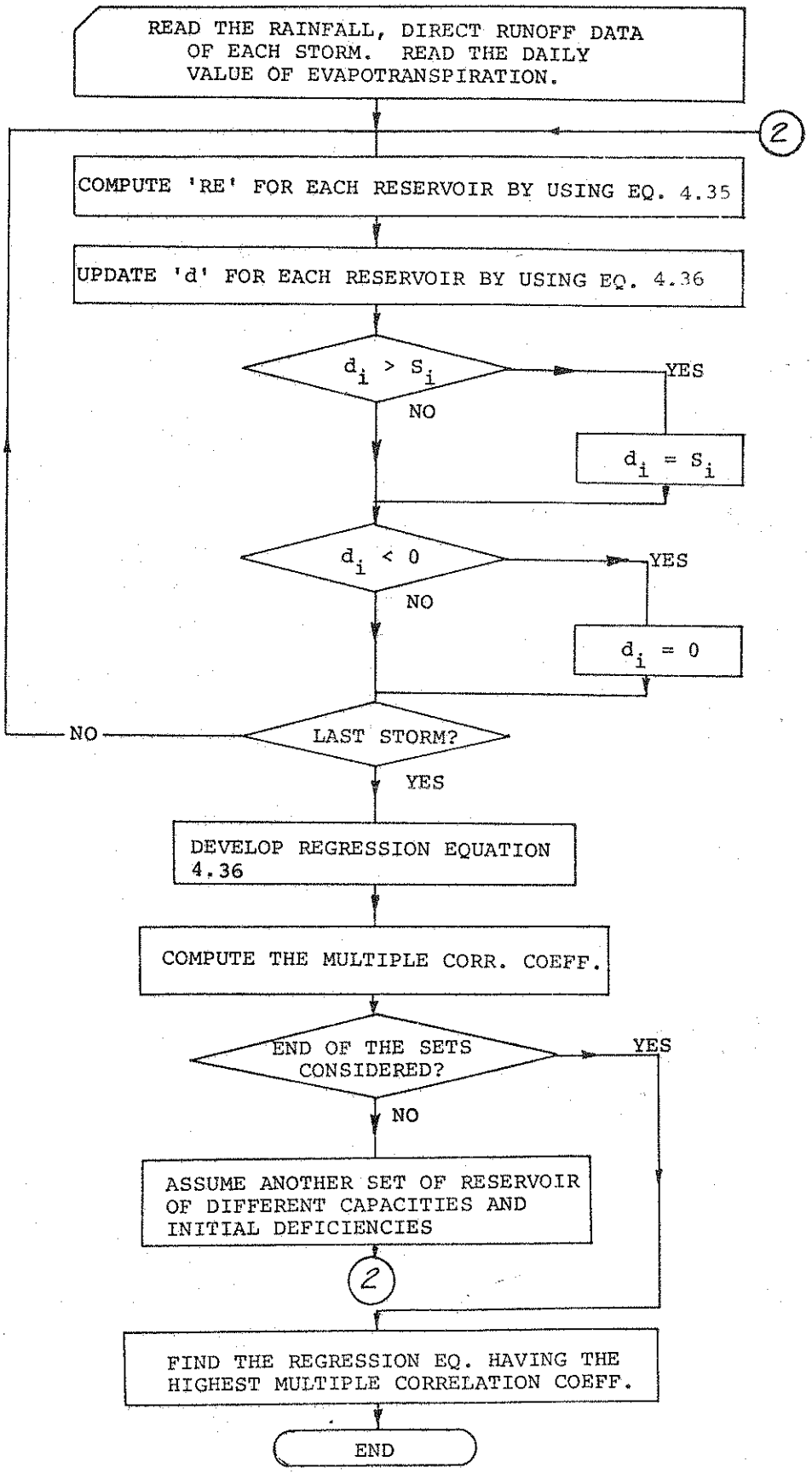

Flow Chart 4.5 Multicapacity Basin Accounting Model

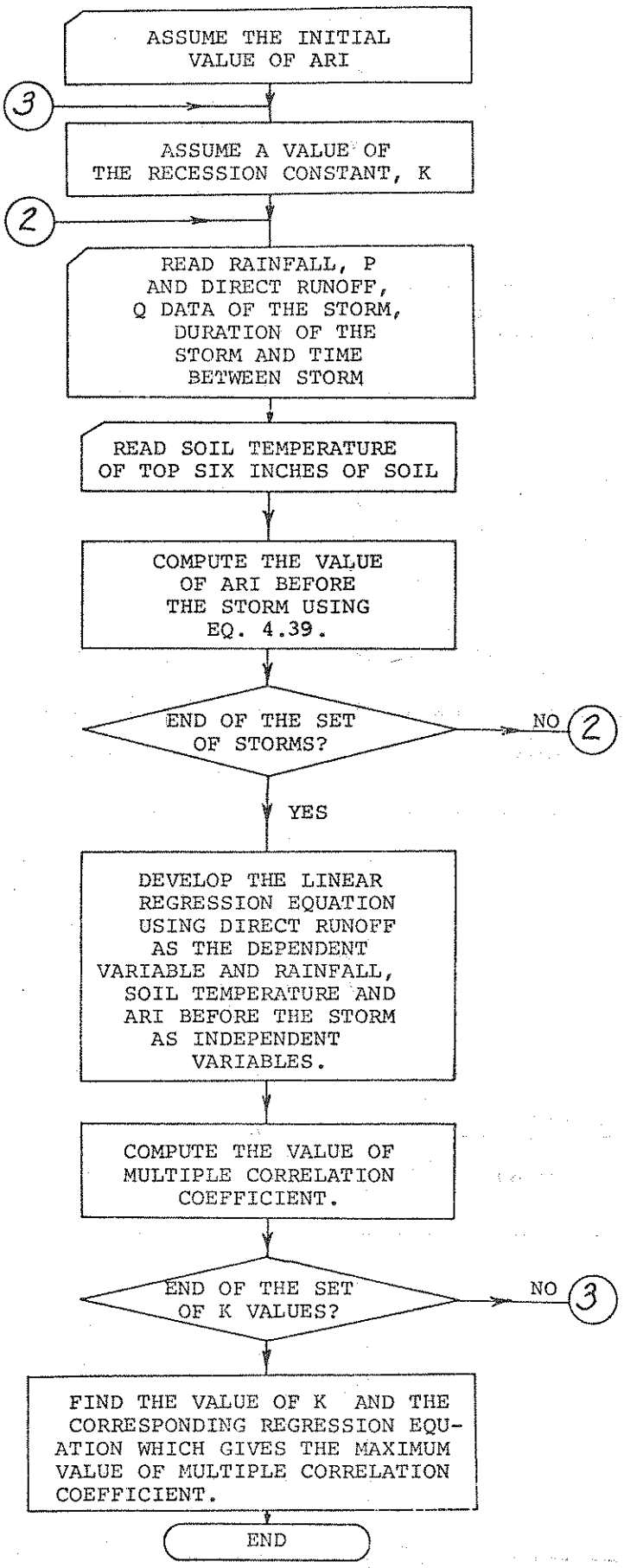

Flow Chart 4.6 Antecedent Retention Index Model

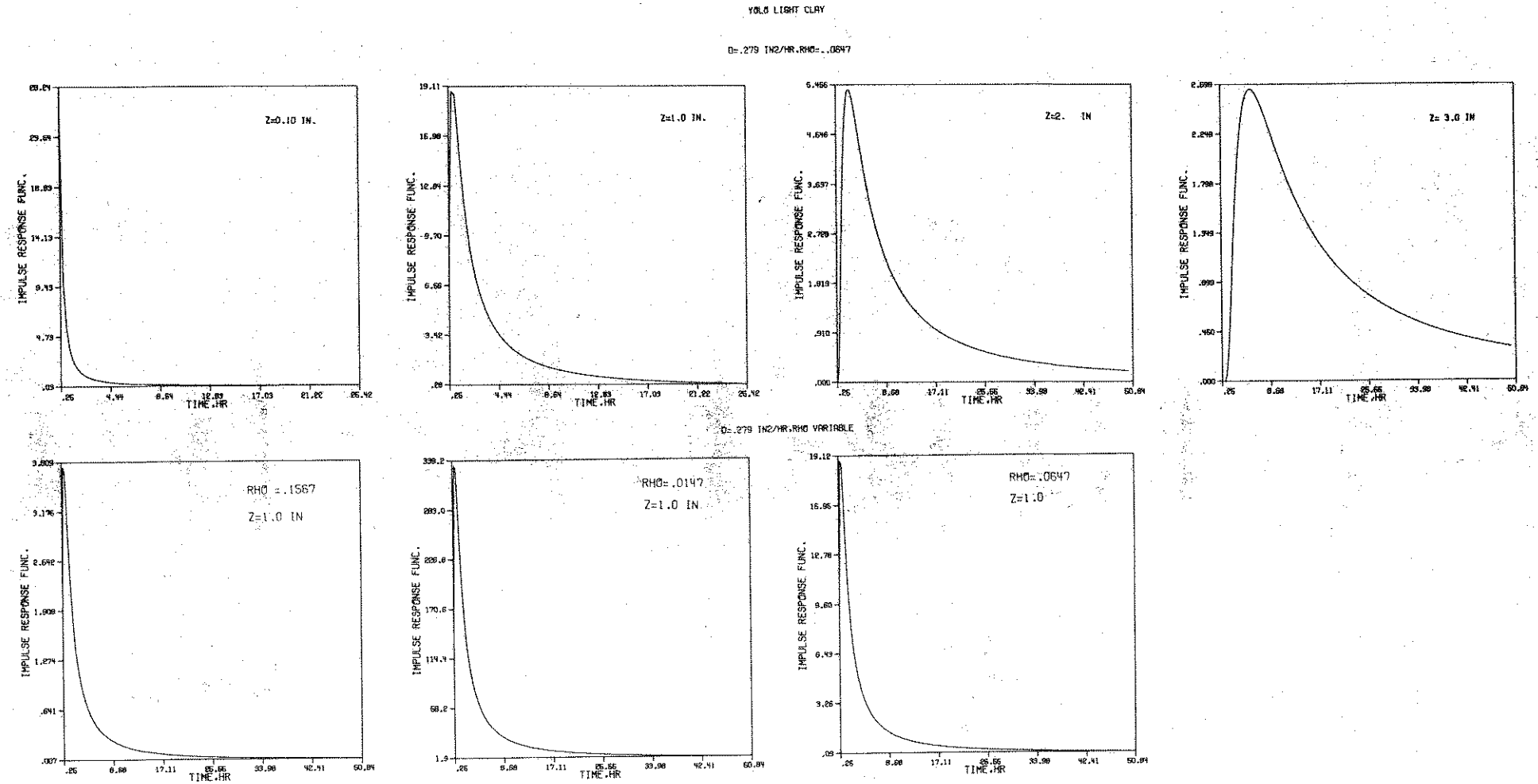

FIGURE 4.1 IMPULSE RESPONSE FUNCTIONS FOR DIFFERENT VALUES OF THE PARAMETERS

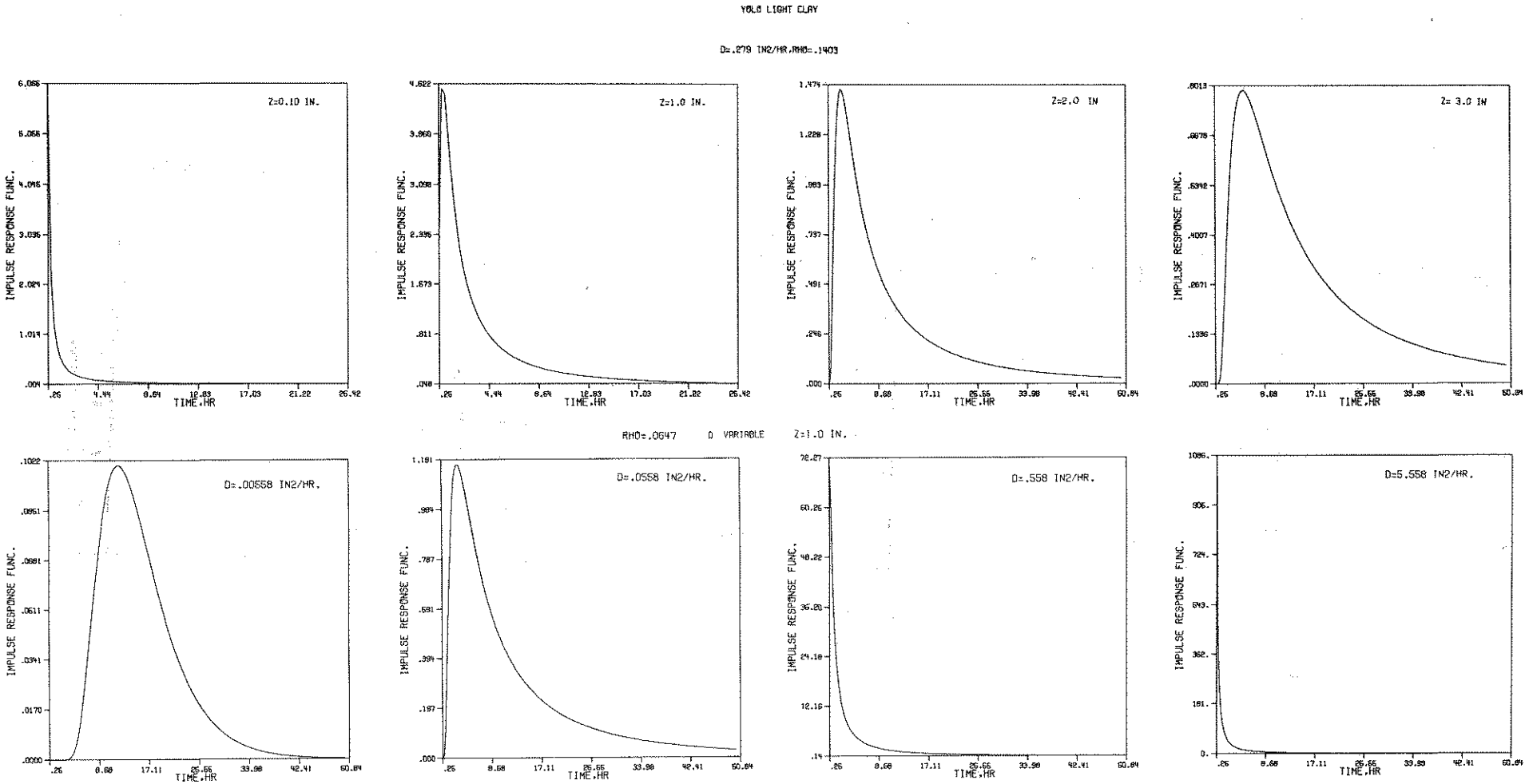

FIGURE 4.1 , CONT.

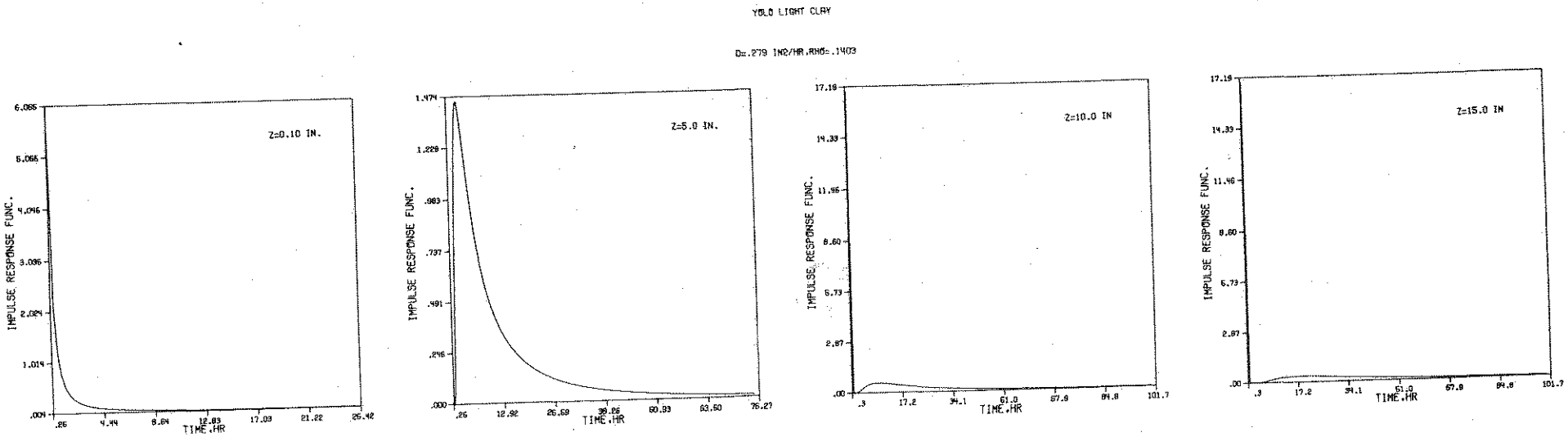

FIGURE 4.1 . CONT.

YOLO LIGHT CLAY

VARIATION OF INFILTRATION RATE WITH CHANGE IN INITIAL MOISTURE CONTENT

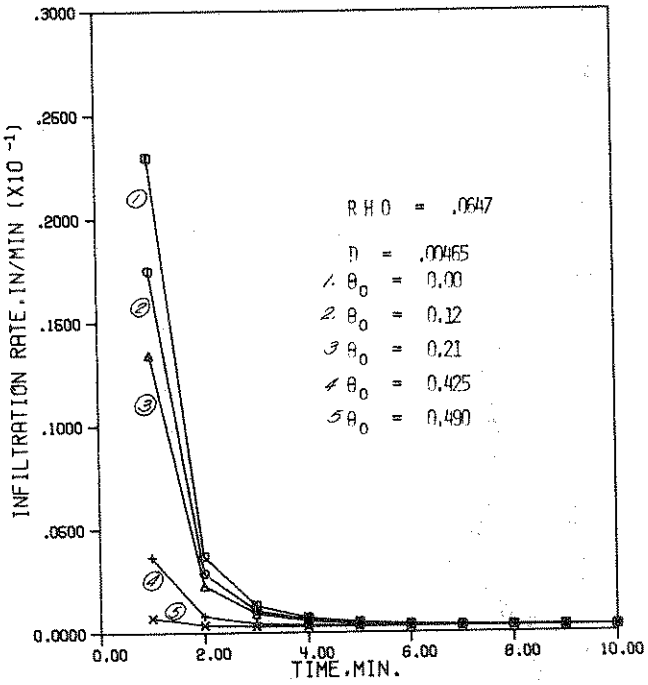

VARIATION OF INFILTRATION RATE WITH CHANGE IN VALUES OF DIFFUSIVITY

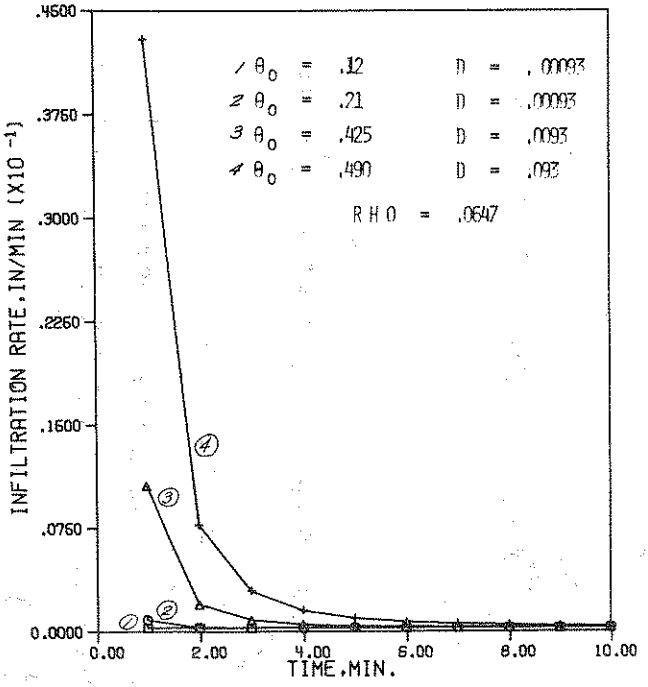

HYDRAULIC CONDUCTIVITY, K IN MIN^{-1} DIFFUSIVITY, D IN IN^2 MIN^{-1}

INITIAL MOISTURE, θ_o POROSITY = 0.499 K = .00029

VARIATION OF INFILTRATION RATE WITH CHANGE IN VALUES OF RHO

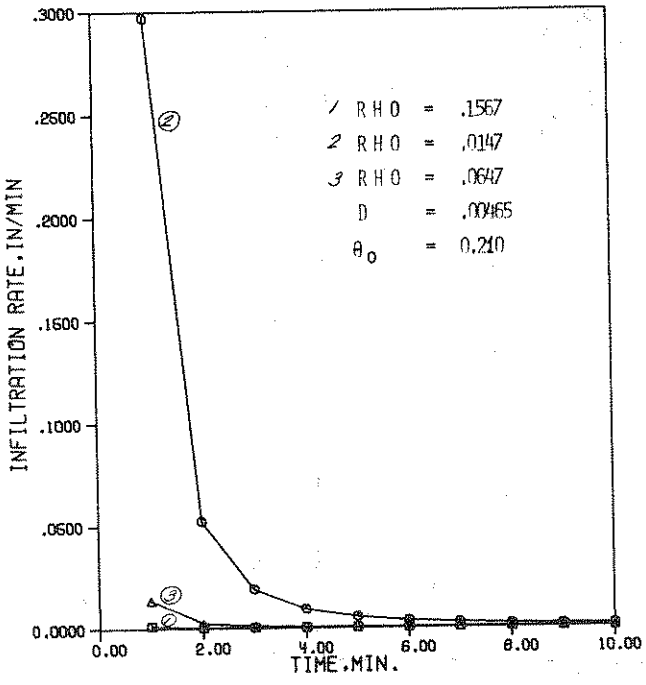

VARIATION OF INFILTRATION RATE WITH CHANGE IN VALUES OF DIFFUSIVITY

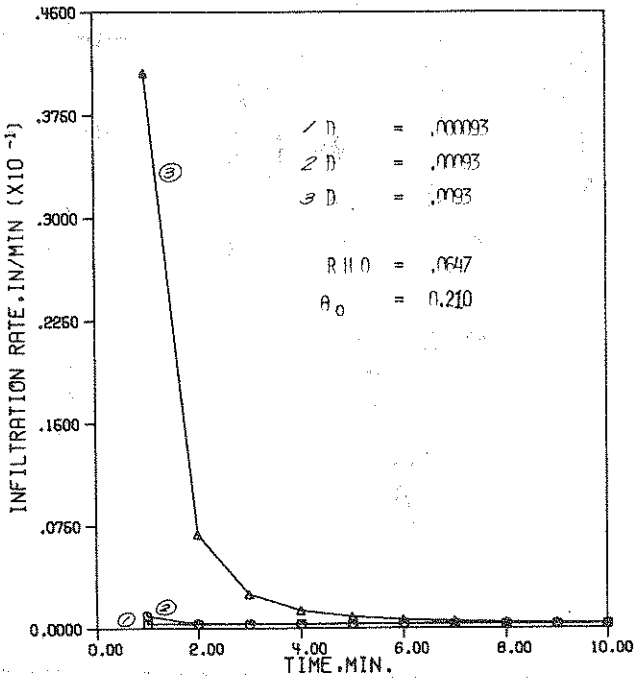

FIGURE 4.2 INFILTRATION CAPACITY FOR DIFFERENT VALUES OF THE PARAMETERS

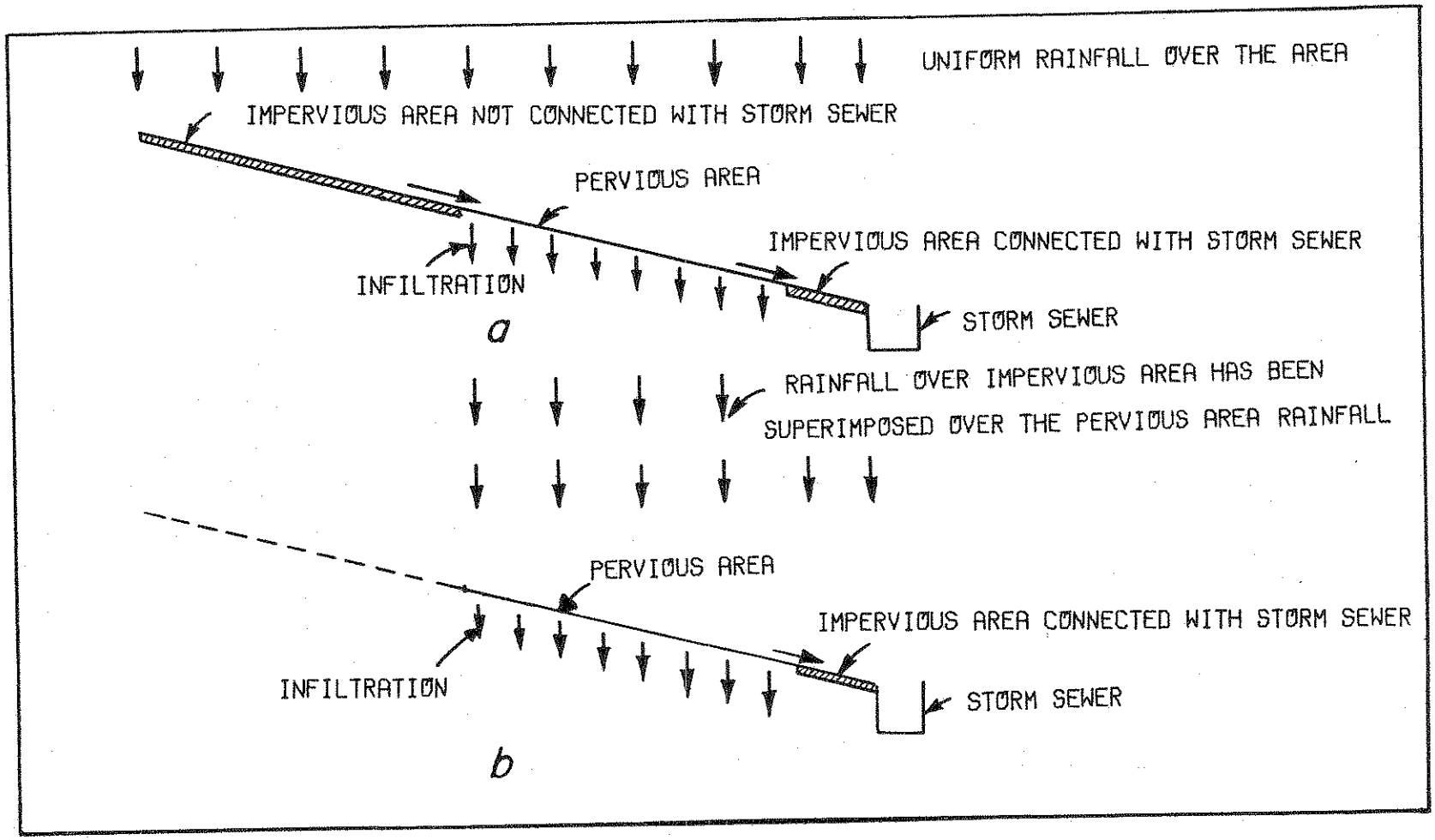

FIGURE 4.3 DEFINITION SKETCH OF URBAN RUNOFF

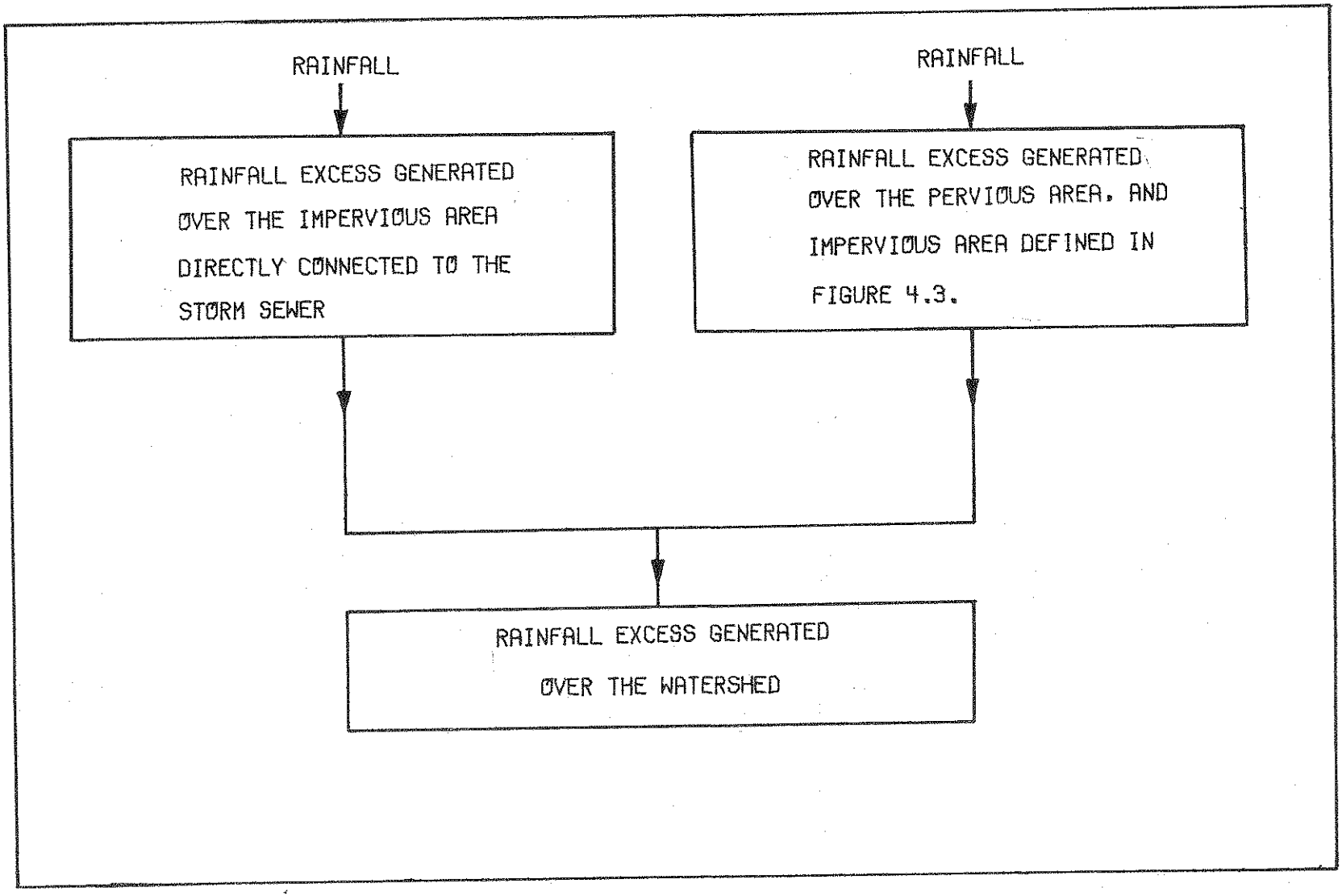

FIGURE 4.4 COMPONENTS OF RAINFALL EXCESS ON AN URBAN WATERSHED

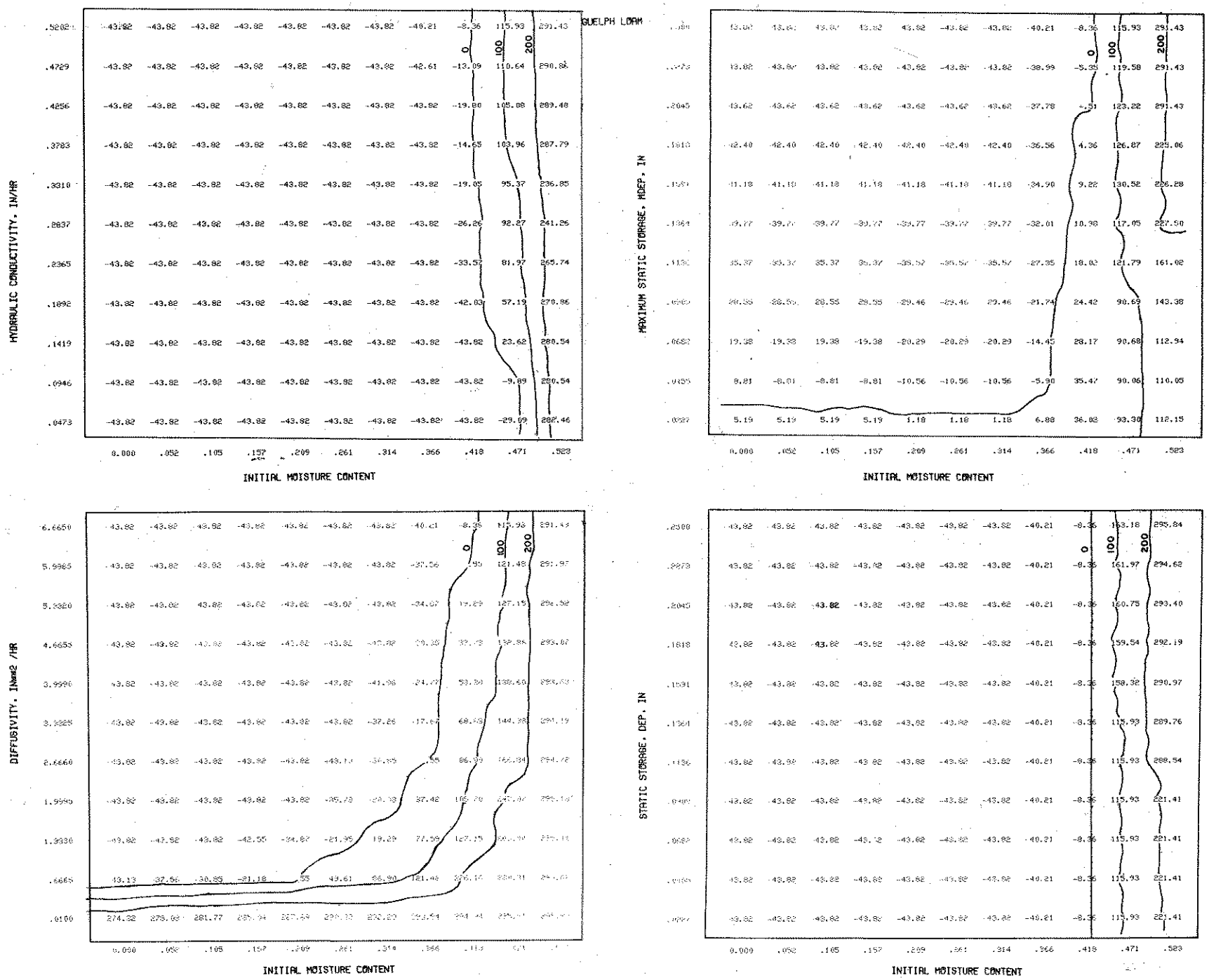

FIGURE 4.5A SENSITIVITY ANALYSIS OF PARAMETERS OF MODIFIED MIT MODEL

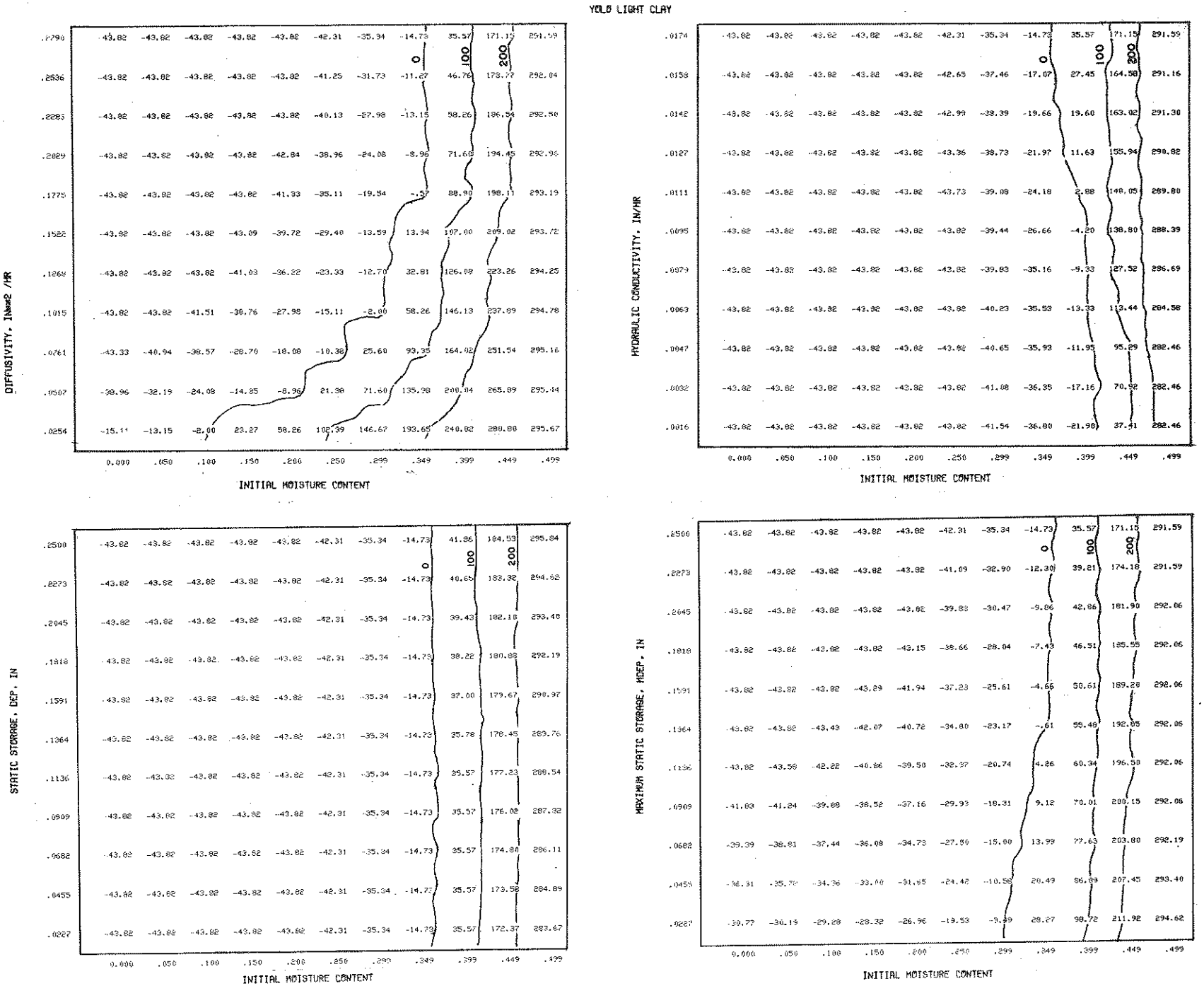

FIGURE 4.5B SENSITIVITY ANALYSIS OF PARAMETERS OF MODIFIED MIT MODEL

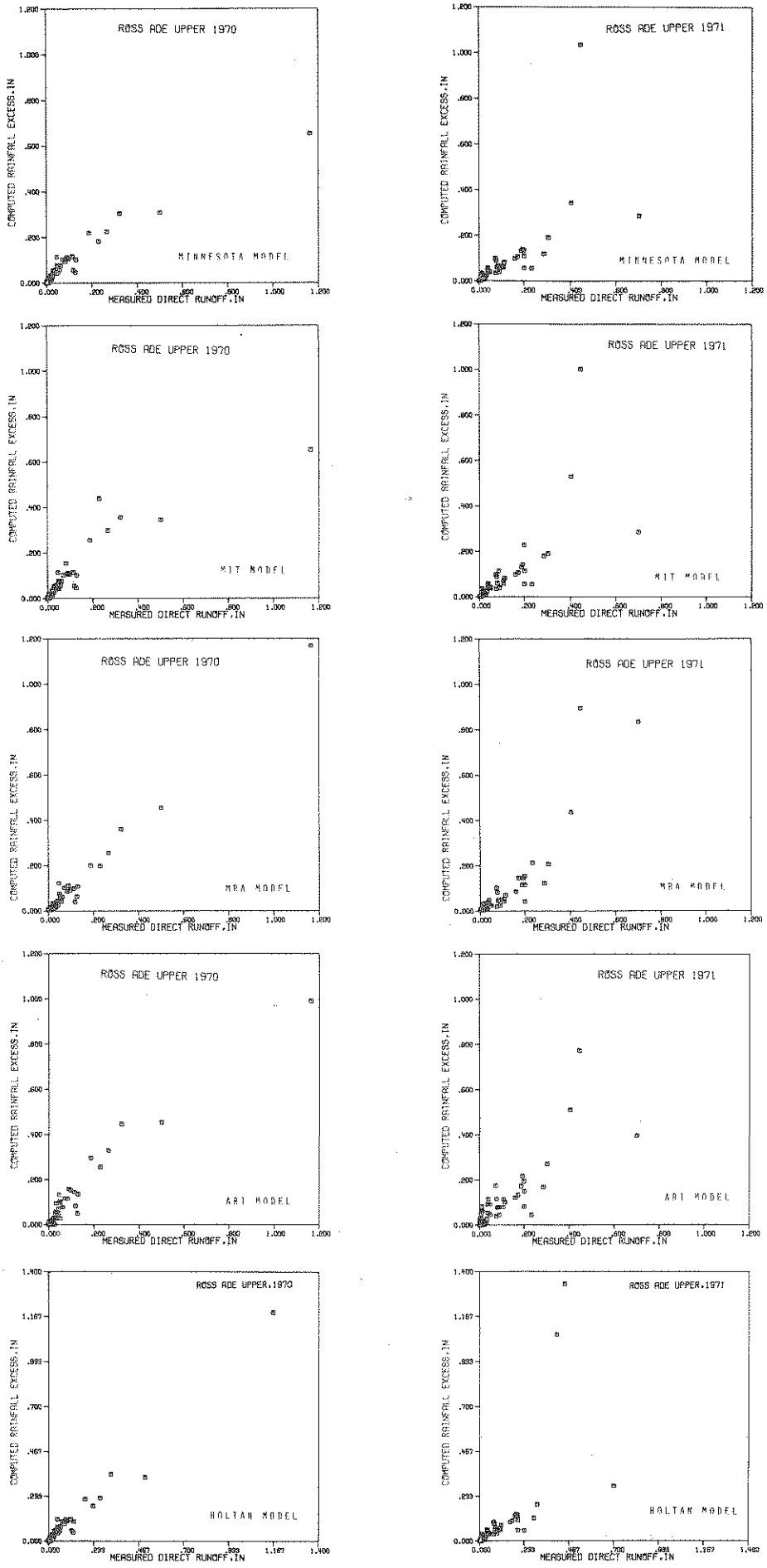

FIGURE 4.6 SCATTER DIAGRAMS OF COMPUTED RAINFALL EXCESS VS MEASURED DIRECT RUNOFF

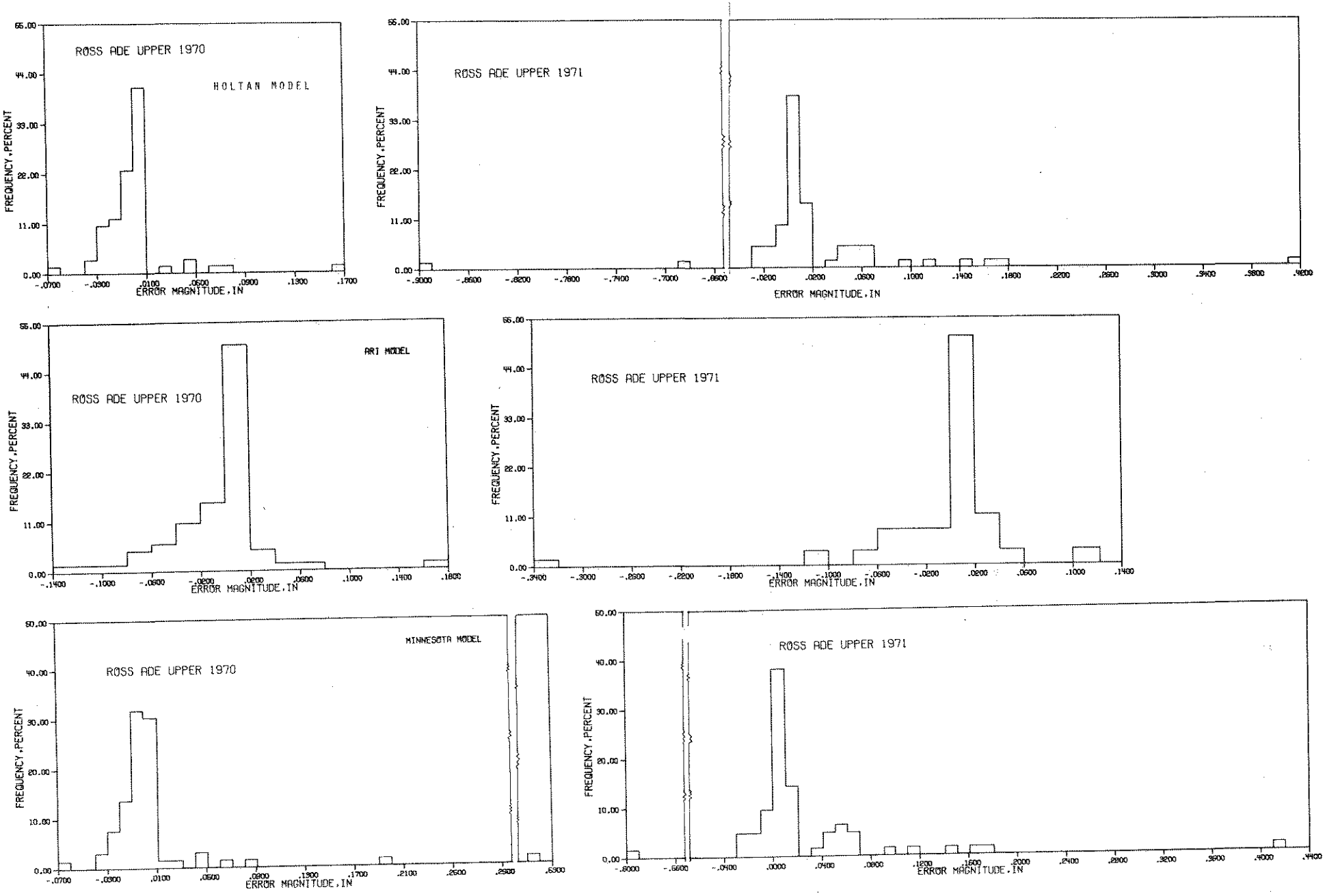

FIGURE 4.7 DISTRIBUTION OF ERROR

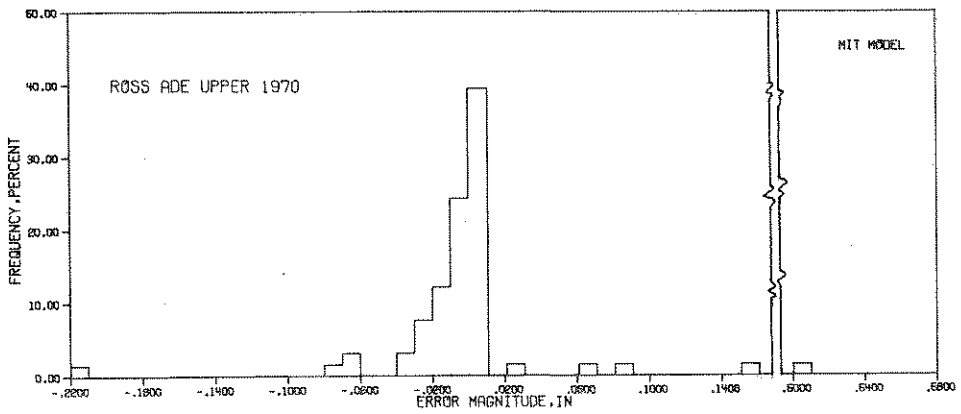

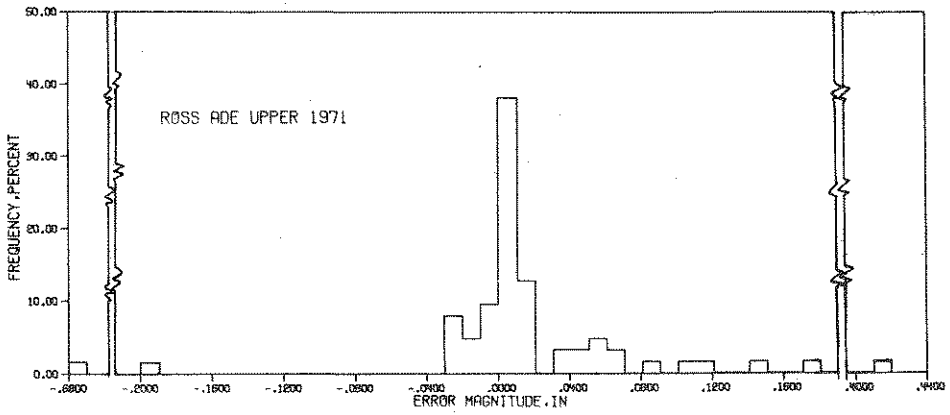

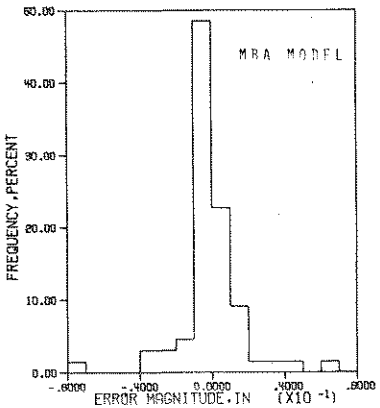

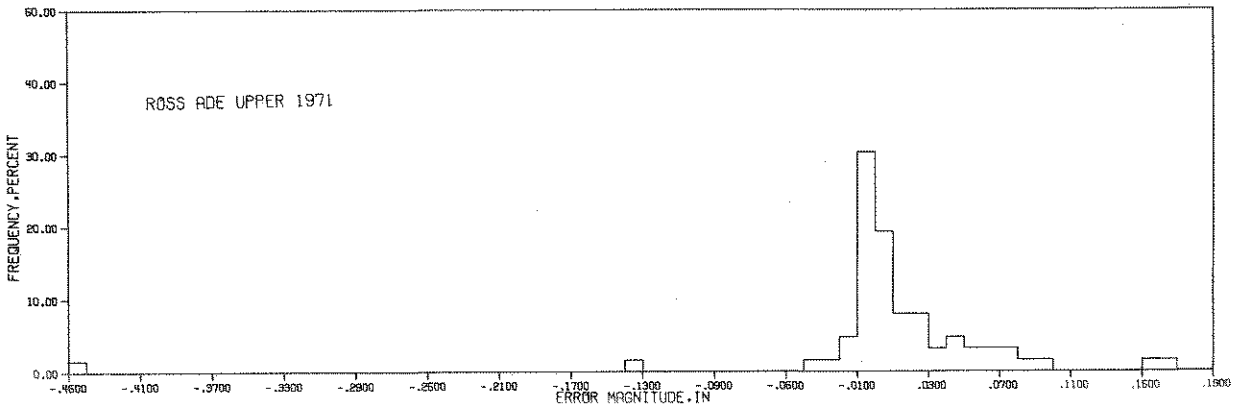

FIGURE 4.7 , CONT.

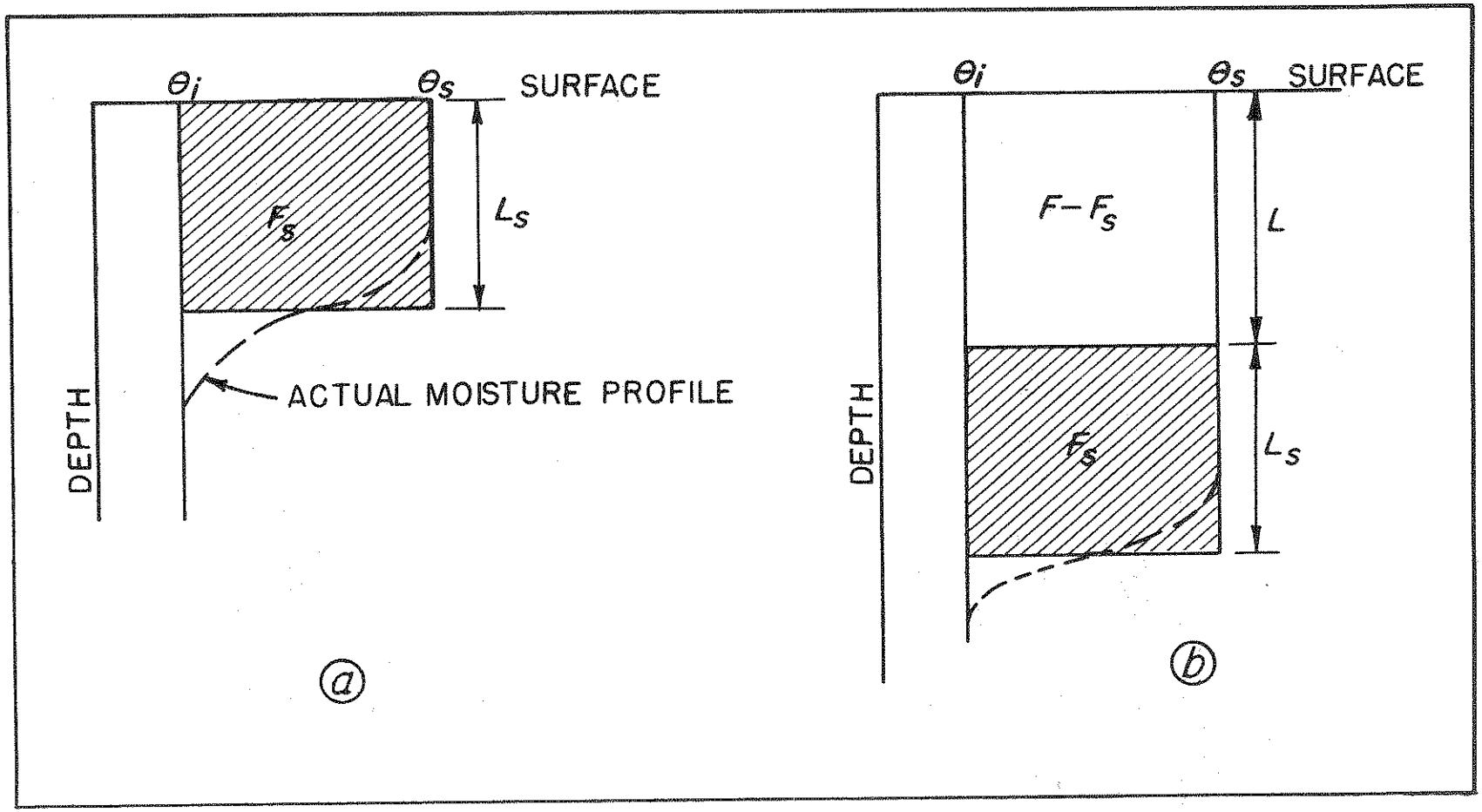

FIGURE4.8 *a* HYPOTHETICAL MOISTURE CONTENT PROFILE AT THE TIME OF SURFACE SATURATION
b MOISTURE CONTENT PROFILE FOR DERIVATION OF EQ.4.31

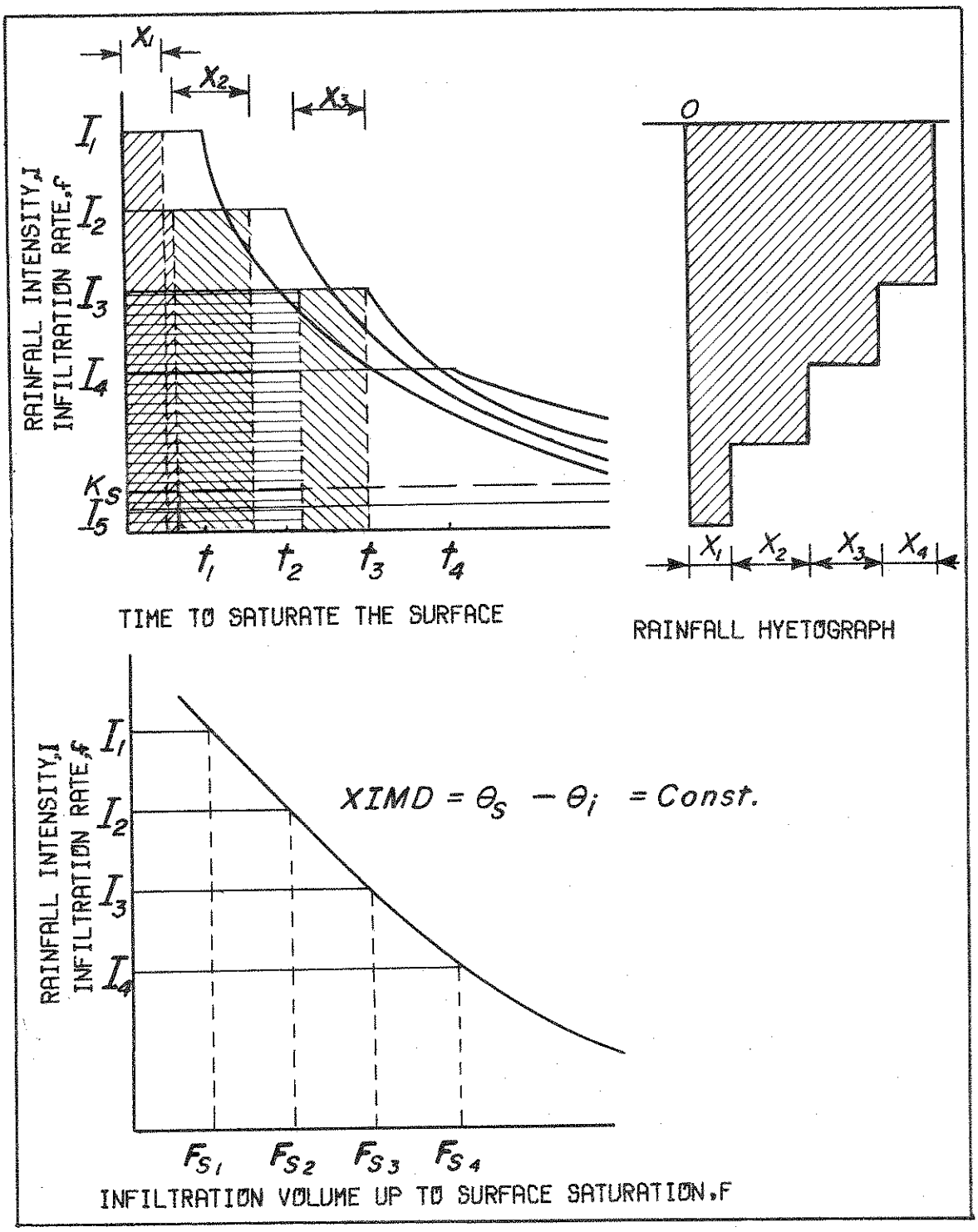

FIGURE 4.9 DEFINITION SKETCH FOR SURFACE SATURATION.

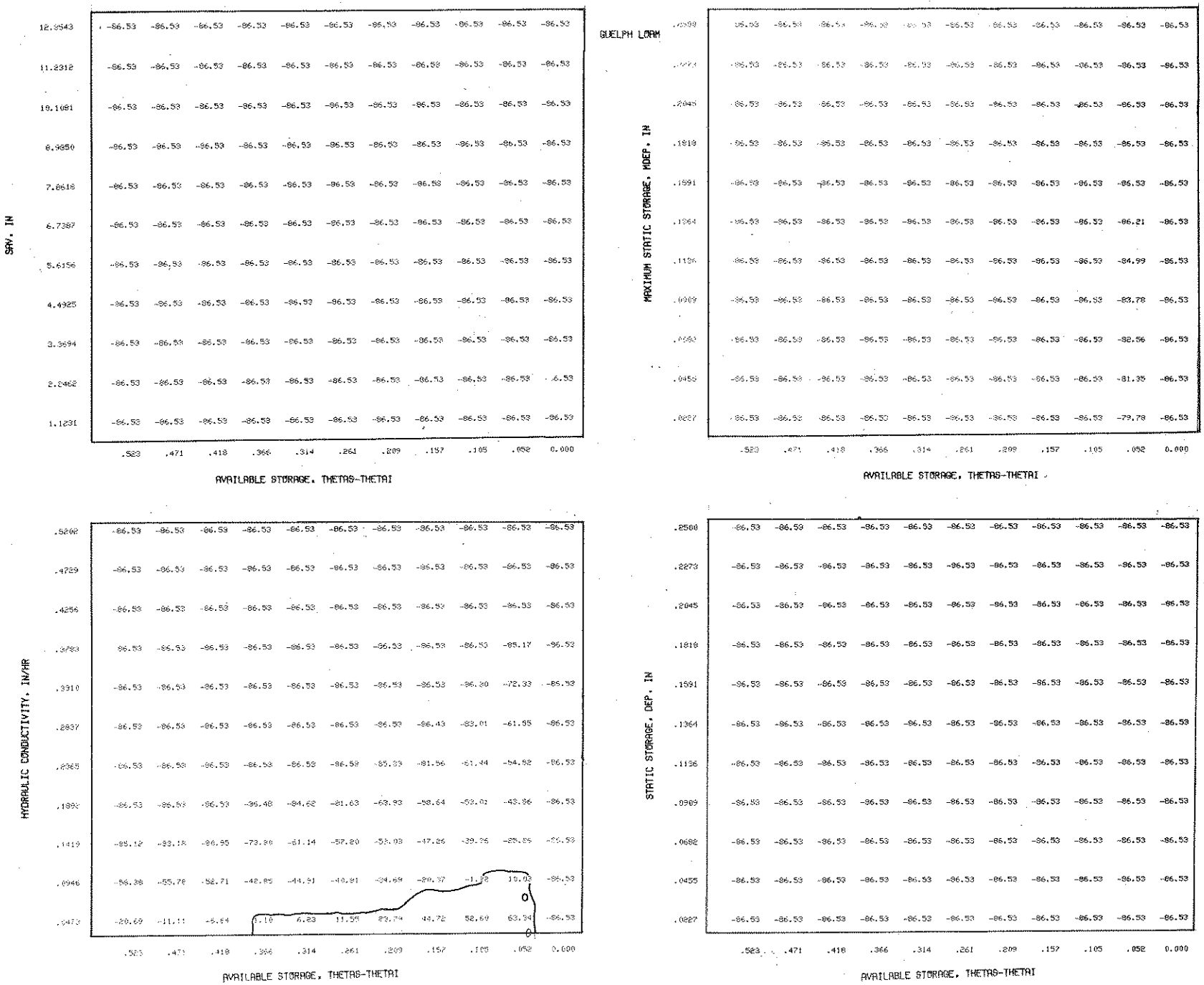

FIGURE 4.10 SENSITIVITY ANALYSIS OF PARAMETERS OF MODIFIED MINNESOTA MODEL

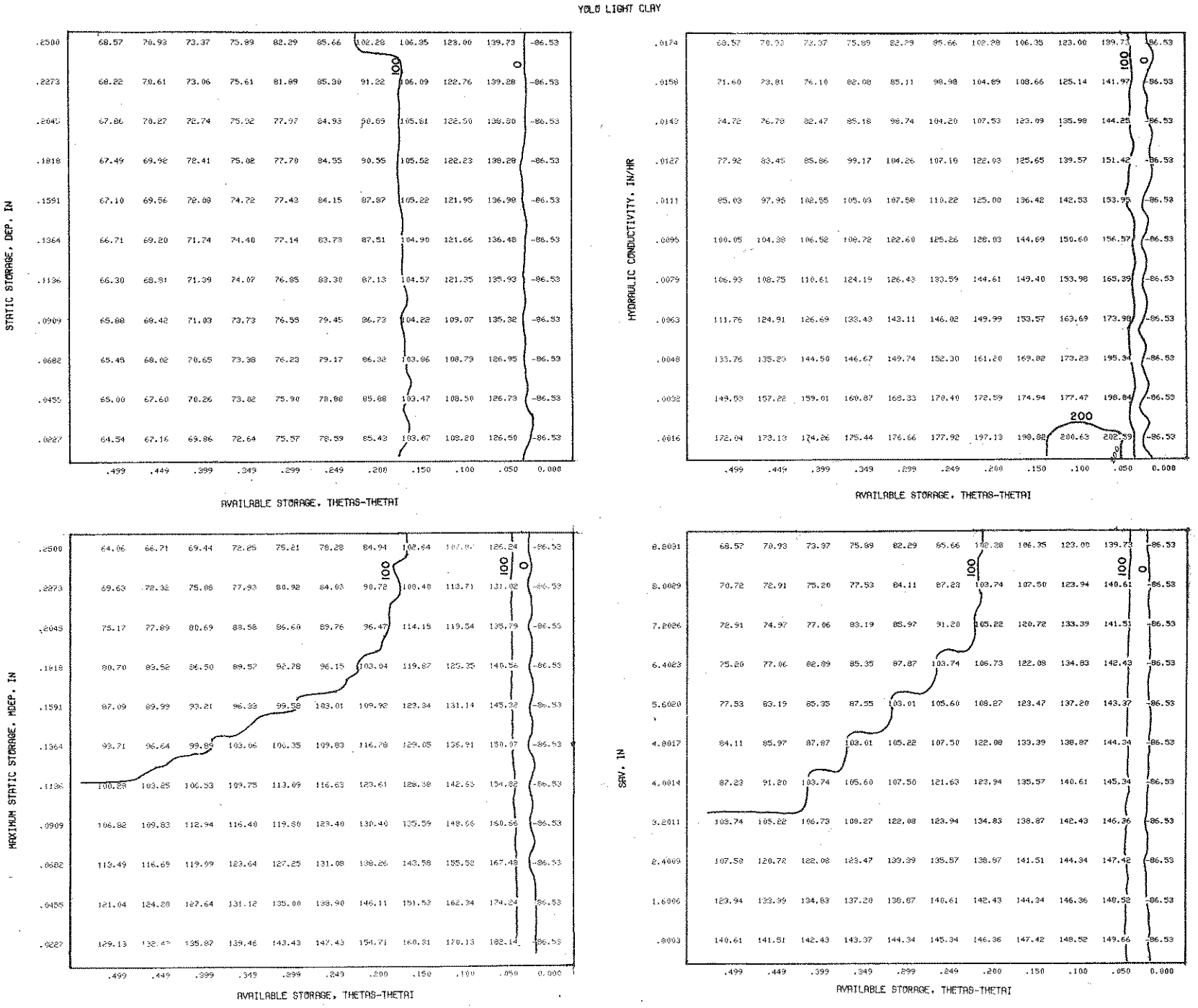

FIGURE 4.11 SENSITIVITY ANALYSIS OF PARAMETERS OF MODIFIED MINNESOTA MODEL

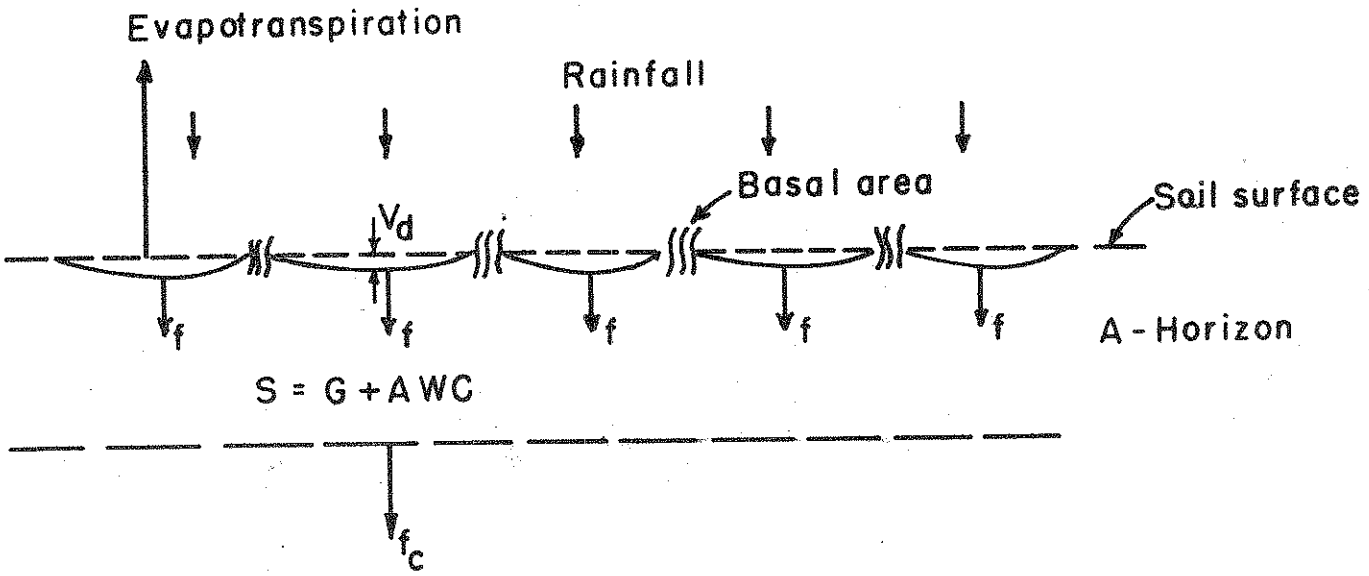

FIGURE 4.12 A DEFINITION SKETCH OF HOLTAN MODEL

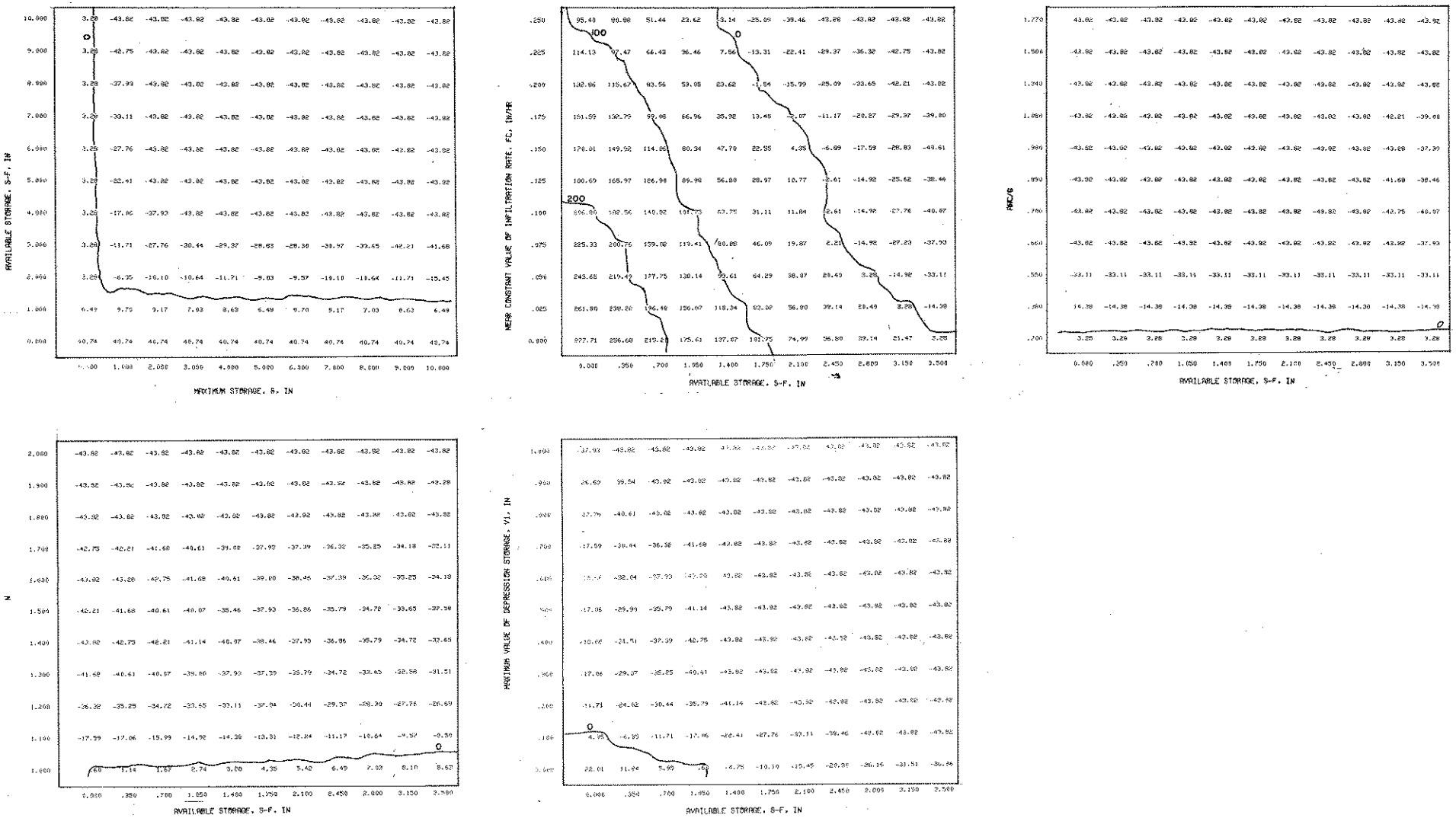

FIGURE 4.12B SENSITIVITY ANALYSIS OF PARAMETERS OF MODIFIED HOLTAN MODEL

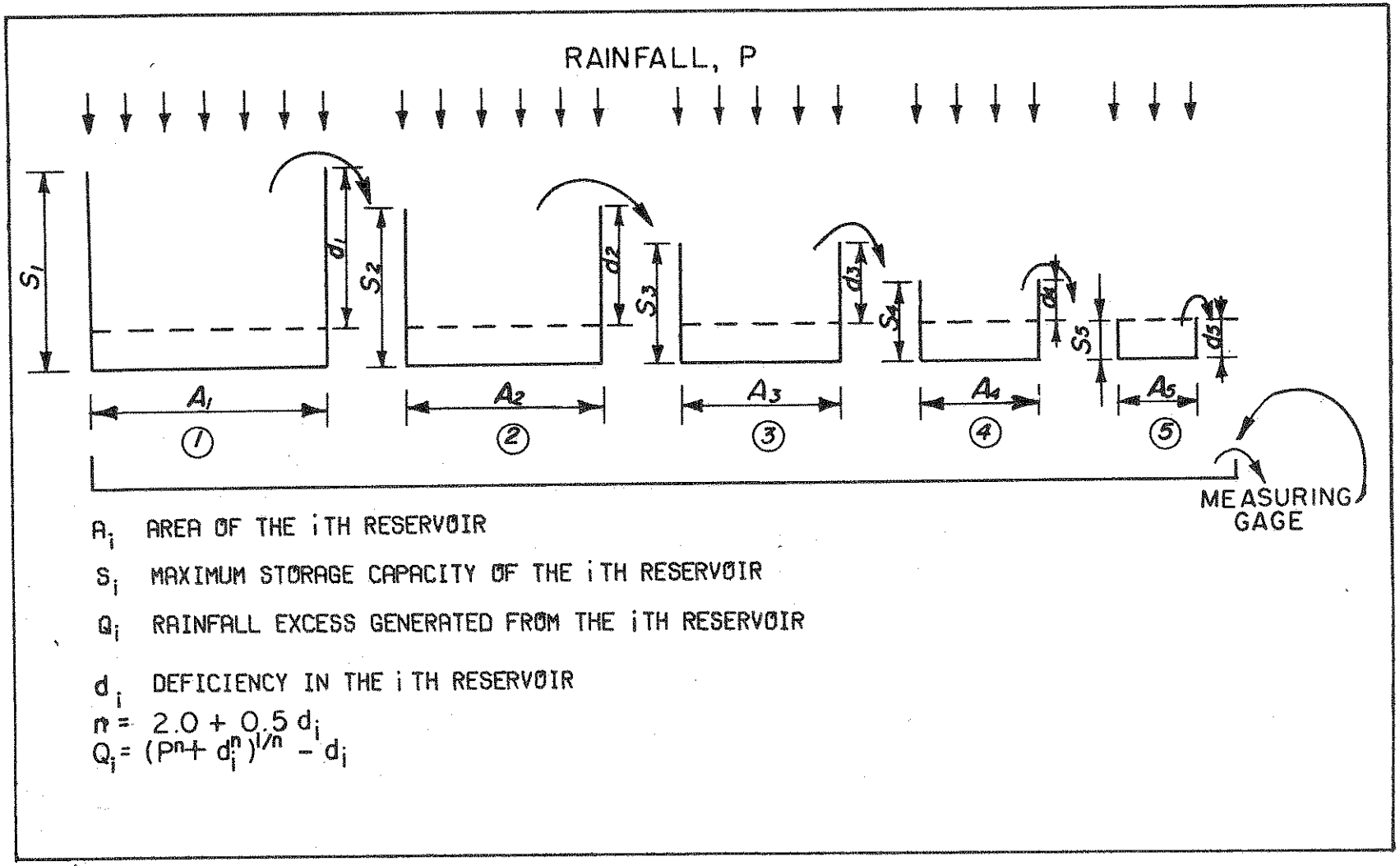

FIGURE 4.13 DEFINITION SKETCH OF THE CONCEPTUAL MODEL

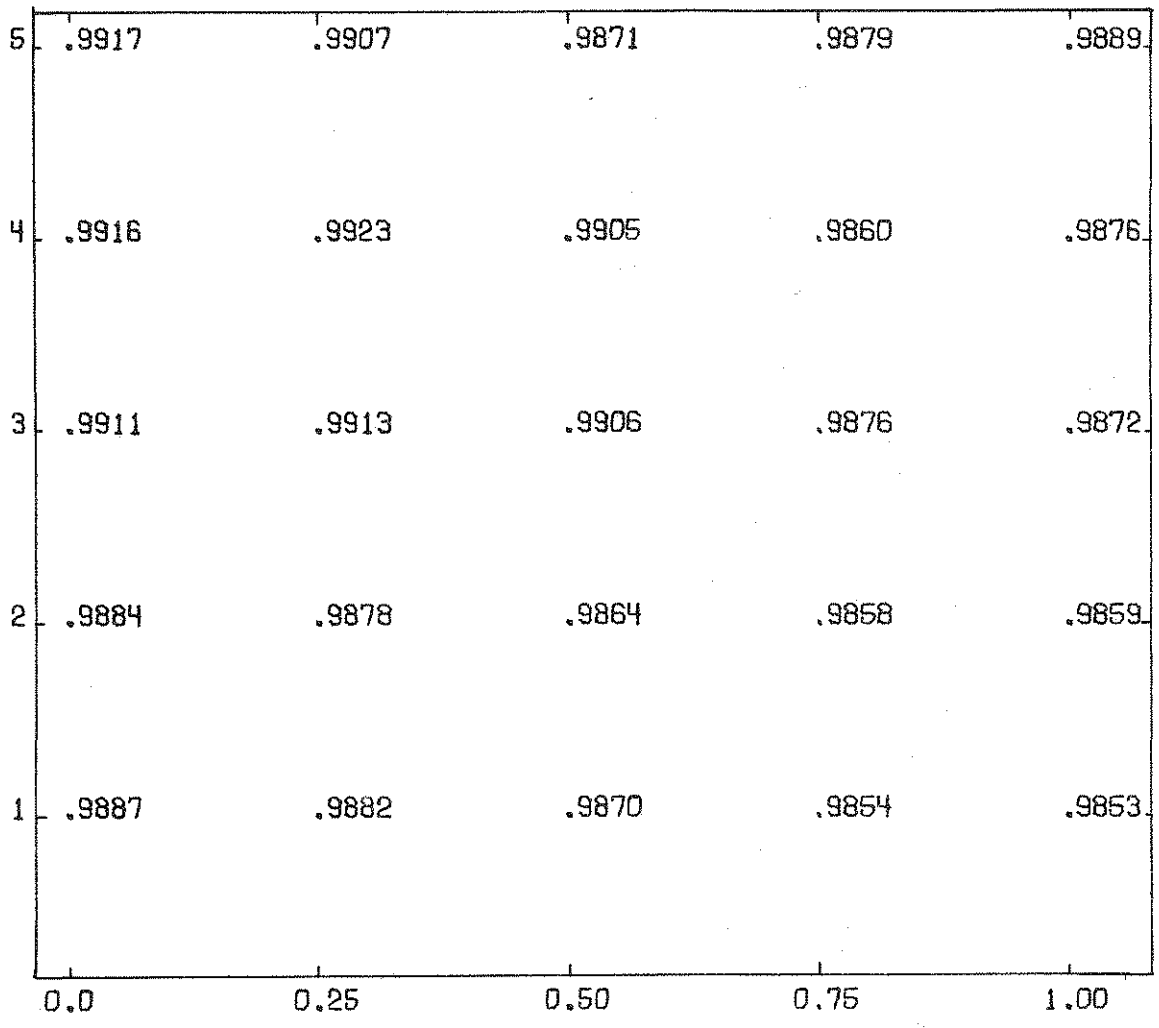

FIGURE 4.14 VARIATION OF MULTIPLE CORR.COEFF.WITH CHANGES IN S AND DEF./MAX. STORAGE

5. ESTIMATION OF DIRECT RUNOFF FROM RAINFALL EXCESS

Direct runoff may be estimated from rainfall excess by using deterministic or stochastic models which may be linear or nonlinear. In the present study, deterministic linear and nonlinear models were used to estimate the direct runoff from rainfall excess. The linear model based on the instantaneous unit hydrograph theory will be discussed first. An exploratory study of a nonlinear model is taken up next, which is followed by a general discussion of both types of models.

5.1 Linear System Approach

The relationship between the input (rainfall excess), $x(t)$, and the output (direct runoff), $y(t)$ is given by the convolution integral (eq. 5.1) when the rainfall excess-direct runoff process is considered as a lumped linear system. In eq. 5.1, $h(t)$ is the kernel function or the instantaneous unit hydrograph (IUH). Several different methods are available to estimate the IUH from rainfall excess and direct runoff data. The Fourier transform method of determination of the IUH which was used in the present study is discussed in detail by Blank et al. (5.1) and Rao and Delleur (5.2). It is sufficient to note for purposes at hand that the impulsive response function $h(t)$ is given by eq. 5.2, where $H(\omega)$ is the Fourier transform of $h(t)$. However, some problems arise in the determination of the IUH when the sampling intervals, Δt, are small. Examples of these problems are the selection of optimum time step to estimate the IUH and the presence of oscillatory kernels. Some of these problems and the methods used to overcome them are discussed below. The use of the kernel functions to predict the direct runoff and the effects of urbanization on the IUH and on the direct runoff are discussed in the following sections.

The basic mathematical relationships governing lumped linear systems are:

$$y(t) = \int_0^t x(t)\, h(t-\tau)\, d\tau \tag{5.1}$$

$$h(t) = \frac{1}{2\pi} \int_{-\infty}^{\infty} H(\omega)\, e^{j\omega t}\, d\omega \; ; \; H(\omega) = R_h(\omega) + j\, X_h(\omega) = \frac{Y(\omega)}{X(\omega)} \tag{5.2}$$

Amplitude of $H(\omega) = [R_h^2(\omega) + X_h^2(\omega)]^{1/2}$ (shown as AMPLITUDE in fig. 5.1), where $X(\omega)$ and $Y(\omega)$ are the Fourier transforms of $x(t)$ and $y(t)$, respectively; and $R_h(\omega)$ and $X_h(\omega)$ are the real and imaginary parts of $H(\omega)$.

5.1.1 Selection of Optimal Time Step

A numerical experiment was conducted to determine the appropriate time step, Δt, at which the rainfall excess and the direct runoff values must be sampled. The experiment consisted of an examination of the variations in the line spectra of the kernel functions and of the regeneration performance. The rainfall excess and the direct runoff values were sampled at 15, 10, 8, 6, 4, 2 and 1 minute intervals. The corresponding Fourier line spectra, the IUH, and the original and regenerated hydrographs of the storm of April 20, 1970, on the Ross Ade watershed are shown in fig. 5.1. At large sampling intervals, Δt, the amplitude spectra of the response functions either do not decay to zero values near the Nyquist frequency, or they approach a constant value near the Nyquist frequency after attaining a large spurious peak value. As Δt decreases, the amplitude spectra approach zero value near the Nyquist frequency. The kernel functions are smooth for large ΔT values but oscillate increasingly with decreasing Δt values. The regeneration performance is not affected by the sampling interval.

The reasons for the presence of large spurious peaks in the line spectrum and the presence of large values near the Nyquist frequency obtained with large sampling intervals, Δt, can be explained by an examination of the amplitude spectra of the inputs and the outputs, a sample of which is shown in fig. 5.2. When $Y(\omega)$, the Fourier transform of the output, does not become zero but remains at a finite value, similar to the Fourier Transform of input $X(\omega)$, the Fourier transform of the IUH [$H(\omega) = Y(\omega)/X(\omega)$] can take large values. Such is the case in figs. 5.1a, b, and c. This effect is reduced when the Δt values are small, although at small values of Δt the noise in the data creates oscillations in the kernel function as shown in figs. 5.1e, f and g. Since a sampling interval which does not introduce spurious peaks in the amplitude spectrum or which does not create oscillatory kernel functions is desirable, a sampling interval Δt of four minutes was

selected for the analysis of the data from the Ross Ade watershed.

5.1.2 Smoothing the Oscillatory Kernel Function

Although an optimal sampling interval Δt may be obtained by following the analysis discussed in the foregoing, the kernel oscillations were found to remain when data of some storms were analyzed. These oscillations must be reduced if not altogether eliminated, if a generalized analysis is to be performed by using these kernels. Such a generalized analysis is discussed in the next section. Three methods, (1) smoothing the kernel function by successive averages, (2) filtering the original data, and (3) increasing Δt may be used to reduce the oscillations in the kernel functions.

The results of smoothing by successive averages clearly show (fig. 5.3) the ineffectiveness of this procedure when the kernel function is smoothed only a few times, and the distortions which result with repeated smoothing. When the Modified Jenkins filter (MJF) (5.2) is used to smooth the raw estimates of h(t) values, the filter may not reduce the oscillations when the order (M) of the filter is small, and will cause some loss of information when M is large as shown in fig. 5.3. Indeed 2M data points are lost for each selected value of M. When the sampling interval Δt is increased, the high frequency oscillations in the kernel function are gradually transformed into low frequency oscillations after a sufficiently large value of Δt is reached, the kernel functions become oscillation-free as shown in fig. 5.3.

None of the three methods of reducing the oscillations in kernel functions may work satisfactorily by itself, but a combination of increasing Δt and filtering appears to give the best result. This conclusion was reached by Rao and Delleur (5.2) also. However, in order to minimize the computational effort, only the Δt values were varied in the present study and the smallest Δt which gave a "smooth" kernel function was used. Analyses similar to the one presently discussed can be found in Rao and Usul (5.3) and Kavvas and Schulz (5.4) also.

5.2 Estimation of the Peak Discharges of the Instantaneous Unit Hydrographs and of the Watershed Time Lags

In order to use the linear system models for the prediction of the direct runoff from the rainfall excess, the instantaneous unit hydrograph must be estimated. A number of previous studies have pointed out the variability of the IUH's from storm to storm (5.1, 5.2) thus invalidating the linear theory. As a result a quasi-linear approach similar in principle to that reported by Rao et al. (5.5) is proposed herein, in which equations 5.1 and 5.2 remain valid for each individual storm, but the IUH is allowed to vary from storm to storm. For this purpose a dimensionless IUH was developed along with the predictive relationships for the two scaling parameters used in the development of the dimensionless IUH. The peak discharge of the IUH's and the time lag were used as the scaling parameters. The time lag used in this study is defined as the time elapsed between the centroid of the rainfall excess hyetograph and the centroid of the direct runoff hydrograph.

The time lag and the maximum ordinate of the IUH were related to the variables listed in table 5.1 by means of nonlinear regression equations. The resulting equations, for the data from watersheds No. 1, 2, 3, 4, 9, and 10 and Table 2.1 are given as eqs. 5.3 and 5.4 in table 5.1. All the variables in eqs. 5.3-5.6 shown in table 5.1 are significant at the 5% level.

In order to investigate the importance of the role of the variables representing the antecedent conditions another set of regression relationships was established by omitting the variables representing these antecedent conditions. The data from Lawrence Creek, Little Eagle Creek, Bean Blossom Creek, and Bear Creek in addition to the data from the watersheds mentioned earlier (watersheds 1 through 10 of Table 2.1) were used for the second set of relationships given as eqs. 5.5 and 5.6 in table 5.1. From the multiple correlation coefficients and from the standard errors of estimates associated with these equations shown in table 5.1, it can be seen that the variables associated with antecedent conditions are not very significant. It is also seen that the antecedent conditions tend to mask the effect of imperviousness on the peak discharge. In eqs. 5.5 and 5.6 the maximum ordinate of the IUH increases and the time to peak decreases with an increase of the fraction of impervious area in the watershed, as is expected. Consequently, eqs. 5.5 and 5.6 were used in the following analysis.

5.3 Dimensionless Instantaneous Unit Hydrograph and Its Use in Prediction

The IUHs computed by the Fourier Transform method were nondimensionalized by dividing the abscissa (time) by the time lag of the storm and the ordinates by the maximum ordinate of the IUH. The dimensionless unit hydrographs so obtained were combined together and a smooth curve was drawn through them to obtain the dimensionless unit hydrograph shown in Fig. 5.4.

For any given rainfall excess volume, the maximum ordinate and the time lag of the IUH can be estimated by using eqs. 5.5 and 5.6 respectively, provided the other variables are known. An IUH appropriate for the storm can be developed from the dimensionless IUH by multiplying its ordinates by the maximum ordinate of the IUH given by eq. 5.5 and by multiplying the time (abscissa) by the time lag value given by eq. 5.6. The area under the IUH generated by this procedure should be adjusted to unity. The area under the IUH was adjusted to unity by varying the ordinates on the recession and rising limbs but by keeping the maximum ordinate of the IUH the same as that obtained by eq. 5.5. This procedure was adopted because the prediction results, especially the prediction of the peak discharge, were sensitive to changes in the maximum ordinate of the IUH computed by eq. 5.5. The IUH so obtained is then convolved with the hyetograph of rainfall excess by eq. 5.1 to obtain the direct runoff hydrograph.

The above procedure was tested by both regeneration and prediction studies. For the regeneration performance analysis, several rainfall excess hyetographs which were used to develop eqs. 5.5 and 5.6 were considered, the IUH's were estimated and the direct runoff hydrographs were computed and compared with observed direct runoff hydrographs. Examples of the results obtained by this analysis are shown in fig. 5.5. The errors in the regeneration of peak discharge, the time to peak discharge, were analyzed and the frequency distribution of these errors is shown in fig. 5.6 for some of the watersheds. The percentage error in peak discharge is given by $[(Q_{po} - Q_{pc})/Q_{po} \times 100]$, the time to peak error is computed by $[(T_{po} - T_{pc})/T_{po} \times 100]$ and the error in time to peak in DT is given by $(T_{po} - T_{pc})$. The subscripts o and c refer to the observed and computed quantities. The percentage error in the time to peak can be very large even if the time to peak is missed by even a single time step Δt, especially if the observed time to peak is very small.

An examination of the results presented in fig. 5.6 demonstrates that the regeneration performance of the present method is good. The percentage of error in the peak discharge regeneration is most frequently within $\pm$ 10% and the percentage error in time to peak regeneration is within $\pm$ 8%. The time to peak is off by $\pm \Delta t$ most frequently. Further results such as those shown in fig. 5.6 may be found in ref. 3.7.

In eqs. 5.3 to 5.6, the average time lag for a watershed is also considered as an independent variable. As in urban sewered watersheds the natural drainage system will be substantially altered; the length (L) and slope (S) variables in eqs. 5.3-5.6 cannot be estimated correctly unless a detailed analysis of the sewer system characteristics is undertaken. Instead of conducting an analysis of the length, slope and roughness characteristics of sewer systems, the average time lag value was used as a composite characteristic representative of the response of sewered areas. Carter (5.6), Eagleson (5.7) and Van Sickle (5.8) have shown that the average time lag values are dependent upon the length and slope of sewers. However, for watersheds which do not have the average time lag information available, eqs. 5.7 and 5.8 can be used without losing any accuracy.

The prediction performance of the present method was tested by using the data from Boneyard Creek, Urbana, Illinois, which were not used either to develop the regression eqs. 5.5, 5.6 or the dimensionless IUH. For several storms the maximum ordinates of the kernel, and the time lag were computed by eqs. 5.5 and 5.6 and these were used to obtain the corresponding kernel functions. The kernel functions were convolved with the known rainfall excess to compute the direct runoff hydrographs. The computed direct runoff hydrographs were then compared with the observed direct runoff hydrographs. The errors in estimating the peak discharge, and the time to peak discharge are given for some storms in table 5.2. The error frequency distributions for the same characteristics are shown in fig. 5.7. Most frequently, the peak discharges were underestimated by -10 to -20%, whereas the time to peak was missed by $\pm \Delta t$. The runoff volume predictions, as can be expected, were very good.

The estimated kernels and the direct runoff values obtained by eq. 5.7 and 5.8 with different levels of urbanization on Lawrence Creek at 38th Street watershed are shown in Fig. 5.8. It should be pointed out

that with the increase in urbanization the amount of rainfall excess for a storm would also increase. This aspect, however, has not been considered in the present analysis.

5.4 Nonlinear System Approach

In the previous sections it was shown that there is no unique IUH for any of the watersheds studied as the IUH varied from storm to storm. This lack of uniqueness in the watershed response has been attributed by Amorocho (5.9) to the possible "misinterpretation of the basin by a linear model". The inherent nonlinearity of the processes of mass and energy transfer in the runoff cycle suggests the consideration of nonlinear models of hydrologic systems. Among the several possible nonlinear models the application of the general representation of the hydrologic system by a functional series was selected because it is the direct extension of the linear kernel method used in the previous sections. The second order nonlinear functional model may be represented by

$$y(t) = \int_0^t h_1(s_1) \cdot x(t-s_1)ds_1 + \int_0^t \int_0^t h_2(s_1, s_2)\, x(t-s_1) \cdot x(t-s_2)ds_1\, ds_2 \qquad (5.9)$$

where $x(t)$ and $y(t)$ are the rainfall input and runoff output, and $h_1(s_1)$ and $h_2(s_1, s_2)$ are the first and second order kernels, respectively. These kernels characterize the system. Amorocho and Brandsteter (5.10) have evaluated them by an expansion in finite series of orthogonal functions. As the function $h_2(s_1, s_2)$ is a three-dimensional surface it is difficult to quantify its characteristics by a small number of parameters that could be related to physiographic or climatologic basin characteristics.

In order to extend the linear system analysis to include some of the second order effects while retaining a level of simplicity similar to that of the linear kernel, it was decided to evaluate a model proposed by Boneh and Diskin (5.11) which considers only the second order kernel, $h_2(t;t)$ along the diagonal in the (s_1, s_2) plane. This kernel is a plane curve which can be characterized in a manner similar to that of the IUH. The following sections contain an exploratory study of this approach and the possible merits of its application to urban hydrology.

Boneh and Diskin (5.11) have shown that if an isolated impulse of a positive magnitude such that

$$x(t) = 0 \text{ for } t \neq 0; \qquad \lim_{t \to 0} x(t) = \infty; \qquad \int_{-\infty}^{\infty} x(t) \cdot dt = A \qquad (5.10)$$

is applied at time = 0 as the input to a second order system, the output obtained by substituting equations (5.10) into (5.9) is expressed by

$$y(t) = A \cdot h_1(t) + A^2 \cdot h_2(t,t) \qquad (5.11)$$

Mass conserving systems must, in addition, satisfy the following conditions:

$$\int_0^{\infty} h_1(t)dt = 1.0; \qquad \int_0^{\infty} h_2(t,t)dt = 0 \qquad (5.12,13)$$

5.4.1 Identification of the First and Second Order Kernels

If the input and output functions are replaced by sets of pulses at equal and constant time intervals, eq. (5.11) can be written for each pulse. For short duration storms the following set of equations can then be written

$$Y_{ij} = X_i H_j + X_i^2 G_j, \qquad i = 1, 2, \ldots, n \qquad (5.14)$$

and solved for H_j and G_j subject to the following constraints:

$$H_j \geq 0 \text{ for all } j; \qquad \sum_j H_j = 1; \qquad \sum_j G_j = 0 \qquad (5.15,16,17)$$

where n = number of storms used, where $n \geq 2$; H_j = discrete ordinate of the first order kernel function; G_j = discrete ordinate of the second order kernel function; Y_{ij} = the j^{th} ordinate of the i^{th} output function (direct runoff); X_i = the i^{th} input function (total rainfall excess of i^{th} storm).

The solution of equations 5.14 subject to the linear constraints 5.15 through 5.17 uses a subroutine which calculates a best least square solution of a system of linear equations by an iterative refinement procedure based on the Gram-Schmidt method (5.12). The procedure is designed to satisfy the constraints 5.16 and 5.17 only. In order to satisfy the constraint 5.15 the negative H_j ordinates were made equal to zero, provided the values of the negative ordinates were very small compared to the positive ordinates. Kernels with large negative H_j values were discarded. The H_j ordinates were then adjusted to meet the constraints 5.16. In order to verify that the solution obtained was the least square solution, the H_j and G_j were systematically perturbed and the sum of squared deviations between the observed and predicted outputs were computed. The procedure requires a substantial central memory space. For more than two storms, it usually required in excess of 150 K "words" on the CDC 6500 computer.

5.4.2 Implementation of the Model

The first and the second order kernels were identified from the rainfall excess and the direct runoff data of pairs of storms for the first 10 watersheds of table 2.1. The identified kernels were used to regenerate the direct runoff. The sum of squared deviations between the measured and the regenerated direct runoffs were computed. The pairs of storms which gave high sums of squares of error (usually greater than 0.02) were rejected. Figure 5.8 shows the first and second order kernels and the measured and regenerated runoffs of two pairs of storms. The distribution of the error of the regenerated peak runoffs and of the times to peak for Waller Creek at 38th Street are given in Figure 5.9.

5.4.3 Effect of the Time Step and of the Number of Storms on the Kernels

The pair of storms of September 6, 1962, and October 21, 1958, on Waller Creek at 38th Street with direct runoff values of 0.4922 and 0.1830 inches respectively were selected to evaluate the effect of the time step on the kernels. The kernel functions were computed for time steps of 15, 22.5, 30, 37.5, 45 and 60 minutes and are shown in Figure 5.10. In general the kernels become smoother as the time step is increased.

A set of eight storms which occurred during the year of 1970 on Ross Ade Upper Watershed was selected to study the effect of the number of storms on the kernels. The effects of increasing the number of storms are shown on Fig. 5.11. The peak value of the kernels and the shape of the kernels are seen to change with the number of storms considered. It appears that the kernels obtained with 2, 3 and 4 storms vary considerably but that the kernels seem to reach a stable shape as the number of storms is increased as can be seen in the case of 6, 7 or 8 storms.

5.4.4 Average Dimensionless Kernels

The number of storms that could be used to compute the first and second order kernels were, in most cases, no more than two because of the large central memory requirement of the procedure used, thus not permitting a satisfactory identification of H and G. The dimensionless kernels were then developed to overcome this difficulty.

The data of watersheds no. 1 through 10 (table 2.1) were used to compute the first and second order kernels for pairs of storms. The kernels were made dimensionless by dividing the ordinates by the respective peak ordinate and the abscissa by the respective time to peak (see fig. 5.12). The dimensionless kernels were plotted for all the pairs of storms for the 10 watersheds and the smoothed average first and second order kernels were obtained graphically. The kernels so obtained are the average dimensionless kernels.

The first and second order kernels may be specified by six parameters: the peak ordinate and the time to peak ordinate of the first order kernel; the peak ordinate and the time to peak ordinate; the minimum ordinate and the time to the minimum ordinate of the second order kernel (see fig. 5.12).

5.4.5 Computational Procedure

The ordinates of H and G are computed by multiplying the dimensionless ordinates of the dimensionless first and second order kernels by the respective peak ordinates, the abscissas (time) are obtained by multiplying the dimensionless abscissas by the values of the respective times to peak. The ordinates of the kernels are adjusted to meet the constraints 5.12, 5.13 and 5.15.

The computational procedures are summarized in Flow Chart 5.1. The following notations are used:

H First order kernel.

G Second order kernel.

HAMX Maximum ordinate of H.

GAMX Maximum ordinate of G.

TMAX1 Time to maximum ordinate of H.

TMAX2 Time to maximum ordinate of G.

TMIN Time to minimum ordinate of G.

5.4.6 Regeneration Performance

The distribution of the differences between the measured and the regenerated values of the peak discharge and of the time to peak discharge in percent for 5 watersheds is shown in Figure 5.13. The percentages of error in the time to the peak discharge were calculated by the relationship:

$$\frac{\text{Measured time to peak - Computed time to peak}}{\text{Measured time to peak}} \times 100$$

If the measured time to peak is one time unit, and the computed time to peak is two time units the percentages of error in time to peak discharge is 100 percent giving an apparent large percentage of error. The actual error in this case is one time unit. For most storm pairs there were no differences between measured and regenerated storm volumes.

5.5 Comparison of Direct Runoffs Computed by Linear and Nonlinear Methods

A set of six storms on Ross Ade upper watershed was selected. (August 10, 1966, December 5, 1966, August 2, 1967, 5:17 p.m., August 18, 1967, 8:35 p.m., and August 26, 1967, 5:31 p.m.). The linear kernels were computed by the Fourier transform method from which an average linear kernel was obtained. The first and second order kernels were estimated by the method given in Section 5.4.1. The direct runoffs of the six storms were regenerated by convolving the average linear kernel with the estimated rainfall excess of the storm and also by eq. (5.14) with the estimated total rainfall excess for the nonlinear method. Figure 5.14 shows the average linear kernel, the first and second order kernels of the nonlinear method and the regenerated runoffs using both methods. Figure 5.15 shows the distribution of the errors by both methods for the peak discharge and for the time to peak for storms not used in developing the kernels but on the same watershed. The regenerated direct runoffs obtained by the nonlinear method appear to be less accurate than those obtained by the average linear kernel.

5.6 Discussion

The first and second order kernels identified from data of two storms yielded a good regeneration performance (Fig. 5.8, 5.9) whereas the regeneration performance of kernels identified from six storms was poor (Fig. 5.14, 5.15). The regeneration performance appears to depend in part on the data used and possibly on the computational procedure.

The time step has an influence on the stability of the first and second order kernels (Fig. 5.10). Larger time steps usually yield smoother kernel functions. There was no change in the regeneration performance of the kernels obtained with different time steps. The first and second order kernels appear to change with the number of storms used (Fig. 5.11). This change is expected as the kernels are obtained as a least square fit to the observed direct runoff values. Thus there is no unique set of kernels for a given watershed. It may be inferred that the quasilinear method appears to be the most satisfactory among the methods studied.

Table 5.1 Regression Equations for Parameters of Linear Kernel

$$y = K \prod_{i=1}^{n} a_i^{C_i} *$$

	K	V	I	M	R1	R2	R3	R4	T1	T2	L	S	U	A	MO	AR	R**	σ***	Eq.
QMA	.20558	.07606	.11105	-.26361	-.01426	.02193	-.01566	.01643	-.14670	-	.70202	.22549	-3.21347	-2.49557			.98	.48	5.3
TL	1.42909	.15826	-.34060	.15723	.04859	-.02841	-	.00366	-.52466	.40606	.64645	-.19094	-2.24638	-	-.60898		.97	.31	5.4
QMA	.01267	-.02562	.10403	-.20080							- .51770	.84921	1.38015	- .83335			.96	.53	5.5
TL	3.47537	.16265	-.19862	.07340							.50529	-.28596	-2.60226	.72326		-.33788	.94	.42	5.6
QMA	.00557	-.04833	.09689	-.15918							-1.20434	1.00825	4.74957				.96	.54	5.7
TL	3.33119	.15911	-.17242	-.15918							.59768	-.21150	-4.30814				.94	.42	5.8

QMA = Maximum ordinate/Area of watershed, $hr.^{-1}$ $mi.^{-2}$
TL = Time lag, hr.
V = Volume of rainfall excess of storm, in.
I = Average intensity of rainfall excess, in. $hr.^{-1}$
M = Maximum intensity of rainfall excess in 1/2 hr., in. $hr.^{-1}$
R1 = Rainfall volume during preceding 7 days, in.
R2 = Seven-day rainfall volume, 1 week before storm, in.
R3 = Seven-day rainfall volume, 2 weeks before storm, in.
R4 = Seven-day rainfall volume, 3 weeks before storm, in.

T1 = Daily mean temperature before storm, °F
T2 = Seven-day mean daily temperature, °F
L = Length of main channel, mi
S = Slope of watershed, ft/mi
U = Urbanization factor 1+u
u = Total fraction of total watershed area which is impervious
A = Average time lag of watershed (Table 2.1)
MO = Maximum ordinate of kernel, $hr.^{-1}$
AR = Area of watershed, mi^2

*The table lists the values of K and of the exponents c_i for the variables appearing in the column heading. All variables are significant to 5% level, **Correlation coefficient, ***Standard error of estimate.

Table 5.2 Results of Predictions of Boneyard Creek Direct Runoff

Date of Storm	Error in Vol., %	Error in time to Peak, Time Step	Error in peak dis., %
4.19.64	0.0	-1.0	-15.64
4.10.64	0.0	-1.0	-16.73
6.27.64	0.1	-1.0	- 3.18
8.18.66	0.0	-2.0	2.50
9.23.61	0.0	1.0	- 6.60
9.03.62	0.0	0.0	15.43
6.19.63	0.0	-1.0	-14.35
7.19.63	0.0	3.0	-16.61
5.25.65	0.0	-1.0	-33.84
7.02.65	0.0	-1.0	-51.39
4.20.66	0.0	0.0	-22.79

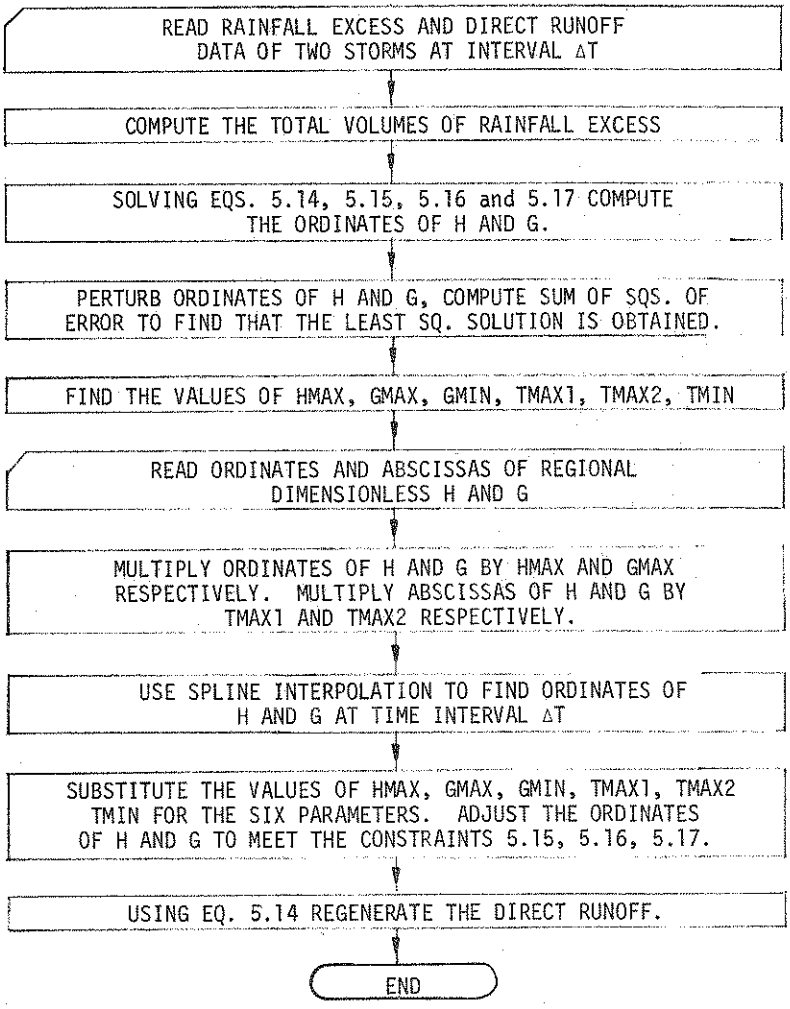

Flow Chart 5.1 Calculation of First and Second Order Kernels Using Average Dimensionless Kernels

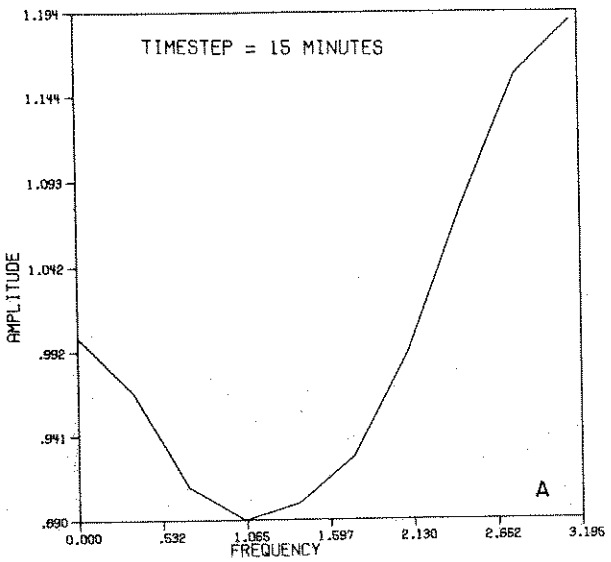

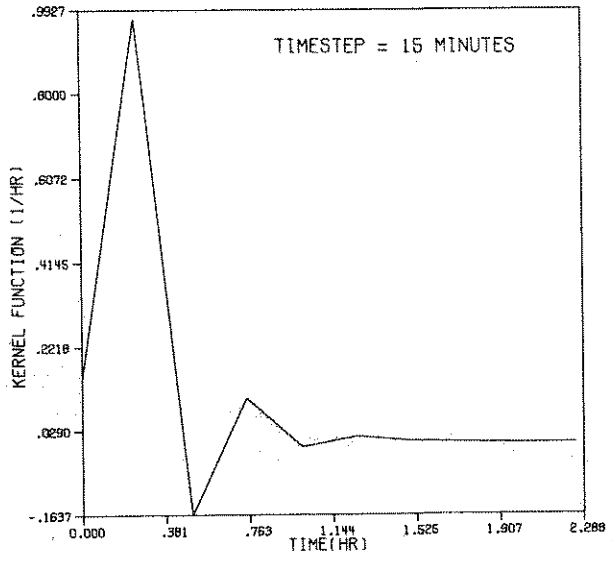

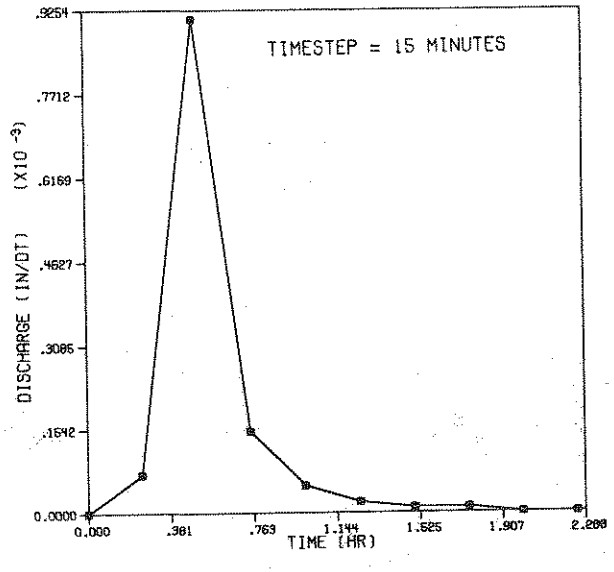

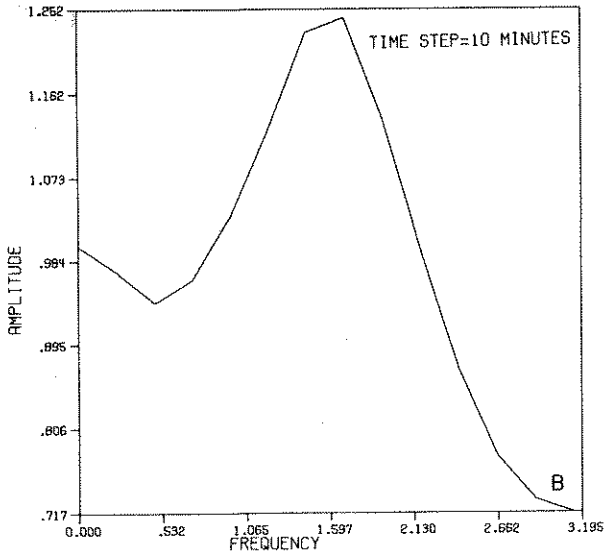

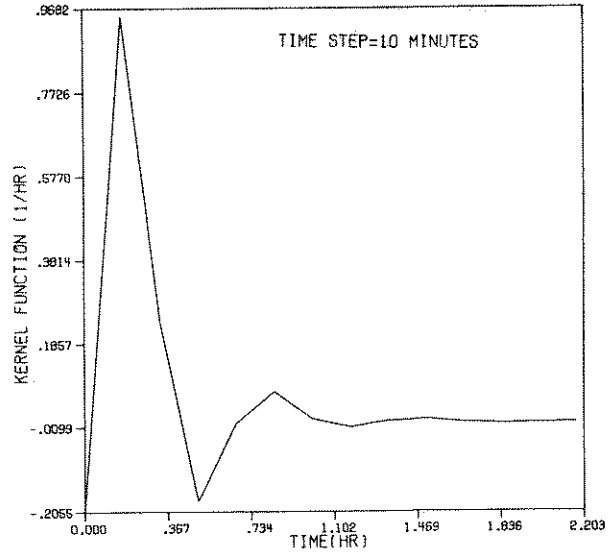

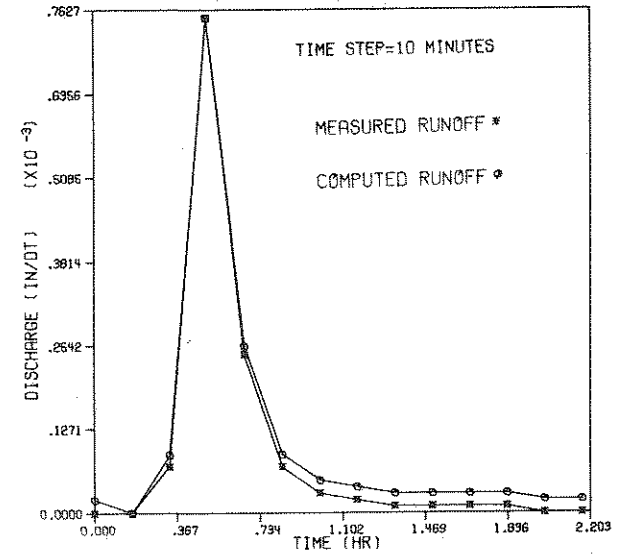

FIGURE 5.1 EFFECT OF TIME STEP ON THE TRANSFER FUNCTION AND THE KERNEL FUNCTION.

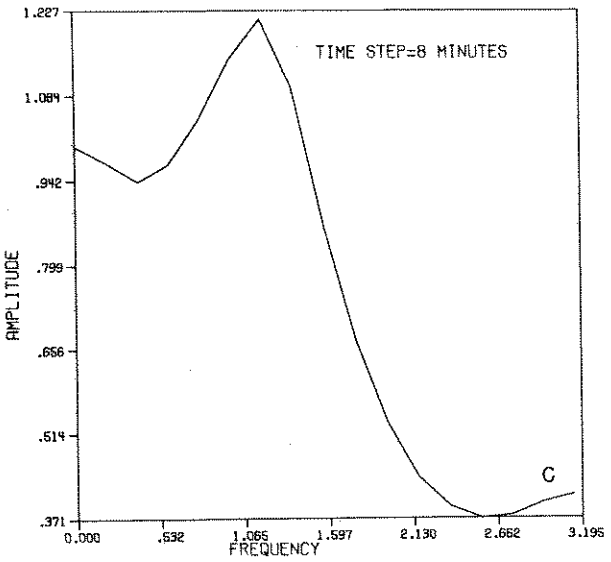

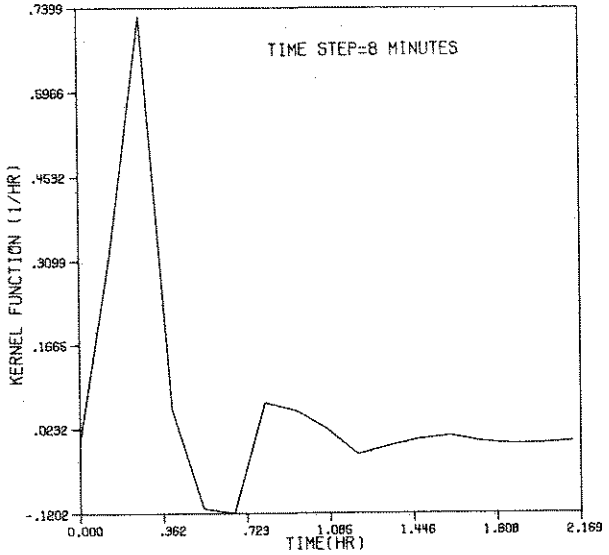

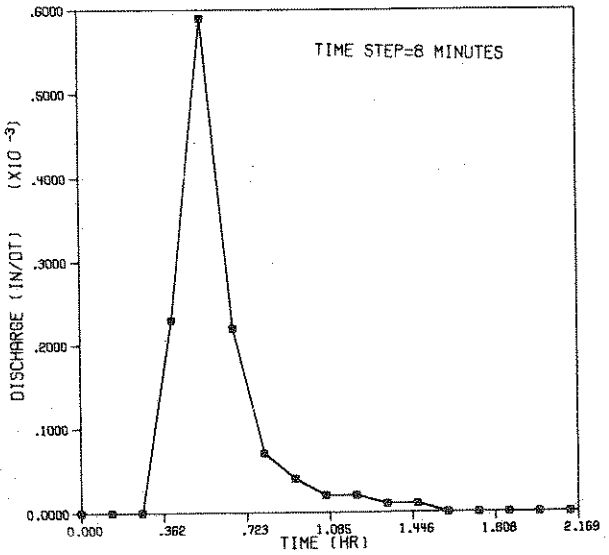

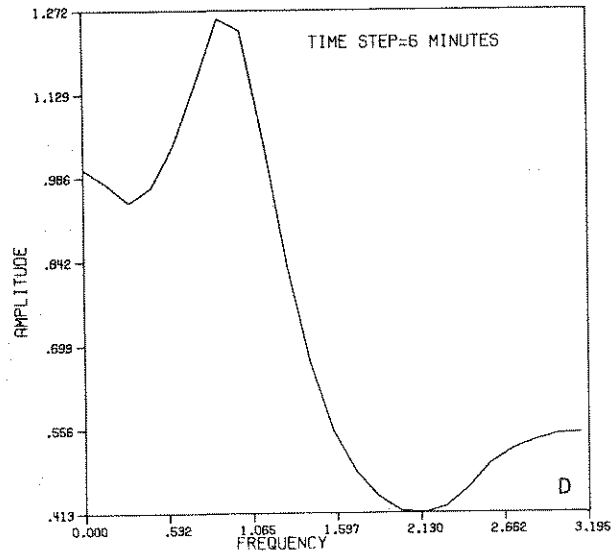

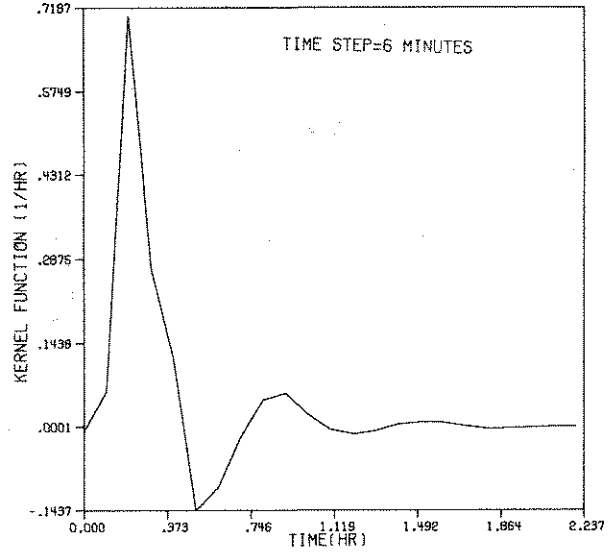

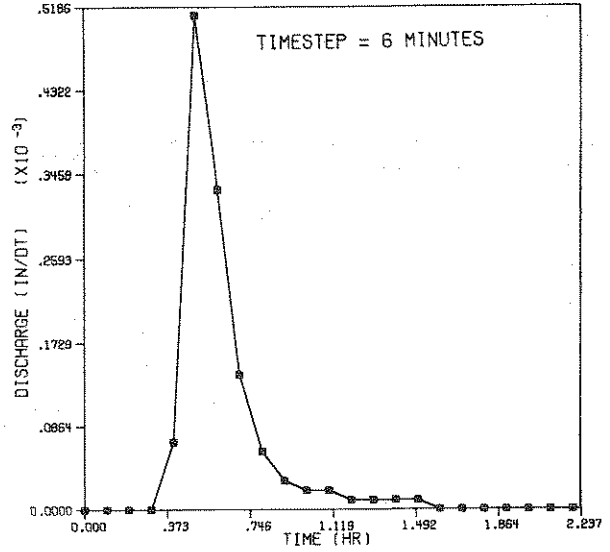

FIGURE 5.1 ,CONT.

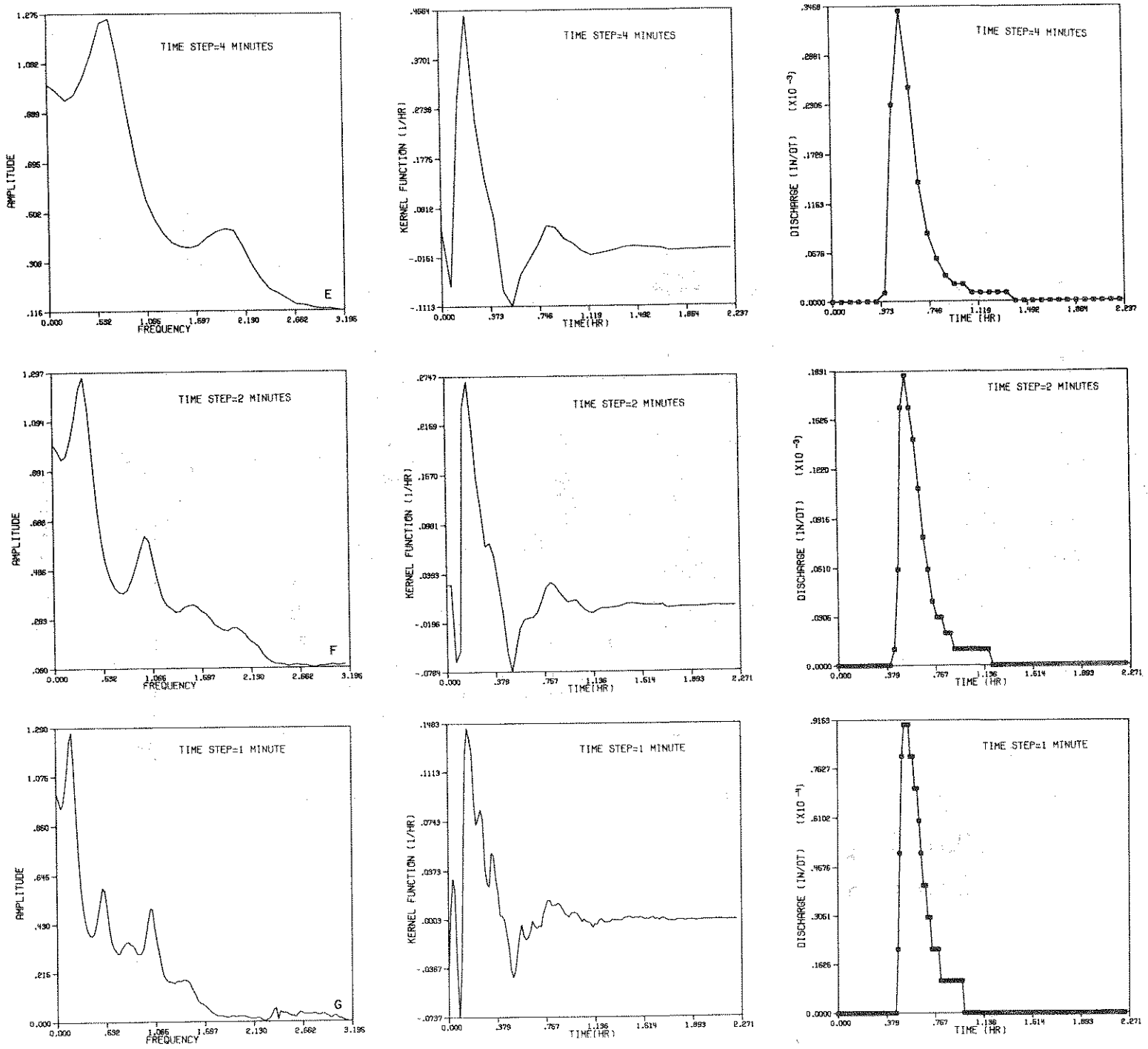

FIGURE 5.J .CONT.

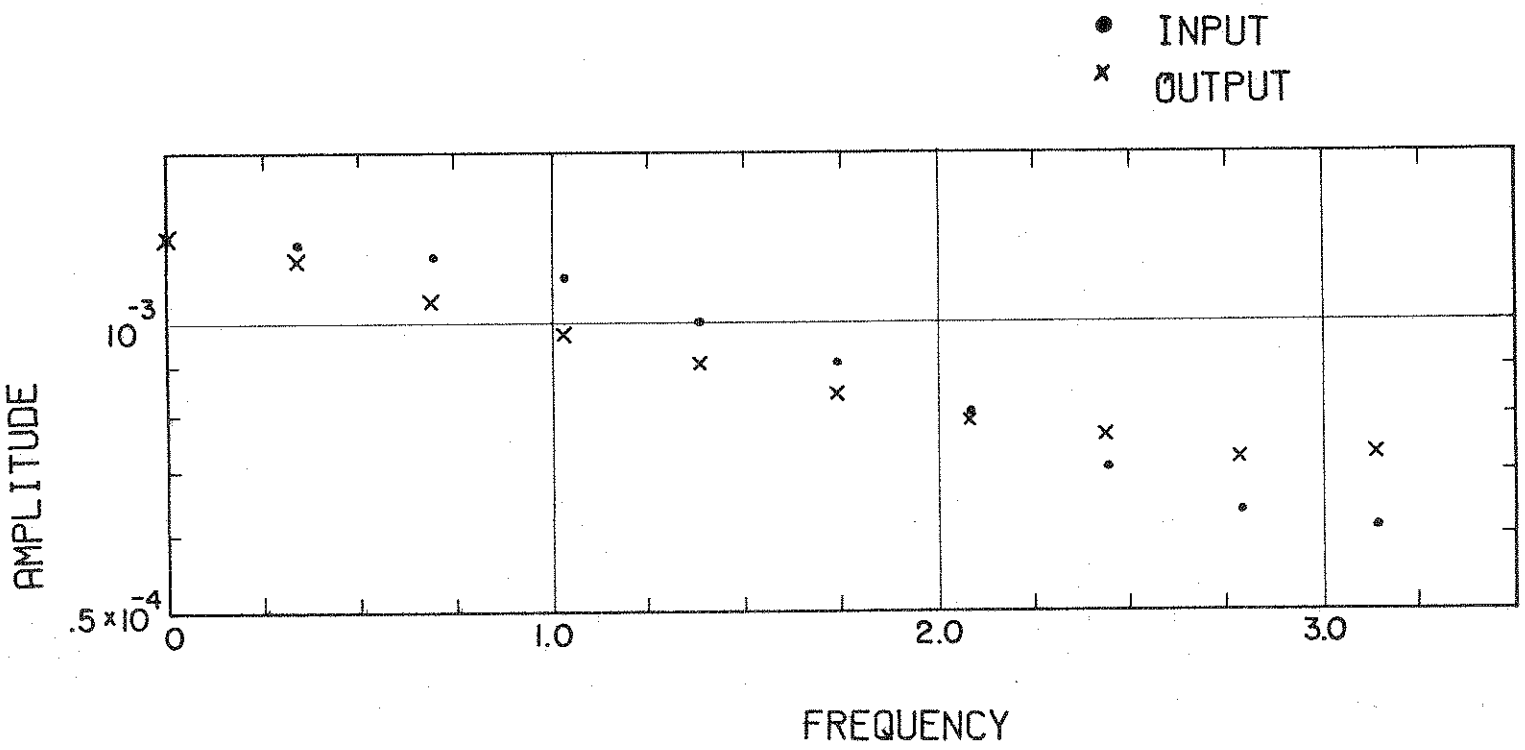

FIGURE 5.2 EFFECT OF TIME STEP ON THE TRANSFORMED INPUT AND OUTPUT

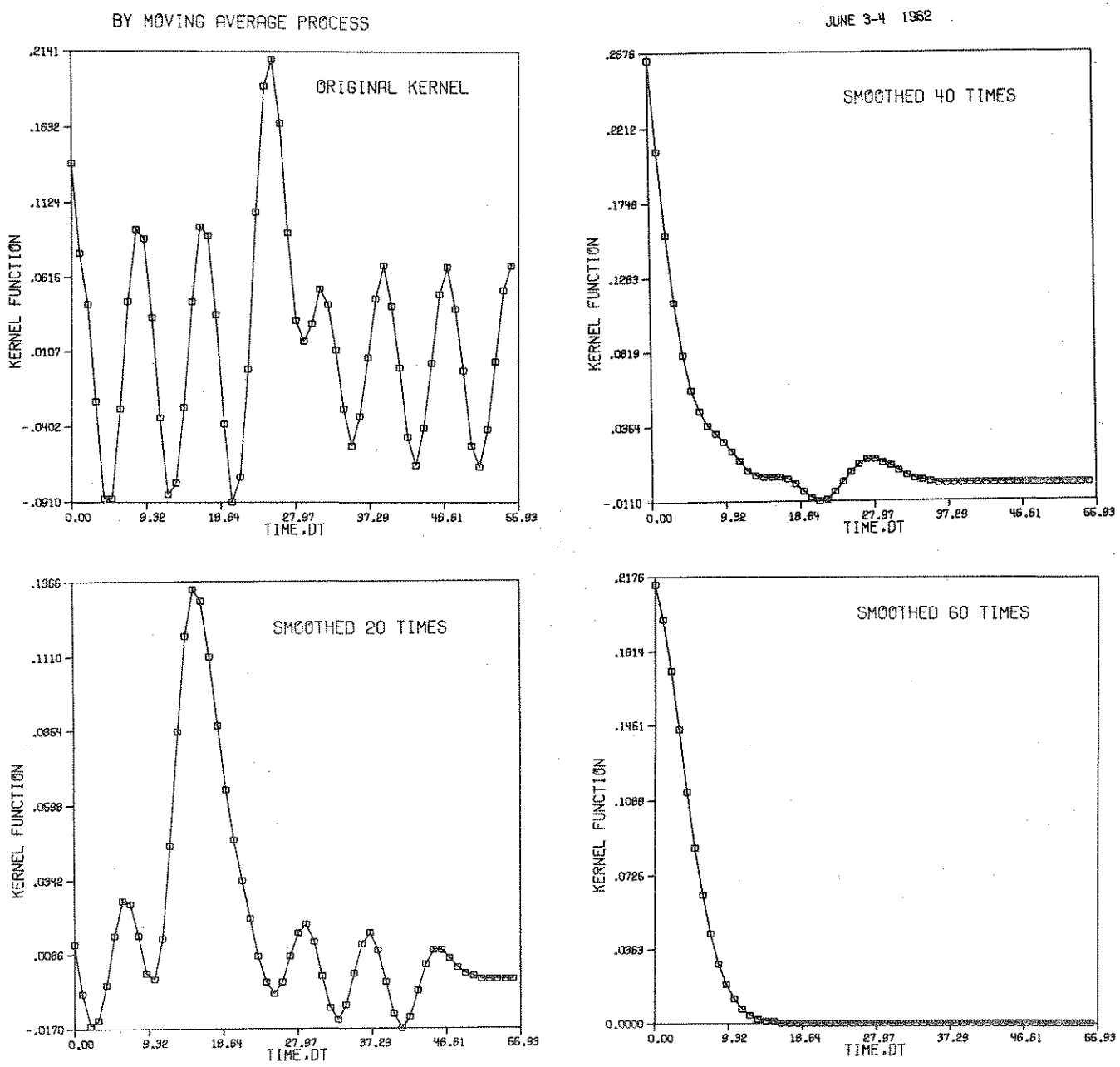

FIGURE 5.3 EFFECT OF SMOOTHING BY MOVING AVERAGE PROCESS, BY FILTERING AND BY INCREASING TIME STEP.

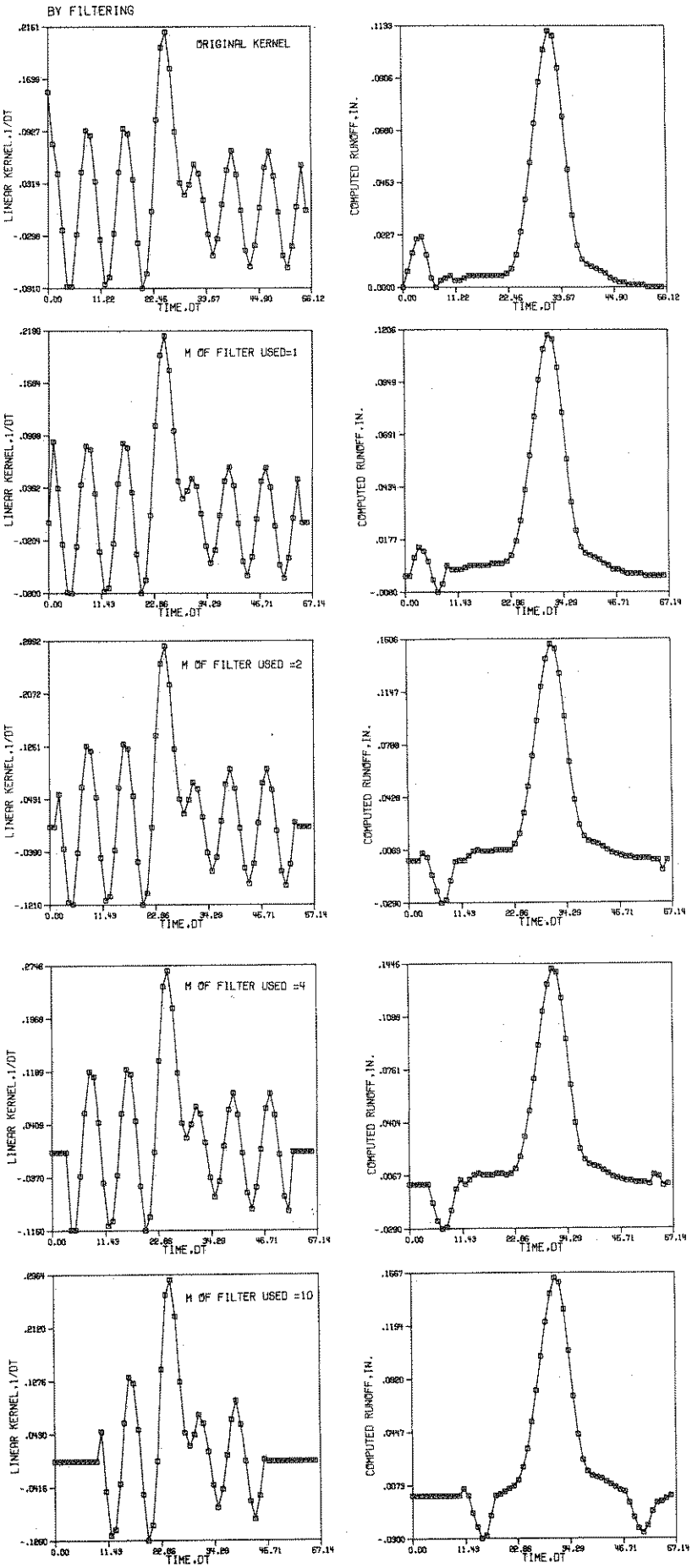

FIGURE 5.3.CONT.

BY INCREASING TIMESTEP

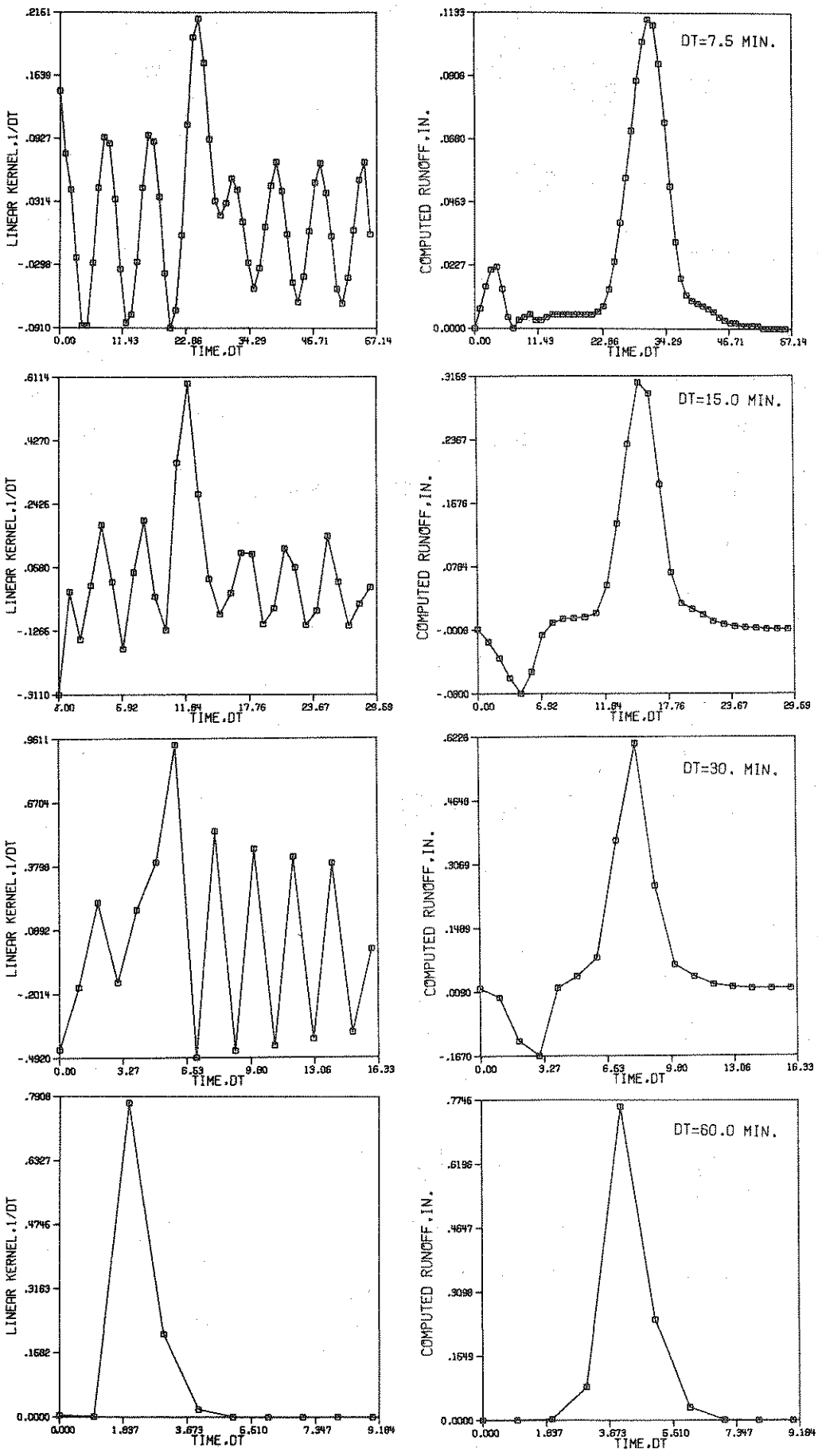

FIGURE 5.3.CONT.

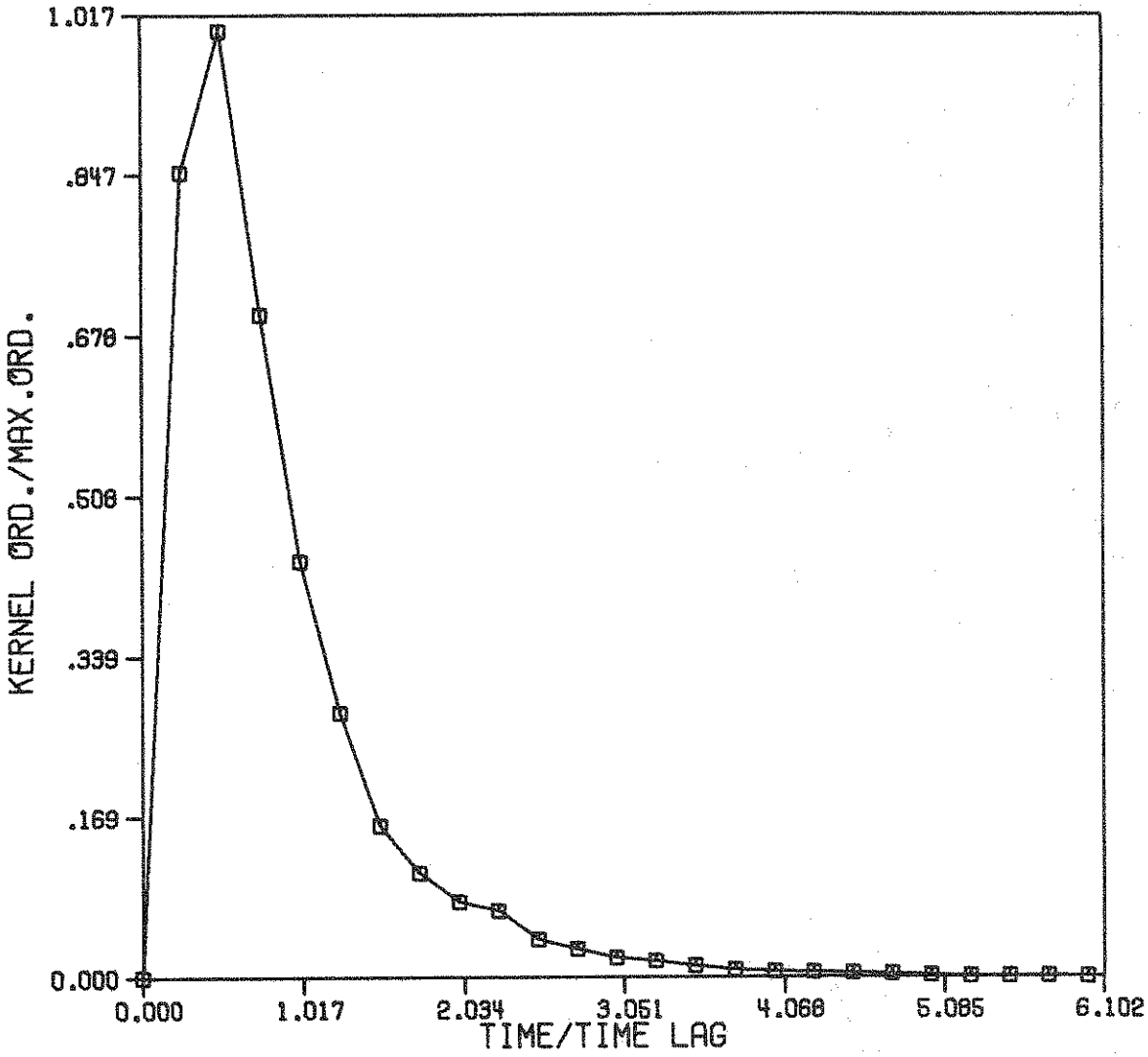

FIGURE 5.4 REGIONAL DIMENSIONLESS IUH

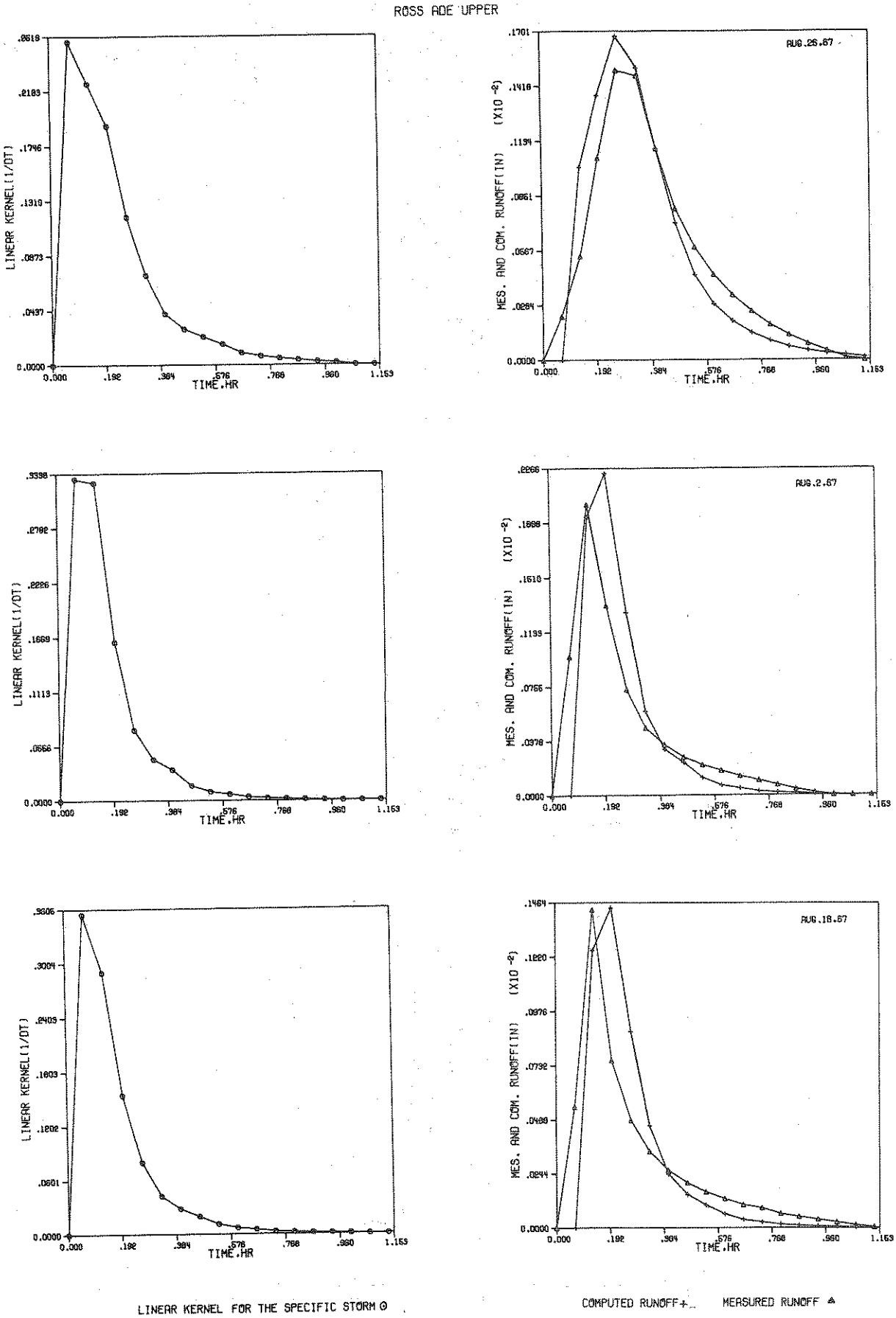

FIGURE 5.5 THE ADJUSTED IUH MEASURED AND REGENERATED RUNOFF.

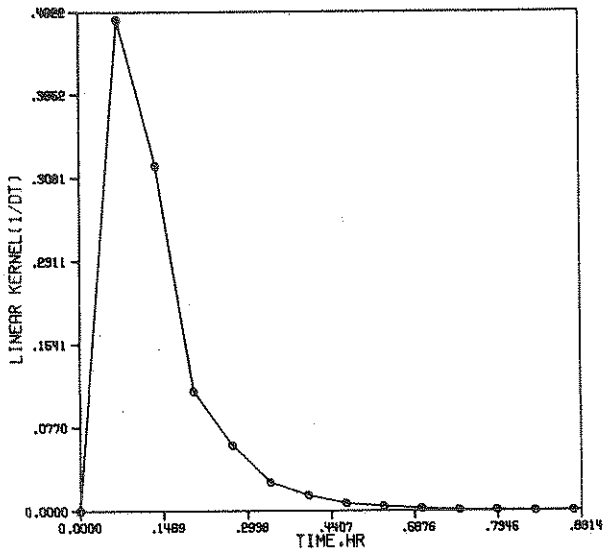

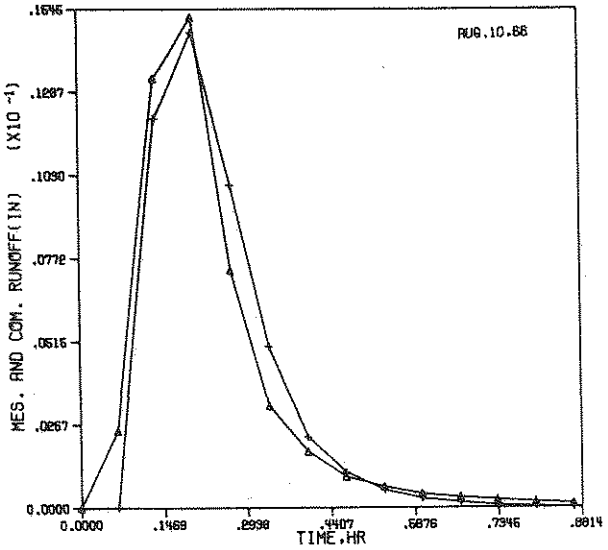

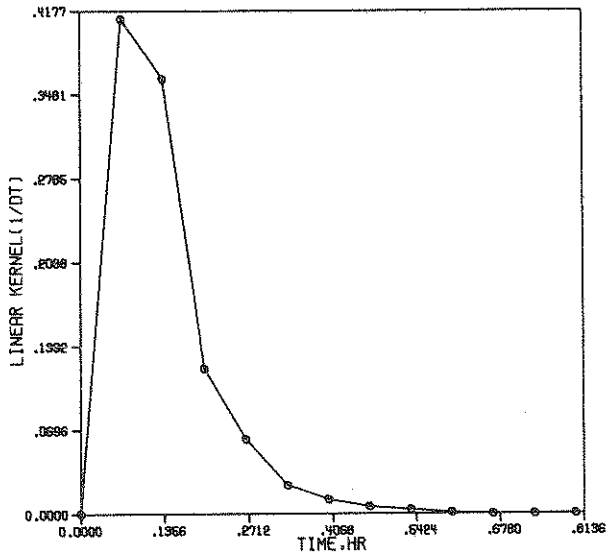

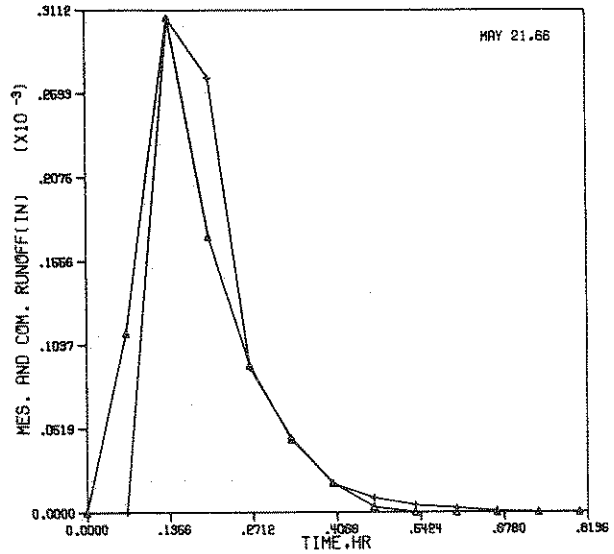

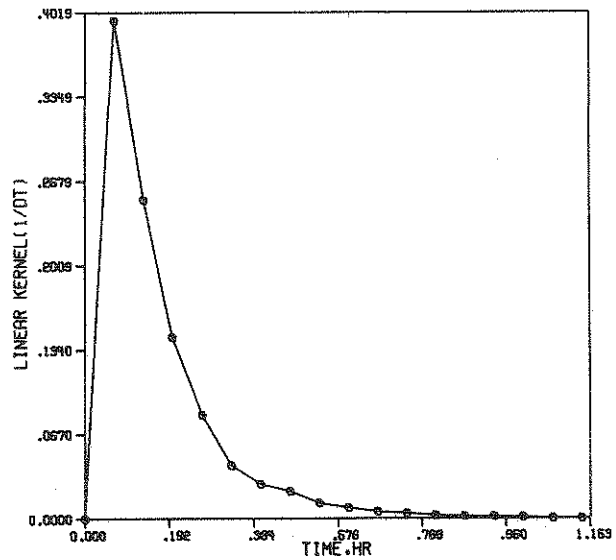

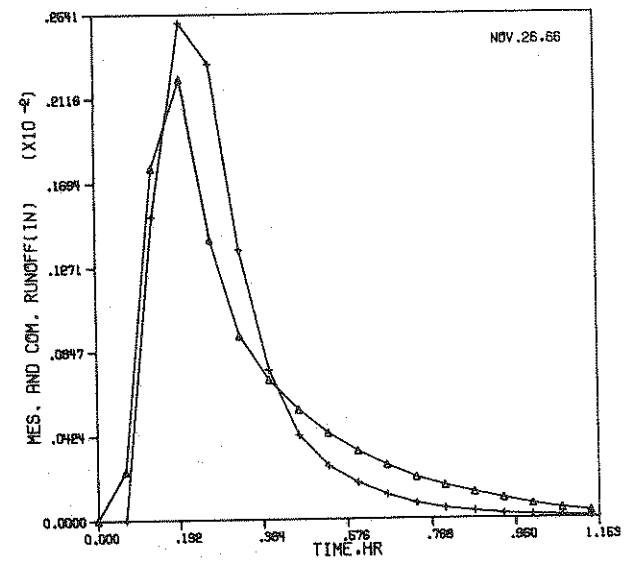

LINEAR KERNEL FOR THE SPECIFIC STORM ⊙

MEASURED RUNOFF △ COMPUTED RUNOFF +

FIGURE 5.5.CONT.

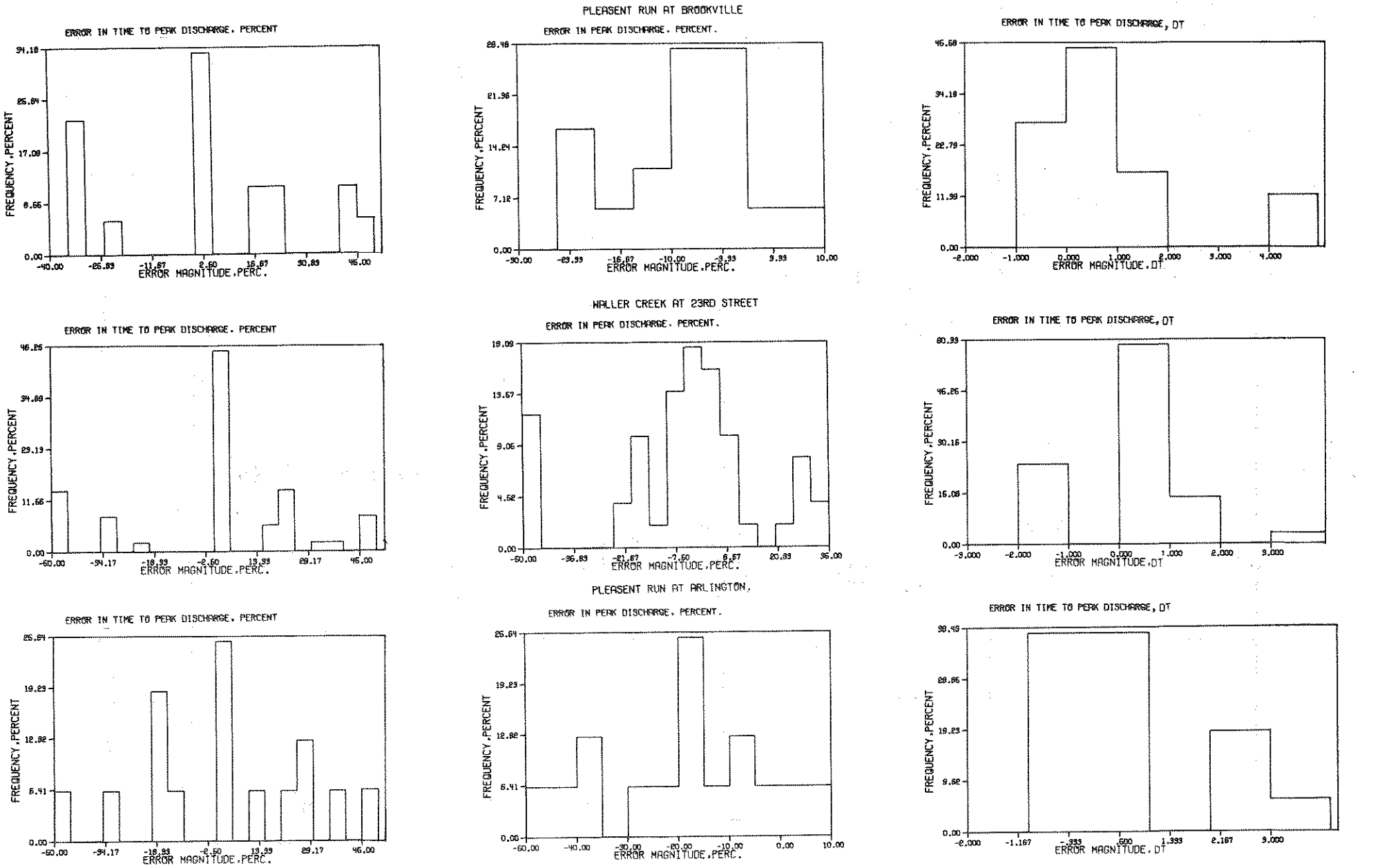

FIGURE 5.6 ERROR DISTRIBUTION OF DIRECT RUNOFF

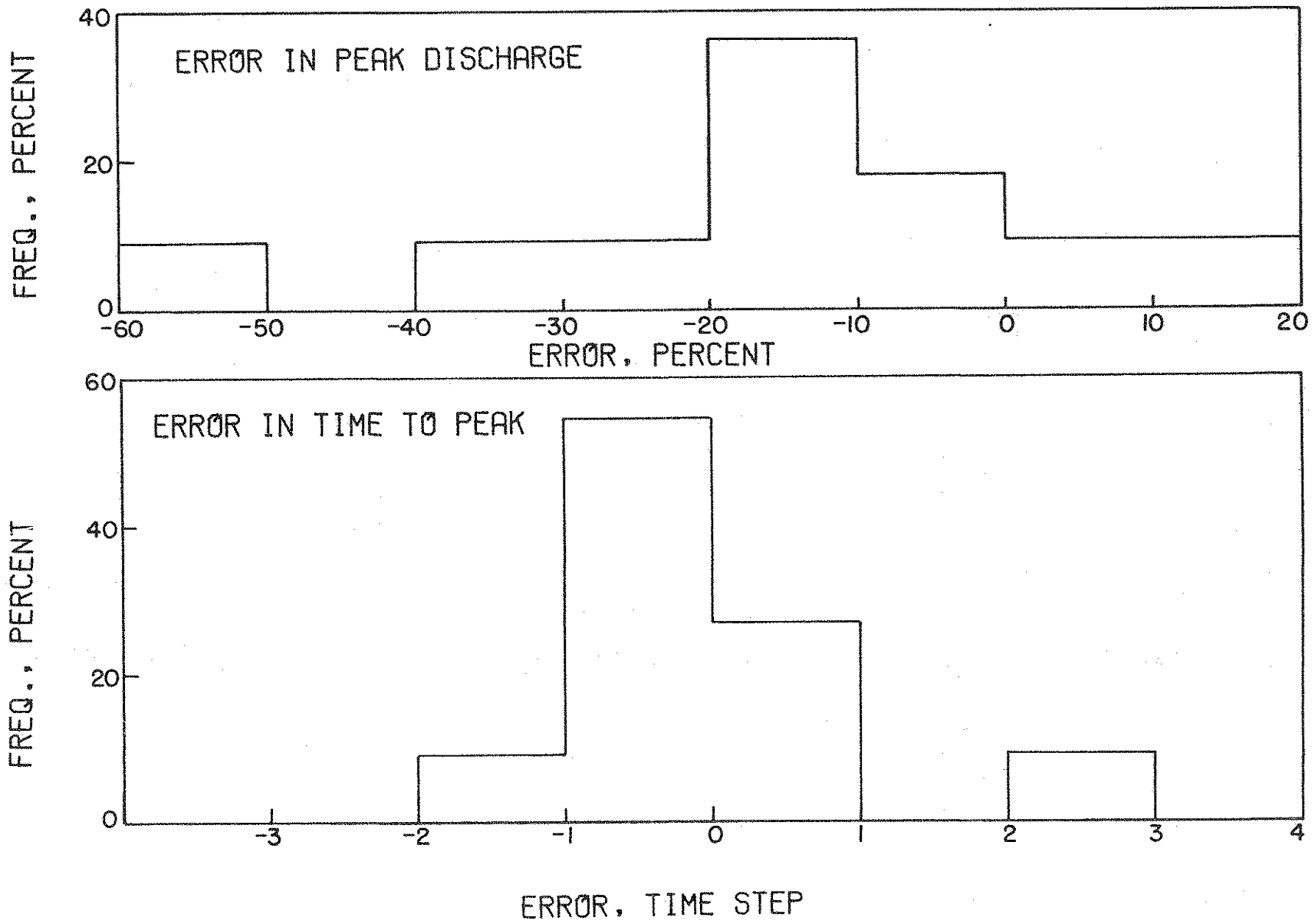

FIGURE 5.7 ERROR DISTRIBUTION OF PREDICTED DIRECT RUNOFF

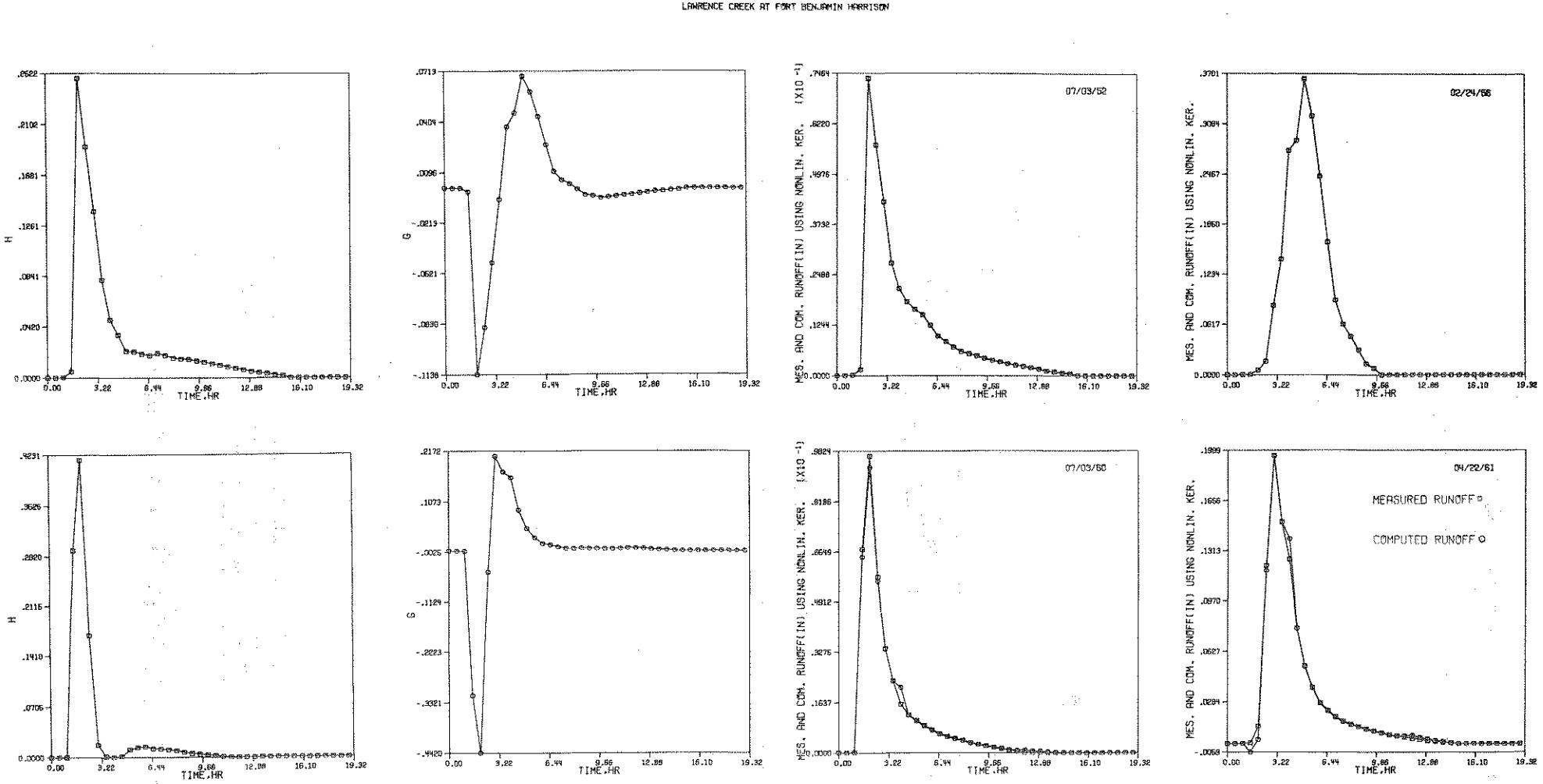

FIGURE 5.8 FIRST AND SECOND ORDER KERNELS, MEASURED AND REGENERATED RUNOFF

WALLER CREEK AT 38 TH ST.

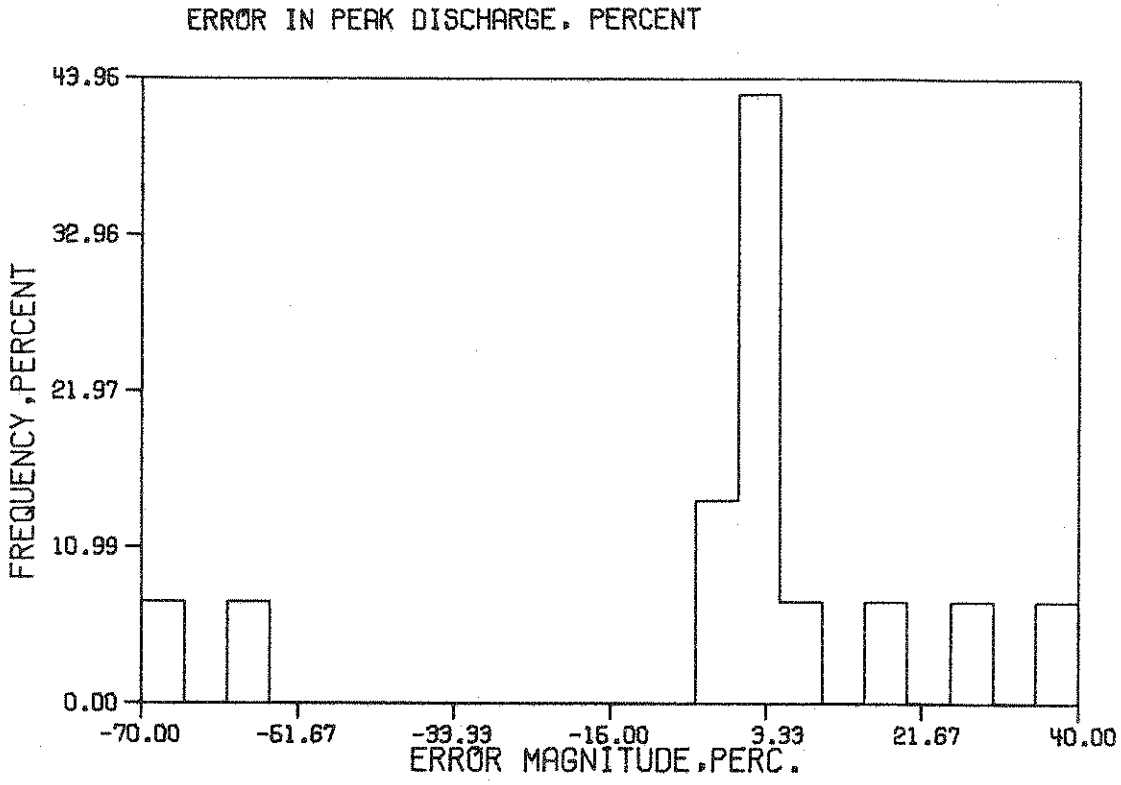

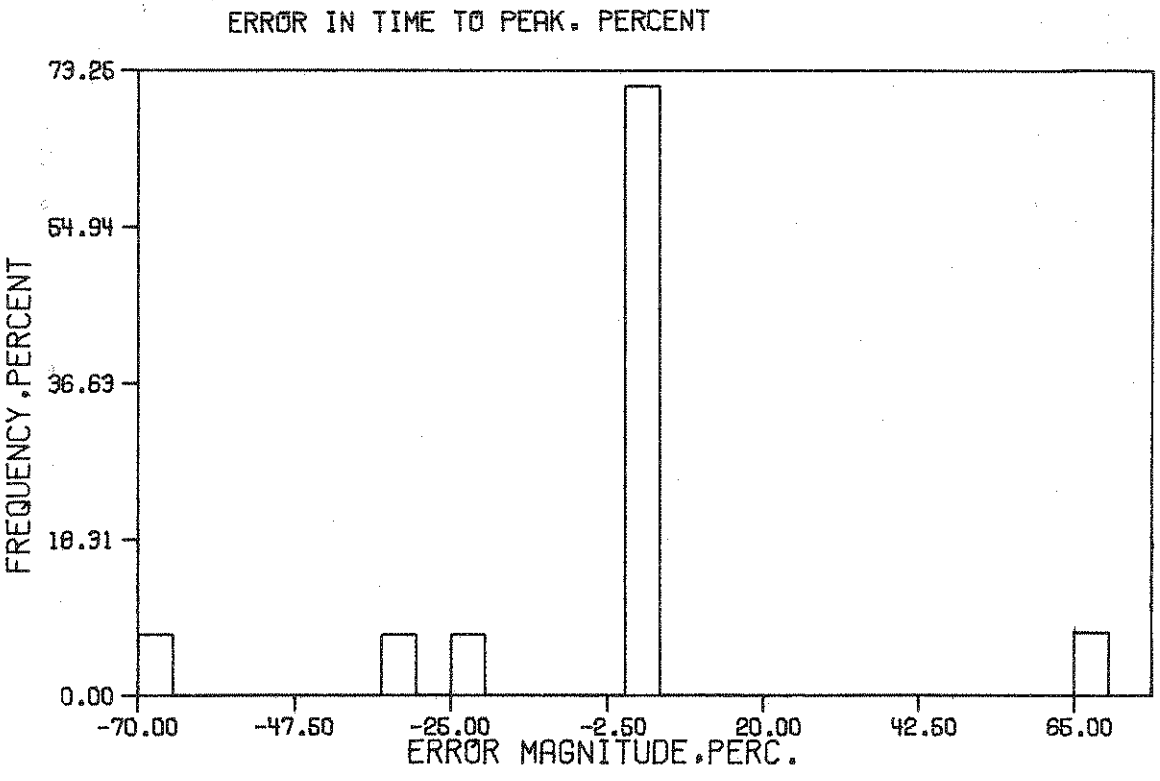

FIGURE 5.9 DISTRIBUTION OF ERROR OF REGENERATED DIRECT RUNOFF

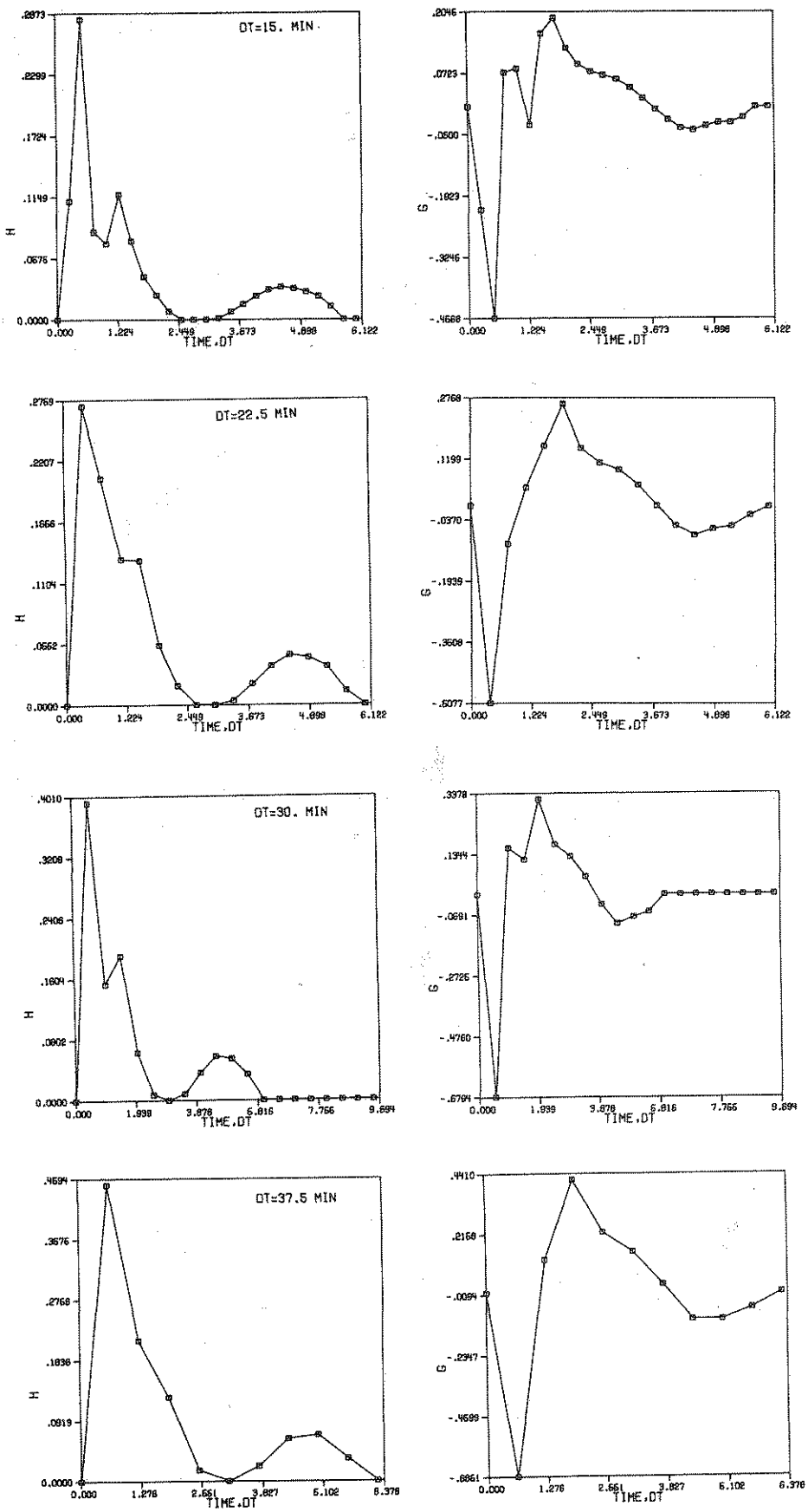

FIGURE 5.10 VARIATION IN FIRST AND SECOND ORDER KERNELS WITH CHANGES IN TIME STEP

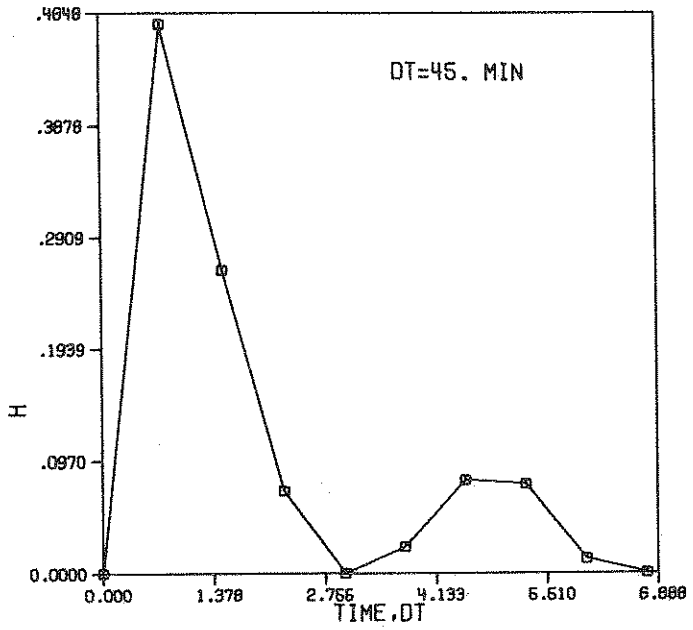

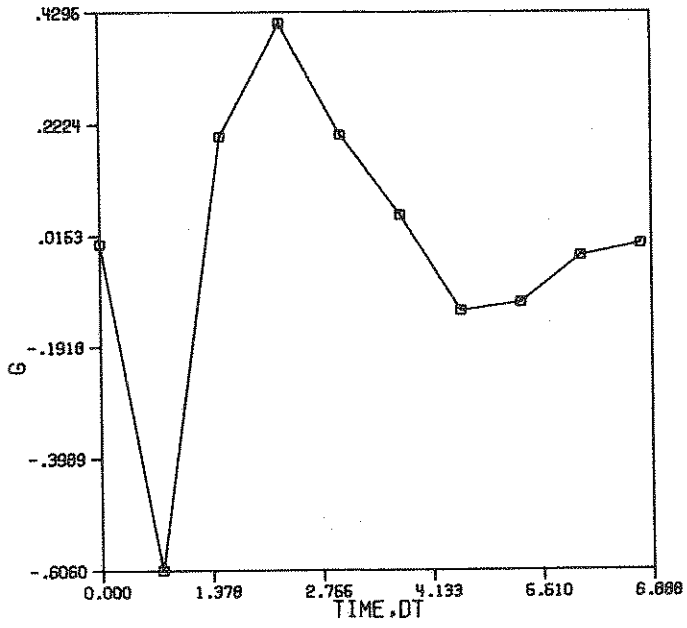

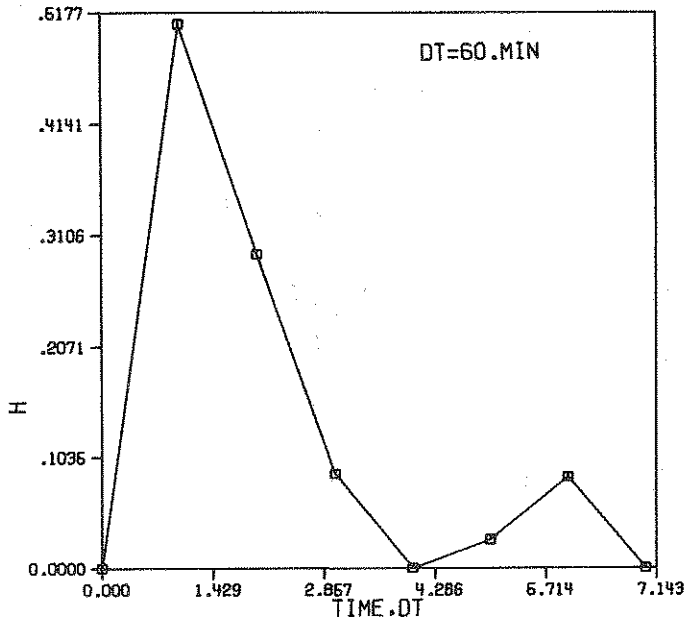

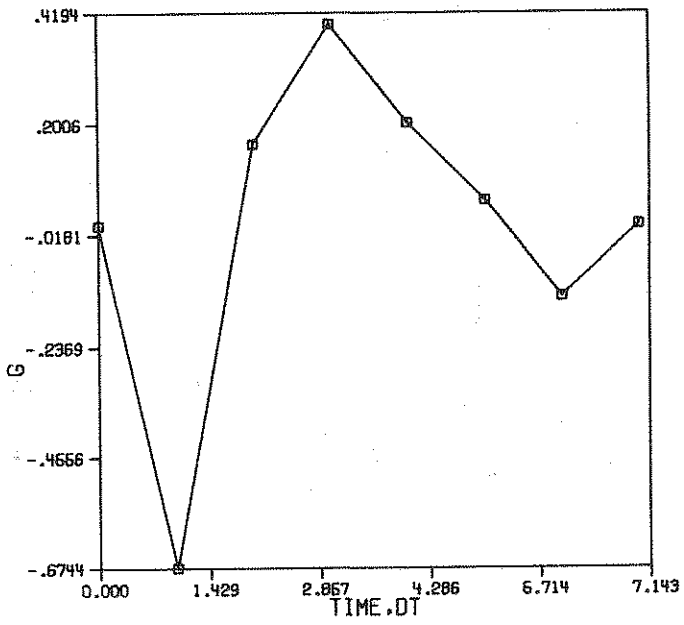

FIGURE 5.10,CONT.

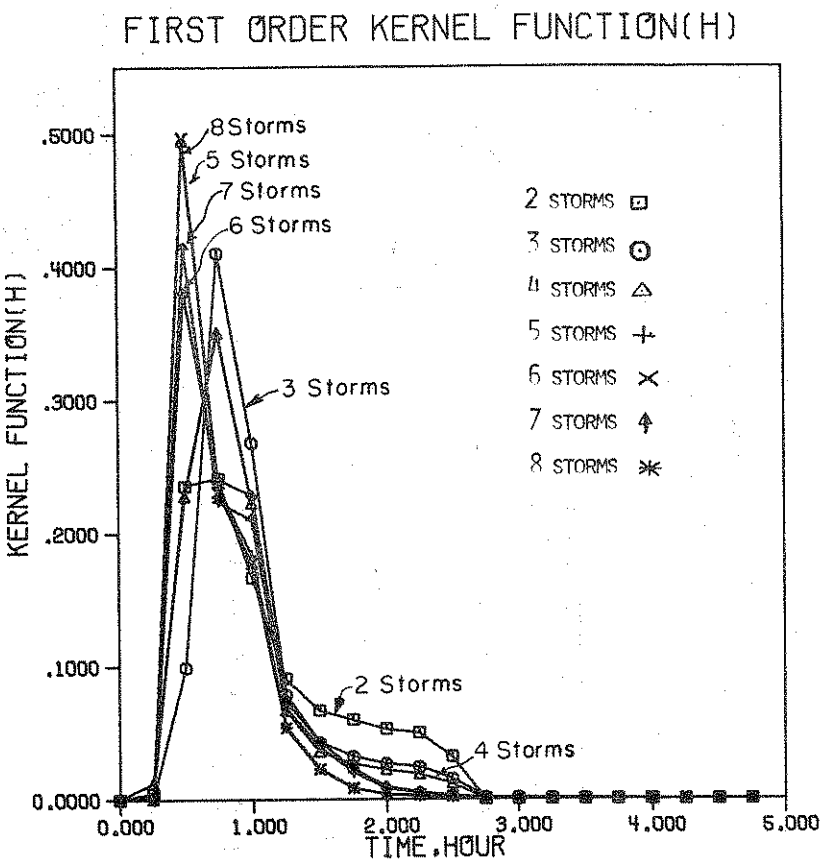

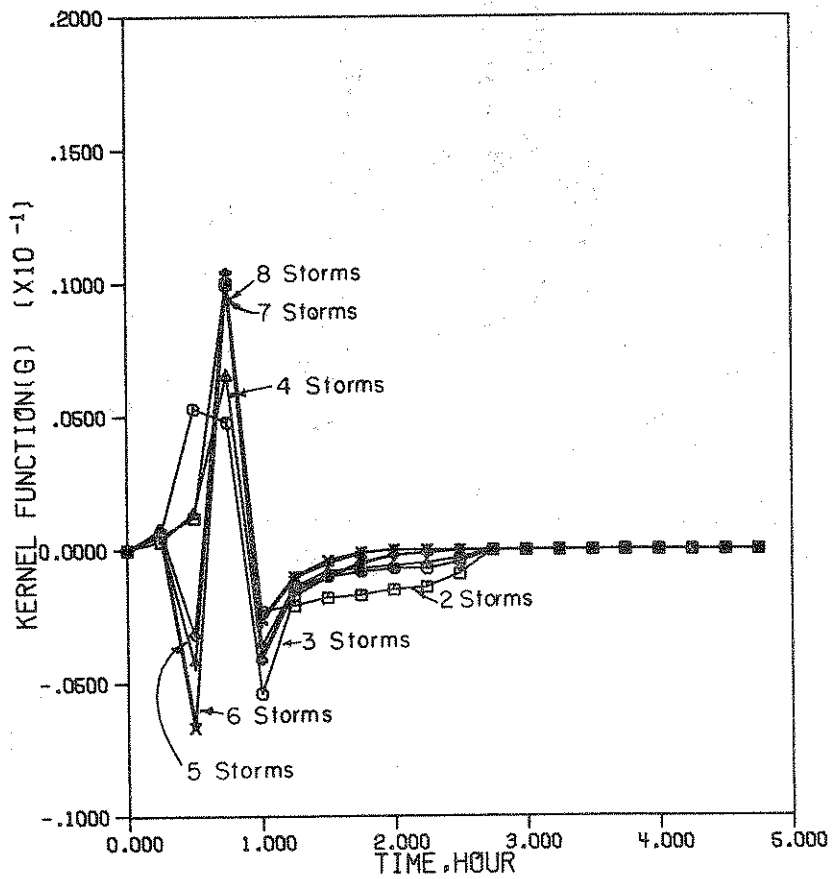

FIGURE 5.11 EFFECT OF NUMBER OF STORMS ON H AND G

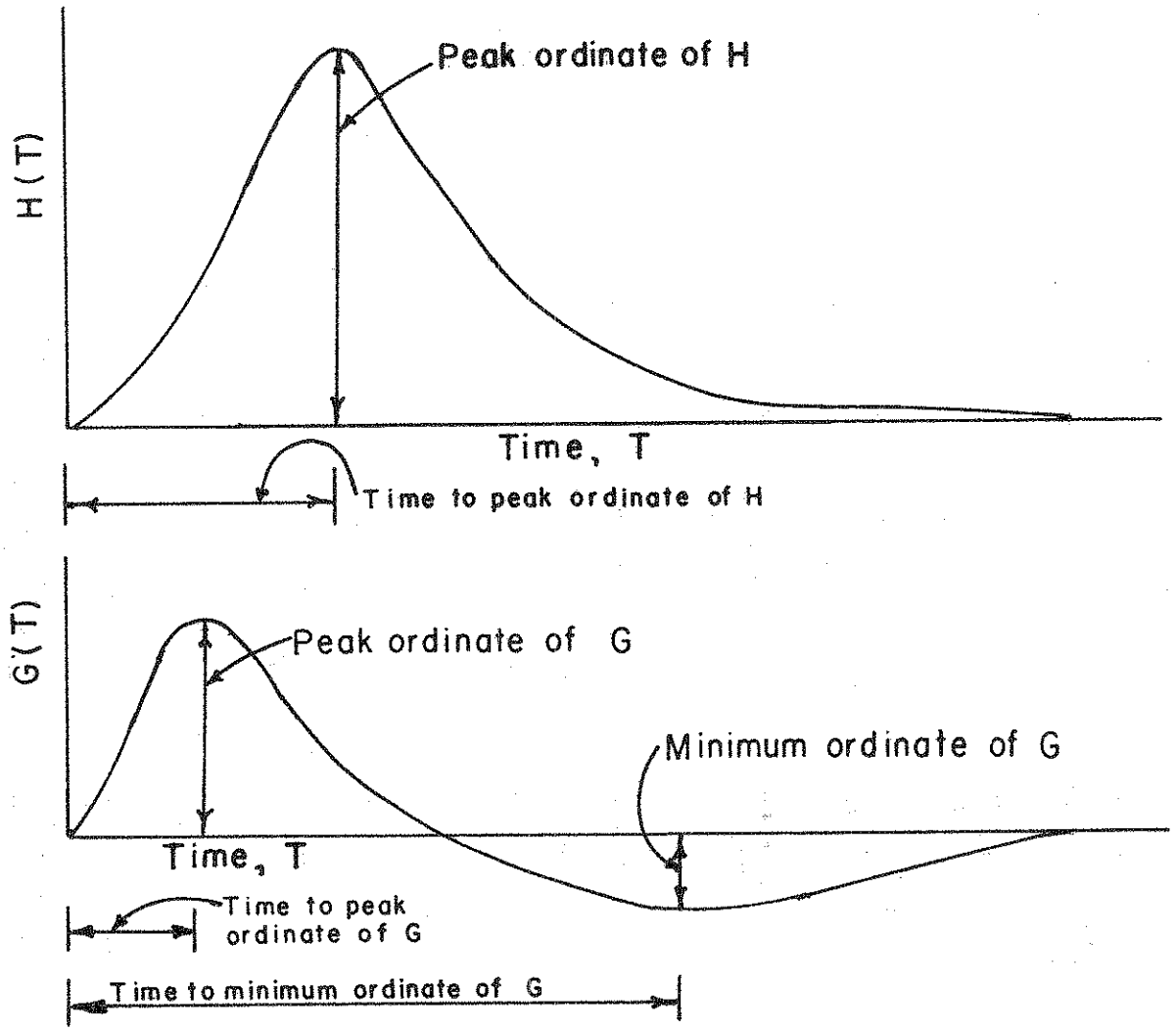

FIGURE 5.12 DEFINITION SKETCH OF FIRST AND SECOND ORDER KERNELS

BEAR CR

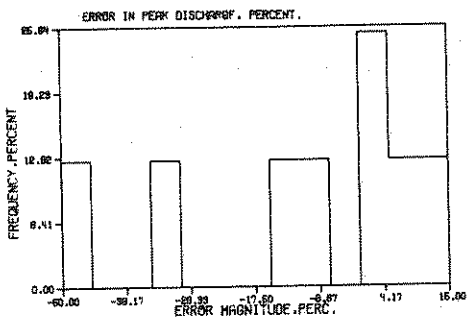

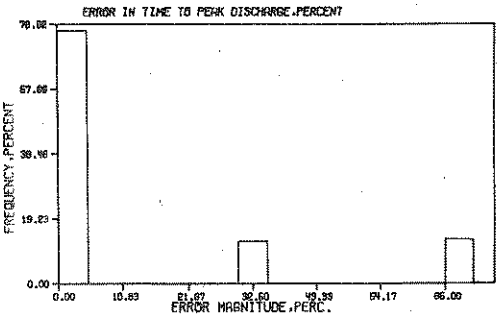

LITTLE EAGLE CREEK

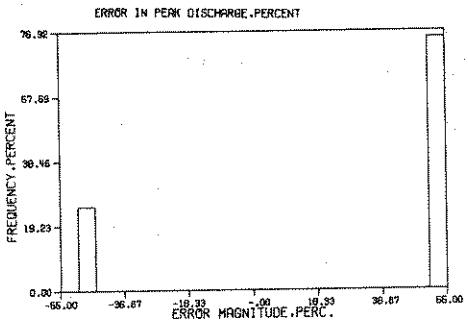

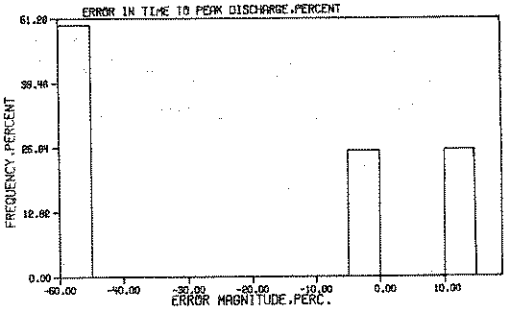

PLEASANT RUN-ARL

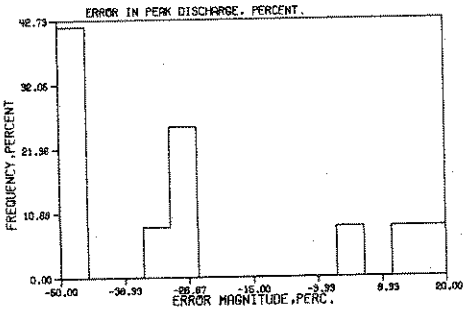

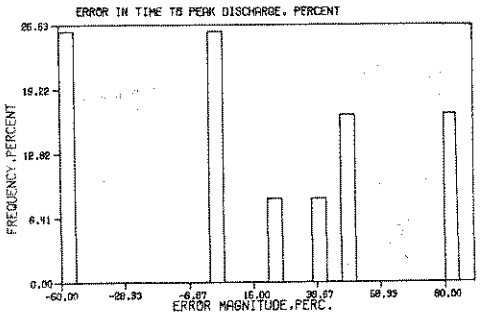

WILBARGER CR

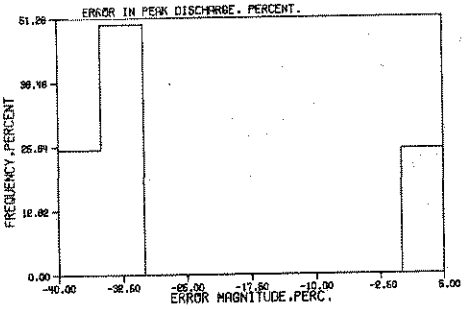

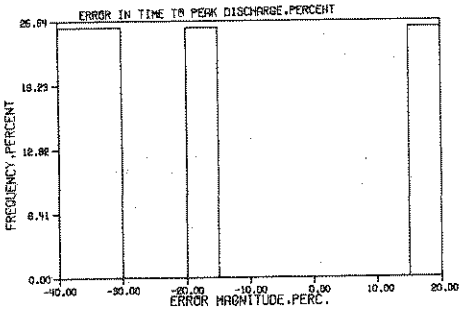

WALLER CR. AT 23RD ST.

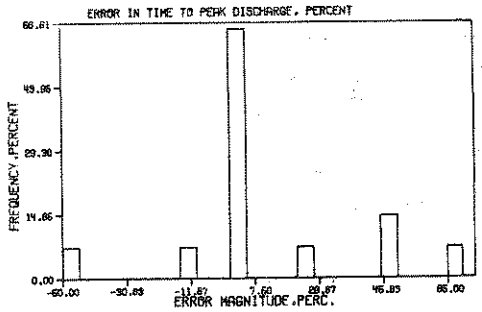

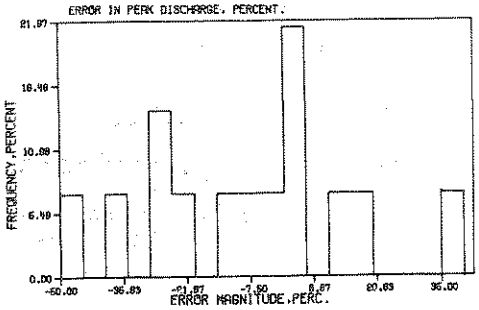

FIGURE 5.13 DISTRIBUTION OF ERROR OF REGENERATED DIRECT RUNOFF

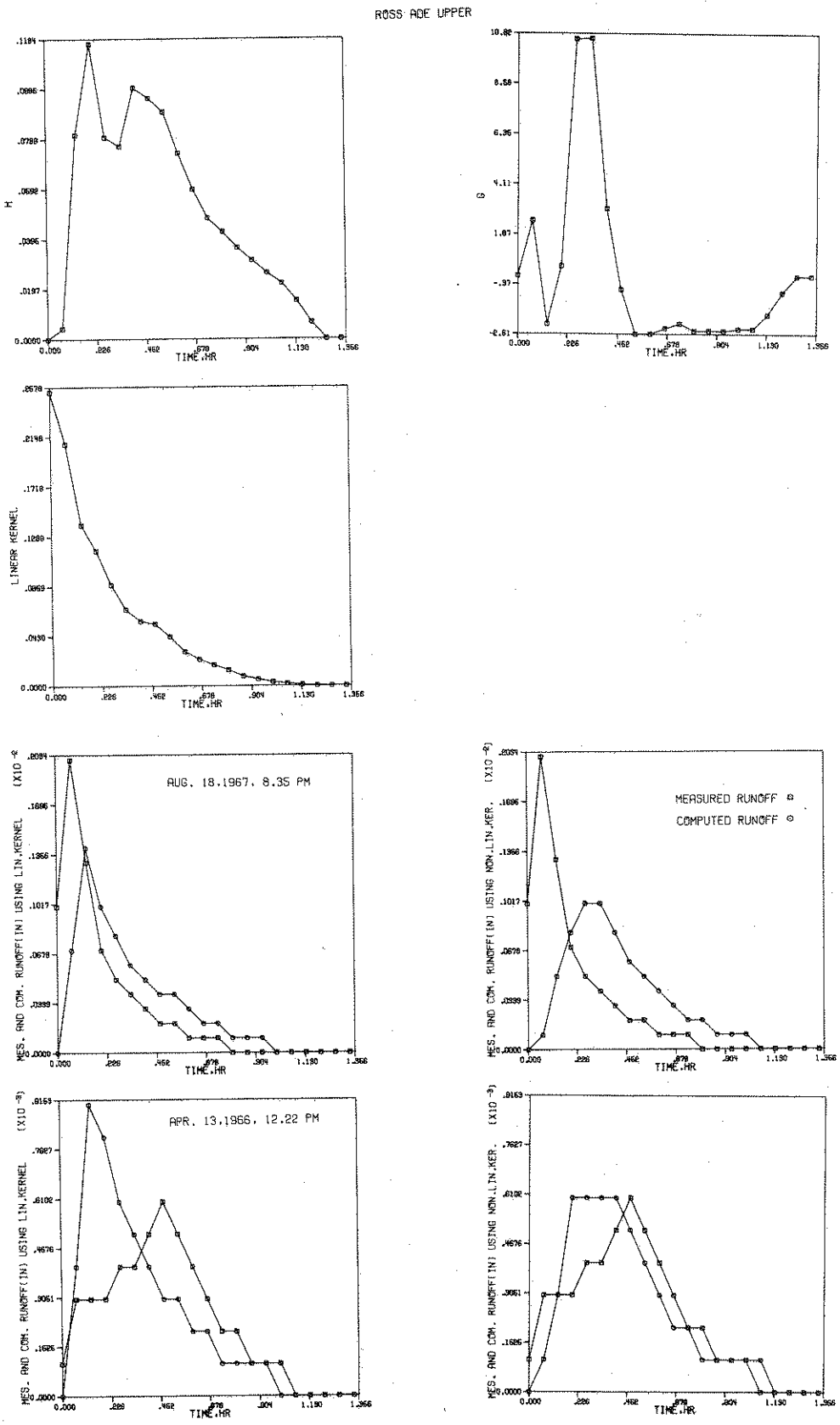

FIGURE 5.14 DIRECT RUNOFF COMPUTED BY USING LINEAR KERNEL AND FIRST AND SECOND ORDER KERNELS

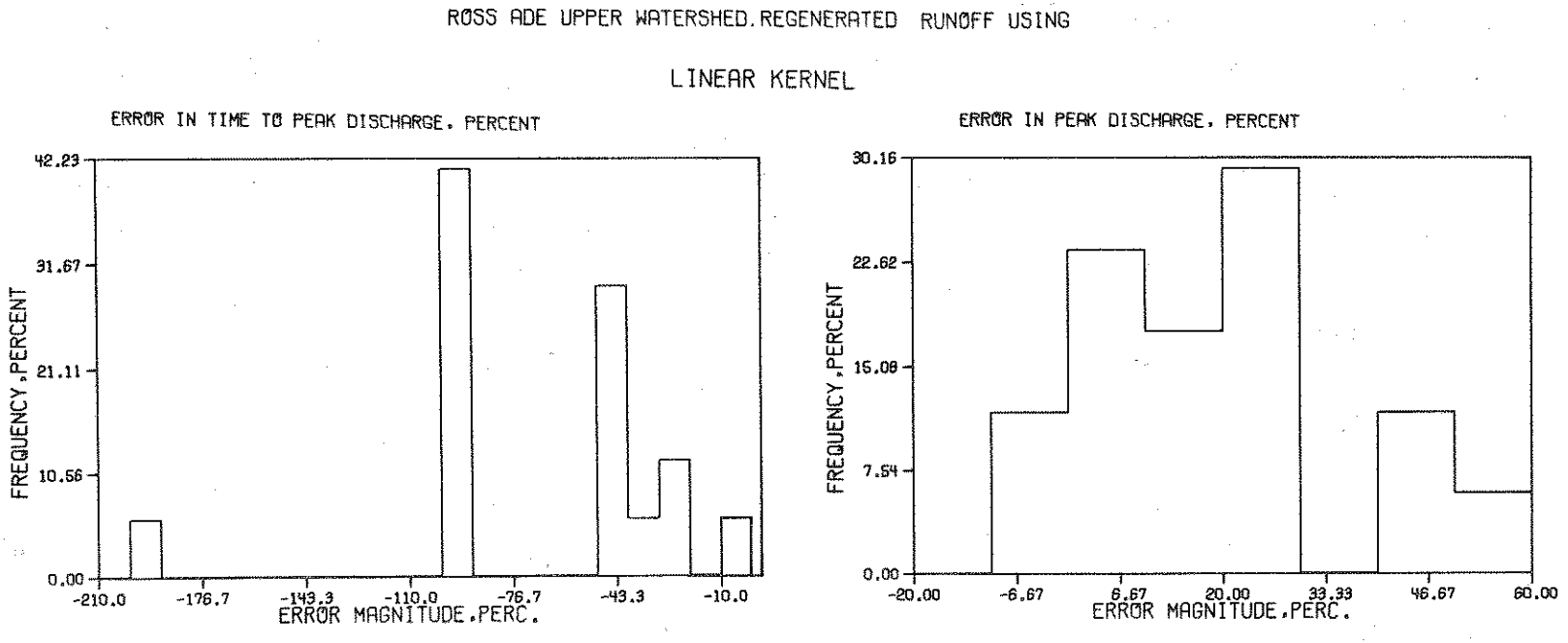

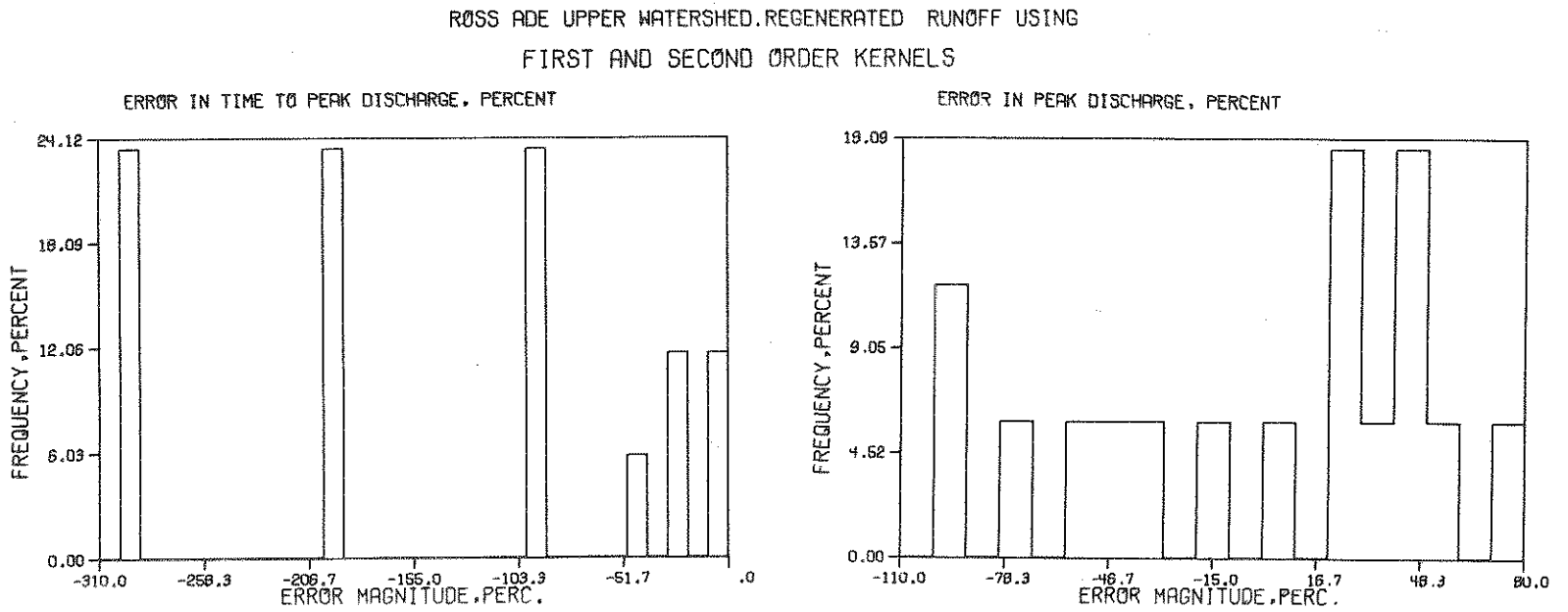

FIGURE 5.15 DISTRIBUTION OF ERROR

6. CONCLUSIONS

i. Four evaporation models were evaluated. They were originally proposed by van Bavel, Kohler, Blaney and Morin and by Blaney and Criddle. van Bavel's model gave the best results, closely followed by Kohler's model. Both are based on the mass transport and energy balance theories. The other two models are empirical and were not originally intended for the estimation of evaporation at short time intervals. Nevertheless the Blaney-Morin model gave reasonable evaporation estimates because of the inclusion of a humidity term. This model is useful in urban hydrology when the radiation and other meteorologic data required by the van Bavel and the Kohler models are not available. The Blaney-Criddle model could not correctly predict the evaporation in a humid climate.

ii. Five rainfall excess models were studied: the modified MIT model, the modified Minnesota model, the modified Holtan model, the Multicapacity Basin Accounting (MBA) model and the Modified Antecedent Retention Index (ARI) model. The first three predict the time distribution of the rainfall excess, the last two the total rainfall excess volume of a storm. Of the five models the ARI model gave the best estimates of the total rainfall excess volume and the MBA model was the next best. Among the three models which predict the time distribution of the rainfall excess, the modified MIT model gave the best results. The Minnesota model, however, is simpler to use. The initial moisture content of the soil profile for the pervious area was the most sensitive parameter for the three models. In an urban watershed, the percentage of impervious area directly connected to storm sewer is an important parameter. The loss from this area is small, nearly all of the rainfall over this area is converted into rainfall excess. In an urbanized watershed connected to storm sewers, the correct identification of the impervious areas is, at least, as important as the estimation of the soil parameters of the pervious area.

iii. The instantaneous unit hydrographs were found to vary from storm to storm on a given watershed. The stability of the IUH depends upon the time interval used in the discretization. Larger time intervals yield smoother IUH curves. The combination of the use of the proper time interval and digital filtering give the most satisfactory results. A quasilinear model of the rainfall excess-direct runoff is proposed. A dimensionless linear kernel was obtained. The IUH for a specific storm on a specific watershed can be obtained by rescaling the dimensionless kernel by using the peak discharge of the IUH and the time lag to watershed and storm characteristics. Good predictions of the direct runoff were obtained by convolving the IUH with the estimated rainfall excess. The variations in the IUH and in the direct runoff due to changes in the urbanization characteristics (primarily increase in imperviousness) can be computed by the proposed quasilinear model.

iv. In the nonlinear system model which was studied the rainfall excess was assumed to consist of a sequence of isolated impulses. The direct runoff output is given as a function of a first and a second order kernel, both of which are plane curves. The first and second order kernels varied with the number of storms used. There was no unique set of kernels for a given watershed. The regeneration performance obtained by the first and second order kernels calculated for pairs of storms was better than that obtained with kernels computed from six storms. The regeneration performance depends in part on the particular set of data used and was not as good as that of the quasilinear model. The predicted runoff hydrographs are sensitive to errors in the second order kernel as the latter is multiplied by the square of the input values.

REFERENCES

2.1 Sarma, P. B. S., J. W. Delleur and A. R. Rao, "A Program in Urban Hydrology - Part II. An Evaluation of Rainfall-Runoff Models for Small Urbanized Watersheds and the Effect of Urbanization on Runoff", Copies are available from NTIS under call number PB 189043.

2.2 Compilation of Hydrologic Data, Austin, Texas, United States Department of the Interior, Geological Survey - Water Resources Division, Texas District, 1968.

2.3 Blank, D. and J. W. Delleur, A Program for Estimating Runoff from Indiana Watersheds - Part I. Linear System Analysis in Surface Hydrology and its Application to Indiana Watersheds, Purdue University, Water Resources Research Center, Tech. Rept. No. 4, August, 1968.

2.4 Soil Survey, Tippecanoe County, Indiana, United States Department of Agriculture, Soil Conservation Service in Cooperation with Purdue University Agricultural Experiment Station, January, 1959.

2.5 Klute, A., Laboratory Measurements of Hydraulic Conductivity of Unsaturated Soil, Methods of Soil Analysis, Am. Soc. Agronomy, Madison, Wisconsin, Part I, pp. 253-261.

2.6 Tucker, L. S., "Availability of Rainfall-Runoff Data for Partly Sewered Urban Drainage Catchments", A.S.C.E. Urban Water Resources Research Program, Tech. Memorandum No. 13, A.S.C.E., New York, March 1970.

3.1 Penman, H. L., "Natural Evaporation from Open Water, Bare Soil and Grass", Proc. Royal Society. (London), Ser. A., Vol. 193, pp. 120-145, 1948.

3.2 Eagleson, P. S., Dynamic Hydrology, pp. 221-241, McGraw-Hill Book Company, New York, 1970.

3.3 van Bavel, C. H. M., "Potential Evaporation: The Combination Concept and Its Experimental Verification", Water Resources Res., Vol. 2, no. 3, pp. 455-467, 1966.

3.4 Kohler, M. A., T. J. Nordenson and W. E. Fox, Evaporation from Pans and Lakes, U. S. Dept. of Commerce, Weather Bureau Res. Paper 38, Washington, May, 1965.

3.5 Blaney, H. F. and W. D. Criddle, "A Method of Estimating Water Requirements in Irrigated Areas from Climatological Data, U. S. Soil Cons. Ser., Washington, 1945.

3.6 Blaney, H. F. and K. V. Morin, "Evaporation and Consumptive Use of Water Formulae", Part I, Trans. Am. Geo. Union, 23(1), pp. 76-83, 1942.

3.7 Hossain, A., "The Effect of Urbanization on Hydrology of Watersheds with Special Reference to Rainfall Excess", Ph.D. Thesis, Purdue University, December 1973.

3.8 Lamoreux, W. W., "Modern Evaporation Formulae Adapted to Computer Use", Monthly Weather Rev., 90(1), pp. 26-38, 1962.

4.1 Swartzendruber, D., "Soil-Water Behavior as Described by Transport Coefficients and Functions", Advances in Agron. 18:327-370, 1966.

4.2 Childs, E. C., The Physics of Soil Water Phenomena, John Wiley and Sons, London, pp. 153-294, 1969.

4.3 Philip, J. R., "A Linearization Technique for the Study of Infiltration", Water in the Unsaturated Zone, Proc. of the Wageningen Symposium, Vol. 1, IASH/IAIHS-UNESCO, pp. 440-451, 1969.

4.4 Harley, M. H., F. E. Perkins and P. S. Eagleson, A Modular Distributed Model of Catchment Dynamics, Rept. No. 133, R. M. Parsons Lab., MIT, 1970.

4.5 Stall, J. B. and M. L. Terstriep, Storm Sewer Design - An Evaluation of the RRL Method, Environmental Protection Tech. Series, No. EPA-R2-72-068, 1972.

4.6 Mein, R. G., "Modeling of the Infiltration Component of the Watershed Rainfall-Runoff Process", Ph.D. Thesis, Agricultural Engr., Univ. of Minnesota, 1971.

4.7 Green, W. H., G. A. Ampt, "Studies on Soil Physics: I. Flow of Air and Water through Soils", Jour. Agr. Sci. 4:1-24, 1911.

4.8 Holtan, H. N., A Concept for Infiltration Estimates in Watershed Engineering, U. S. Dept. of Agriculture, Agr. Res. Service, ARS, p. 25, 1961.

4.9 Wang, F. C., and Lakshminarayana, "Mathematical Simulation of Water Movement through Unsaturated Non-Homogeneous Soils", Soil Science, Am. Proc., 32, pp. 329-334, 1968.

4.10 Holtan, H. N., C. B. England and W. H. Allen, Jr., "Hydrologic Capacities of Soils in Watershed Engineering", Proc. International Hydro. Symp., Ft. Collins, pp. 218-226, 1967.

4.11 Soil Conservation Service, SCS National Engineering Handbook, Section 4, Hydrology, Part 1 - Engineering Planning, Ch. 1-10, 1964, U. S. Dept. of Agriculture, Washington, D. C.

4.12 Chow, V. T., "Handbook of Hydrology", McGraw-Hill Book Company, New York, N.Y., 1964.

4.13 Holtan, H. N., and Lopez, N. C., "USDAHL-70 Model of Watershed Hydrology", Agricultural Research Service, U.S.D.A., Tech. Bull. No. 1435, Nov. 1971.

4.14 Kohler, M. A. and M. M. Richards, "Multicapacity Basin Accounting for Predicting Runoff from Storm Precipitation", Jour. of Geophysical Research, Vol. 67, No. 13, pp. 5187-5197, 1962.

4.15 Saxton, K. E. and A. T. Lenz, "Antecedent Retention Indexes Predict Soil Moisture", Jour. of Hyd. Div. Proceedings of the ASCE, pp. 223-241, 1967.

5.1 Blank, D., J. W. Delleur and A. Giorgini, "Oscillatory Kernel Functions in the Linear Hydrologic Models", Water Resources Res., Vol. 7, No. 5, pp. 1102-1117, October 1971.

5.2 Rao, R. A. and J. W. Delleur, "The Instantaneous Unit Hydrograph: Its Calculation by the Transform Method and Noise Control by Digital Filtering", Tech. Rept. 20, Purdue University Water Resources Research Center, Lafayette, Indiana, June, 1971.

5.3 Rao, A. R., N. Usul, "Sensitivity Analysis of Lumped Linear System Models of the Rainfall-Runoff Process", Tech. Rept. No. 43, Water Resources and Hydromechanics Laboratory, Purdue University, School of Civil Engineering, West Lafayette, Indiana, 47907, pp. 138, May 1973.

5.4 Kavvas, M. L. and Schulz, E. F., "Removal of Unit Hydrograph Oscillations by Filtering", Proc. of the Second International Symposium in Hydrology, Ft. Collins, Colo., Sept. 11-13, 1972. "Floods and Droughts", p. 167-174, Water Resources Publications, 1973.

5.5 Rao, R. A., J. W. Delleur and P. B. S. Sarma, "Conceptual Hydrologic Models for Urbanizing Basins", Jour. of the Hydraulics Div. ASCE Vol. 98, No. HY7, pp. 1205-1220, July, 1972.

5.6 Carter, R. W., "Magnitude and Frequency of Floods in Suburban Areas", U.S.G.S. Prof. paper 424-B, Art. 5, pp. 9-11, 1961.

5.7 Eagleson, P. S., "Unit Hydrograph Characteristics for Sewered Areas", Proc. ASCE, Jour. Hyd. Div., Vol. 88, No. HY2, pp. 1-25, March, 1962.

5.8 Van Sickle, D., "Experience with the Evaluation of Urban Effects for Drainage Design", in "Effects of Watershed Changes on Stream Flow", Eds. W. L. Moore, and C. W. Morgan, Univ. of Texas Press, Austin and London, pp. 229-254, 1969.

5.9 Amorocho, J., "Nonlinear Hydrologic Analysis", in Advances in Hydroscience, V. T. Chow, Ed., Vol. 9, 1973, pp. 203-250.

5.10 Amorocho, J. and A. Brandstetter, "Determination of Nonlinear Functional Response Function in Rainfall-Runoff Processes", Water Resources Res., Vol. 7, No. 5, October, 1971.

5.11 Boneh, Arnon and M. H. Diskin, "Demonstration of Nonlinear Effects of a Second Order Surface Runoff Model", Proc. of the Second International Symposium in Hydrology, Sept. 11-13, 1972, Ft. Collins, Colo., "Floods and Droughts", pp. 157-166, Water Resources Publications, 1973.

5.12 Bjork, A., "Iterative Refinement of Linear Least Squares Solutions I", IT 7(1967), pp. 257-278 and part II, BIT, 8(1968), pp. 8-30.